The implementation of Arctic ice management

Counteracting the annual Arctic sea ice loss by distributing sea water on top of sea ice

L.L. (Laura) van Dijke

TU Delft

The implementation of Arctic ice management

Counteracting the annual Arctic sea ice loss by distributing sea water on top of sea ice

by

L.L. (Laura) van Dijke

To obtain the degree of Master of Science
in Offshore & Dredging Engineering
at the Delft University of Technology.
To be defended publicly on Friday October 14, 2022 at 15:00.

Student number:	4563476	
Project duration:	January 14, 2022 – October 14, 2022	
Thesis committee:	Dr. ir. H. Hendrikse,	Supervisor, TU Delft
	Dr. F. Ypma	Supervisor
	Ir. C.C. Owen	Supervisor, TU Delft
	Dr. ir. P. van der Male	TU Delft
	Ir. J.S. Hoving	TU Delft

Cover image: Polar bear wandering around on Arctic sea ice by Fruchtzwerg's world [2011].

TU Delft

Preface

The topic of this Master thesis is not an everyday concept and the question I got asked the most was: '*But why should we do something like that?*' Without going into the details of this research, this question is one to be asked on different levels. As motives can differ, the aim to use our knowledge to contribute is often common. However, using modern technologies to deliberately intervene in nature might not be something everyone believes in, which I partly agree with. Nevertheless, without researching these topics, we wouldn't even know the safe opportunities out there. For this reason, I am excited to use my knowledge to explore what is possible.

I am very grateful to Hayo Hendrikse and Fonger Ypma for letting me join their project and for their enthusiasm for this research to succeed. This allowed me to explore both realistic and less realistic methods to find answers to the questions raised. I appreciate your time to listen to my findings, suggestions and questions and keeping me on my toes at all times. Furthermore, I would like to thank Cody Owen for his time and help during my experiments (and challenging me to guess the ice thicknesses).

At last, I owe a big thank you to the friends I made since I started studying in Delft, my boyfriend and my family for their valuable advice and endless support during the past years and hopefully the years to come.

L.L. (Laura) van Dijke
Delft, October 2022

Abstract

The Arctic is warming more rapidly than other latitudes, which can result in the release of additional greenhouse gasses, global sea level rise and increase in extreme weather events. Additionally, this causes the rapid decline of sea ice and an ice free Arctic might occur during the summer in the 2040s. The decreasing sea ice cover accelerates the warming of the Arctic, which is known as the albedo feedback system. Solar radiation management (SRM) can be a solution to diminish or possibly stop sea ice decline. Within SRM a proposed technology, known as Arctic Ice Management (AIM), is distributing water on top of existing sea ice to increase the ice thickness enough to survive the summer melt. This raises the question: What water volume should AIM distribute on top of existing sea ice to counteract the annual Arctic sea ice volume loss? Based on data obtained during the period 1979-2020, the September trends for ice extent, ice area and ice volume are -83 400 km^2yr^{-1}, -49 200 km^2yr^{-1} and -322 km^3yr^{-1} respectively. The ice volume is considered as target parameter, as it accounts for both absolute areal ice loss and overall decreasing ice thickness. There are two main ice drift patterns in the Arctic: The Beaufort Gyre in the Beaufort Sea and the Transpolar Drift, of which the latter exports ice through Fram Strait into the Greenland Sea. Literature shows the ice remains within the Arctic for about five years when located in the Beaufort Sea and one to two years when located in the Transpolar Drift. For both locations, the ice decay is determined using an analytical approach first. This approach shows resemblance for ice located in the Beaufort Sea, but generally overestimates the ice decay in the Transpolar Drift. For this reason, an empirical approach is developed to determine the survival ice thickness. This results in accurate trends for ice decay of -2.1 to -2.7 cm day^{-1} in the Beaufort Sea and -0.8 to -1.4 cm day^{-1} in the Transpolar Drift. Considering 91 melting days results in an average survival thickness of 2.18 and 1 m respectively. AIM can be used to increase the ice thickness beyond this survival thickness and an AIM model is developed to show ice growth including AIM. The model concludes the AIM thickness, initial ice thickness prior to flooding and freezing duration after AIM define the effective ice thickness increase. The model is validated with small scale experiments, which indicate a delay between the flooding phase and continued natural ice growth. This delay can be the effect of the duration required to restore the temperature profile in the ice after flooding as shown by COMSOL Multiphysics simulations. Considering the AIM model, it is discouraged to implement AIM on ice thicknesses below 0.6 m and suggested for ice thicknesses approaching 1 m or higher to optimize the effective increase. The required water volume to compensate the annual sea ice volume loss highly depends on the location, initial ice thickness and target ice thickness and varies between 707 to 1095 km^3 in the Beaufort Sea and between 386 to 464 km^3 in the Transpolar Drift for the methods discussed in this research. To pump up this water volume, the expected power requirements are 4.5 to 7.0 GW and 2.5 to 3.0 GW respectively.

Contents

List of Figures

List of Tables

Nomenclature

Abbreviations

Abbreviation	Definition
AIM	Arctic ice management
AO	Arctic oscillation
FDD	Freezing degree days
FYI	First year ice
IMB	Ice mass balance (buoy program)
MYI	Multi year ice
SRM	Solar radiation management
TDD	Thawing degree days

Symbols

Symbol	Definition	Unit
a	Albedo coefficient	[-]
d	Day of year	[-]
$C_{P,w}$	Heat capacity at constant pressure sea water	[J kg^{-1} K^{-1}]
$C_{P,i}$	Heat capacity at constant pressure ice	[J kg^{-1} K^{-1}]
C_t	Heat transfer coefficient	[-]
e_{air}	Vapour content air	[mb]
f	Cloud fraction	[-]
F_r	Shortwave radiation	[W m^{-2}]
F_L	Longwave radiation	[W m^{-2}]
F_s	Sensible heat	[W m^{-2}]
F_l	Latent heat	[W m^{-2}]
h_s	Snow layer thickness	[m]
H	Ice thickness	[m]
I_o	Radiative energy penetrating the ice	[W m^{-2}]
k_i	Thermal conductivity ice	[W m^{-1}K^{-1}]
k_s	Thermal conductivity snow	[W m^{-1}K^{-1}]
k_w	Thermal conductivity sea water	[W m^{-1}K^{-1}]
l_i	Latent heat of ice	[J kg^{-1}]
q_c	Thermal heat conduction	[W m^{-2}]
q_o	Oceanic heat flux	[W m^{-2}]
S	Solar constant	[W m^{-2}]
T_a	Atmospheric temperature	[°C]
T_f	Freezing temperature of sea water	[°C]
T_o	Surface temperature ice	[°C]
Z	Zenith angle	[°]
α	Conversion factor FDD to seconds	[-]
δ	Solar declination	[°]
ϵ_{air}	Emissivity air	[-]
ϵ_{ice}	Emissivity ice	[-]
ρ_i	Density ice	[kg/m^3]
ρ_s	Density snow	[kg/m^3]

Symbol	Definition	Unit
ρ_w	Density sea water	[kg/m^3]
σ	Stefan-Boltzman constant	[W m^{-2}K^{-4}]
ϕ	Latitude	[$^\circ$]

1 Introduction

The Arctic region is warming faster than other latitudes resulting in the rapid loss of Arctic sea ice [Perovich & Richter-Menge, 2009; Screen & Simmonds, 2010; Walsh, 2014]. This increased warming is known as Arctic amplification and is also a result of Arctic sea ice loss. In other words, the decreasing ice cover shows the effects of climate change [J. Overland et al., 2019], but also drives climate change [Euskirchen et al., 2013]. The increased warming of the Arctic influences sea ice, land ice and permafrost, directly affecting the regional flora and fauna. At the same time, worldwide effects are expected, such as increasing global temperatures due to thawing permafrost releasing additional greenhouse gasses, global sea level rise due to land ice melting and possible global increase in extreme weather events due to a decreasing temperature gradient between higher and lower latitudes [Francis & Wu, 2020; Moon et al., 2019].

Arctic amplification is widely explained by different feedback systems [Goosse et al., 2018; Previdi et al., 2021], and one of these systems is the surface albedo feedback. Albedo tells us how much of the incoming radiation on a certain substance is reflected, i.e. it indicates the "whiteness" of a material. The albedo effect was observed as early as 1875, arguing that snow and ice reflect more incoming radiation than other materials [Croll, 1875]. The variations in albedo 'a' in the Arctic region are significant, with $a = 0.06$ for the open ocean, $a = 0.5$ for bare ice and $a = 0.9$ for ice covered with snow. The basic principle of the surface albedo feedback is explained by Serreze & Francis [2006] among many others. As the sea ice area decreases, more open ocean appears resulting in a lower surface albedo. A lower albedo results in less reflection and more absorption of radiation, followed by warming of the surface temperatures and further sea ice decline. In many papers it is argued if the surface albedo feedback is [Crook et al., 2011; Screen & Simmonds, 2010; Taylor et al., 2013] or is not [Hall, 2004; Pithan & Mauritsen, 2014; Winton, 2006] the main cause of Arctic amplification. Nevertheless, all papers express the significant contribution of the albedo feedback on Arctic amplification and, therewith, the importance of Arctic sea ice. However, predictions by the Coupled Model Intercomparison Project (CMIP) show that all Arctic seas will become ice free during the summer months within the 2020s. The central Arctic is expected to reach this state in the 2040s and the Barents Sea is expected to be ice free all year round in the 2050s [Årthun et al., 2021; Notz & Community, 2020; Onarheim et al., 2018; J. E. Overland & Wang, 2013].

Different proposals have been presented to diminish or even stop Arctic amplification. These techniques can be grouped in either negative emission technologies (removing carbon dioxide from the atmosphere) or solar radiation management (increasing the surface albedo) [Miller et al., 2020]. Solar radiation management (SRM) is often linked to either stratospheric aerosol injection [Berdahl et al., 2014; Lenton & Vaughan, 2009] or restoration of the sea ice, referred to as Arctic Ice Management (AIM). Ice restoration proposals are for example highly reflective glass microspheres distributed on low reflective young sea ice [Field et al., 2018] or by pumping water onto the ice to increase the ice thickness. The latter idea was first proposed by Flannery et al. [1997], who suggested the required energy might be retrieved from temperature gradients between ice and water. Continuing this idea, Desch et al. [2017] analysed the feasibility of installing wind powered pumping systems. However, some questions concerning the implementation remain. What it takes to counteract the annual Arctic sea ice loss is considered fundamental for the development of AIM. This has lead to the following research question:

What water volume should Arctic ice management distribute on top of existing sea ice to counteract the annual Arctic sea ice volume loss?

The question is divided in five aspects. First of all, why the annual sea ice volume loss is set as the aim for this research is discussed in Chapter 2 and a target value for AIM implementation is defined.

Secondly, Chapter 3 describes how ice dynamics and natural processes can influence AIM implementation based on literature findings. In third place, an empirical approach is created to predict the ice thickness decrease during one summer and this is compared to an analytical approach in Chapter 4. Thereafter, Chapter 5 discusses natural ice growth and how AIM might affect natural ice growth. This results in the development of an ice growth model including AIM in Chapter 6, which is validated and verified using small scale experiments and COMSOL Multiphysics simulations. Finally, Chapter 7 combines the results of all five aspects to show possibilities of AIM implementation. This report ends with a conclusion and discussion including recommendations in Chapters 8 and 9.

2

Annual Arctic sea ice loss

Both the mean ice thickness and the areal coverage are decreasing. The decrease of the Arctic ice cover can be seen from passive-microwave data starting in November 1978 [Parkinson et al., 1999]. At present, 43 years of data are available for analysing the trend of the Arctic ice cover. Within research, several parameters are used to define sea ice decline and these are discussed in this chapter. First, the areal extent is covered in Section 2.1, followed by ice volume and ice thickness in Section 2.2. Finally, Section 2.3 discusses the best target parameter for AIM implementation.

2.1. Sea ice cover

The Arctic region can be divided into the central Arctic, multiple seas and several straits. The different regions as provided by the National Snow and Ice Data Center (NSIDC) are shown in Appendix A. The analysis of the Arctic ice cover is generally presented in either sea ice area or sea ice extent (hereafter referred to as ice area and ice extent). Ice extent defines the area of the ocean surface which is covered with at least 15% ice [Parkinson & Cavalieri, 2008]. This definition is also used to define the ice edge and depends on the ice concentration. An example of the ice concentration is shown in Figure 2.1 as given by the NSIDC. Ice area defines the actual area covered with ice. By these definitions the ice area is always smaller than the ice extent.

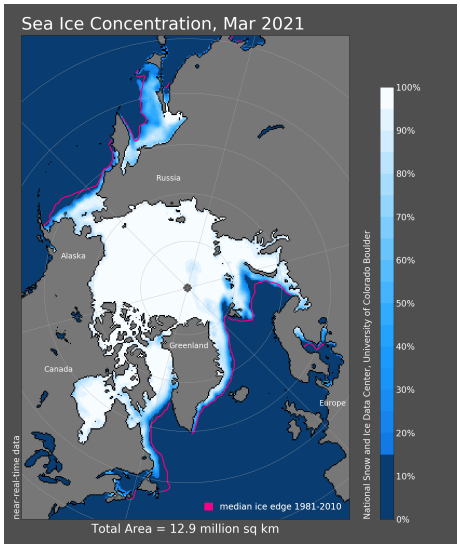

Figure 2.1: Sea ice concentration in March 2021. Image credit: National Snow and Ice Data Center.

The trend of the ice extent and ice area are analysed in many papers. The year the paper was written defines how many years of data were available and included in the research. This results in different outcomes when recent years are added and this is the main reason certain values in the coming sections can differ from one another.

The paper by Cavalieri & Parkinson [2012] covering the period 1979-2010, analyses the decreasing trend over 32 years and compares it to earlier performed analysis over 28 years (1979-2006) [Parkinson & Cavalieri, 2008] and over 18 years (1979-1996) [Parkinson et al., 1999]. Table 2.1 shows the trend for both ice extent and ice area concerning these three time series. The results indicate that, according to the data up to and including 2010, every two years the ice extent decreases with approximately the size of Iceland and the table shows an accelerated decrease in both ice extent and ice area [Cavalieri & Parkinson, 2012]. The effect on the annual trend due to the addition of the last four years (2006-2010) emphasises the importance of continuously updating the data.

Table 2.1: Annual trend for extent and area [Cavalieri & Parkinson, 2012; Parkinson & Cavalieri, 2008; Parkinson et al., 1999]

	1979-1996	1979-2006	1979-2010
Annual ice extent ($km^2\ yr^{-1}$)	$-34.0 \cdot 10^3$	$-45.1 \cdot 10^3$	$-51.5 \cdot 10^3$
Annual ice area ($km^2\ yr^{-1}$)	$-29.3 \cdot 10^3$	$-41.0 \cdot 10^3$	$-49.6 \cdot 10^3$

Besides annual trends, data is often divided into regional [Cavalieri & Parkinson, 2012] and seasonal trends. The AIM installation targets the entire Arctic ice loss and does not focus on regional trends. Regional ice, and indirectly regional trends, play a role in choice of location and will be discussed in Chapter 5.2. The seasonal trends are discussed in Section 2.1.1. Furthermore, trends are subject to change over longer periods and, therefore, Section 2.1.2 discusses the decadal trends.

2.1.1. Seasonal trends

Due to seasonal variations, the average ice extent during the period 1979-1996 had a maximum in March and a minimum in September of respectively 15.4x10^6 km^2 and 7.0x10^6 km^2 [Parkinson et al., 1999]. These variations are clearly visible for each line shown in Figure 2.2, with a maximum ice extent around March (end of winter) and a minimum around September (end of summer). Furthermore, the figure shows the average for the last four decades using the latest data by the NSIDC [Fetterer et al., 2017].

The seasonal effect is also visible on the inter-annual trend. Available data shows a decline in ice extent for all months, but the decadal changes in the Arctic ice cover are stronger during summer than winter [Comiso, 2012]. The satellite data up to 2017 shows a decline for September with approximately -83 000 km^{2}yr^{-1} (-1.1% per year), compared to the smallest absolute trend of -34 000 km^{2}yr^{-1} (-0.26% per year) in May [Serreze & Meier, 2019]. This suggests an accelerated process to a seasonally ice free Arctic when compared to annual trends. The general understanding of 'seasonally ice free' is less than 1.0x10^6 km^2 of ice. Figure 2.2 shows similar results with the largest intervals around September and the smallest in May.

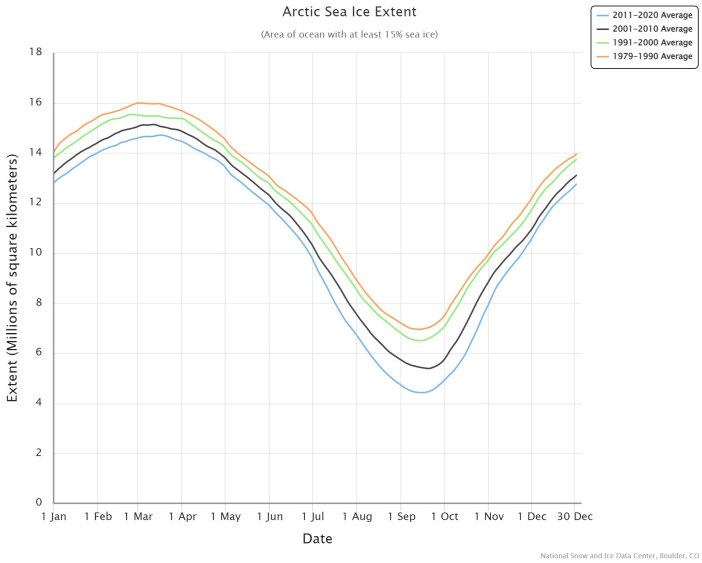

Figure 2.2: Seasonal variations and decadal trends for ice extent. Image credit: Sea Ice Index, National Snow and Ice Data Center.

The decline in ice extent is often expressed in monthly values. Using data of the NSIDC [Fetterer et al., 2017] for ice extent, up to and including 2021, results in Figure 2.3. This figure shows the trend for the maximum ice extent (March), minimum ice extent and simultaneously the strongest relative trend (September) and the maximum absolute inter annual difference (October), which can be due to delayed initial ice growth as a result of warmer ocean water and/or surface temperatures. During the interval 1979-2020[1] the according trend values are -40 600 km^{2}yr^{-1} (-0.26% per year) in March, -83 400 km^{2}yr^{-1} (-1.19% per year) in September and -84 300 km^{2}yr^{-1} (-0.95% per year) in October. The percentage changes are given relative to the 1979-1996 average.

[1]The NSIDC splits the sea ice index data in a near-real-time product (NRTSI product, used to extend the record to present day) and a final product (GSFC product). The GSFC product (*Sea Ice Concentrations from Nimbus-7 SMMR and DMSP SSM/I-SSMIS Passive Microwave Data* [Cavalieri et al., 1996]) is obtained from the Goddard Space Flight Center and considered as higher quality, but is not received at the NSIDC until roughly a year later. For this reason the trends are calculated for the GSFC product only until and including 2020

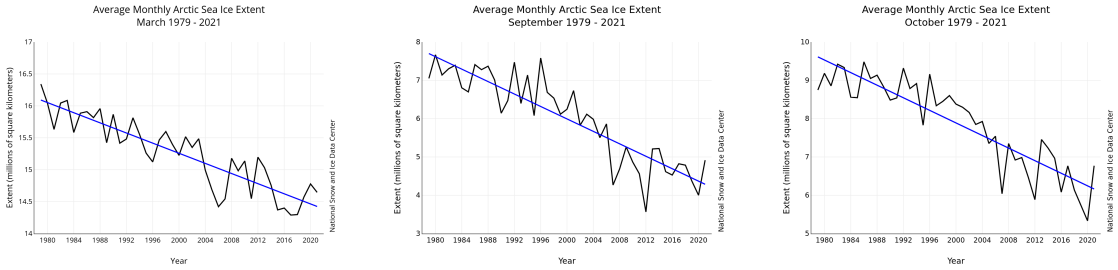

(a) March 1979-2021 **(b)** September 1979-2021 **(c)** October 1979-2021

Figure 2.3: The decreasing monthly trends for ice extent. Image: Sea Ice Index, National Snow and Ice Data Center.

Similar trends can be calculated for ice area using data of the NSIDC [Fetterer et al., 2017]. Like ice extent, the average ice area had a maximum in March of 13.2x10^6 km^2 and a minimum in September of 4.8x10^6 km^2 during the years 1979-1996. During the years 1979-2020, the ice area decreases with approximately 3800 km^2yr^{-1} (-0.03% per year) in March and 49 200 km^2yr^{-1} (-1.03% per year) in September. Similarly, the strongest absolute trend occurs in October with -56 600 km^2yr^{-1} (-0.83% per year). The percentage changes are given relative to the corresponding monthly average during the period 1979-1996. The NSIDC makes a remark about the values measured for the ice areas. The sensors detect melt ponds on top of the ice cover as open ocean instead of ice covered with water. For this reason, the summer ice area is most likely underestimated.

2.1.2. Decadal trends

The trends for ice extent and ice area show the decrease during the period 1979-2020. However, as mentioned earlier in this chapter, the trend changes depending on how many and which years are included in the data. Figure 2.4 shows the decadal trends for ice area and extent in March and September. When comparing both figures, the September ice trend suggests a stabilisation during the last decade, while the March trend remains similar (extent) or accelerates (area). The stabilisation has been recognised before concerning summer ice extent by Francis & Wu [2020]. They conclude that in (roughly) every year the winter and spring months suggest hitting a new minimal record. However, in August and September the trend turns and they explain this pattern with low pressure formation resulting in clouds and winds, which positively affects the ice cover. They also suggest early snow melt might result in an atmospheric shift initiating a negative feedback for the ice extent.

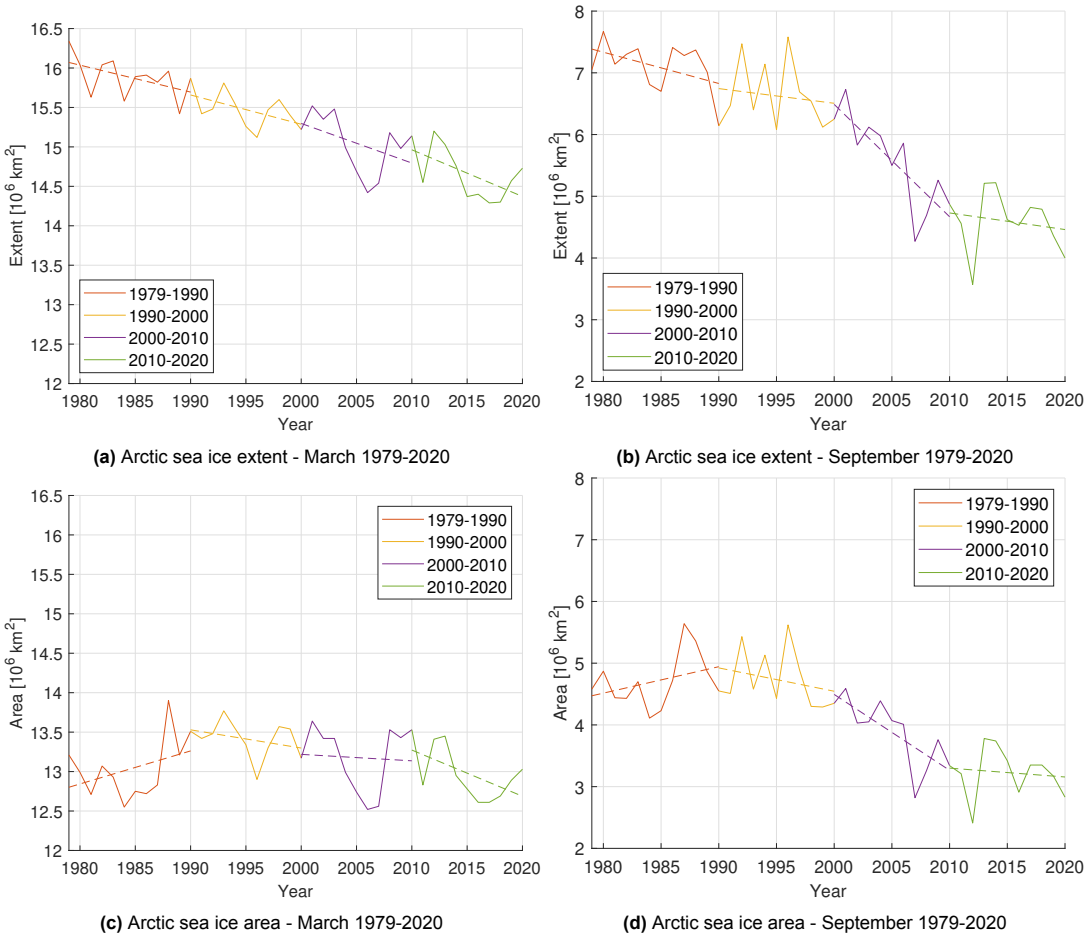

(a) Arctic sea ice extent - March 1979-2020

(b) Arctic sea ice extent - September 1979-2020

(c) Arctic sea ice area - March 1979-2020

(d) Arctic sea ice area - September 1979-2020

Figure 2.4: The decadal trends for ice extent and area during 1979-2020. Data: Sea Ice Index, National Snow and Ice Data Center, Fetterer et al. [2017].

2.2. Sea ice volume

Besides ice extent and ice area, sea ice volume is used to discuss ice trends in the Arctic (hereafter referred to as ice volume). Figure 2.5 shows the seasonal variation of the ice volume for similar intervals as used for ice extent. It is noticeable that the ice volume reaches its annual maximum slightly later (April: average 30 381 km^3 during the period 1979-1996), than the ice extent (March). The annual minimum still occurs in September (average 14 396 km^3 during the period 1979-1996).

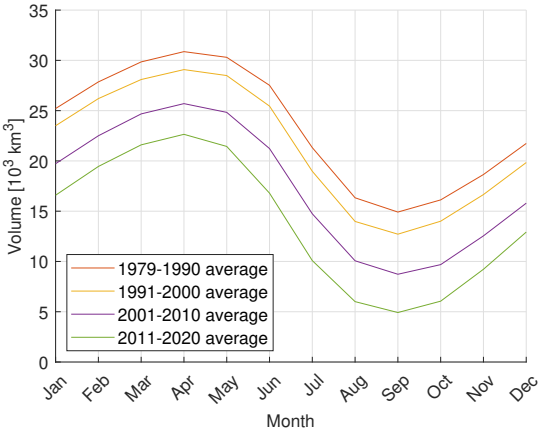

Figure 2.5: Seasonal variations and decadal trend for ice volume. Data: PIOMAS Ice volume time series provided by Polar Science Center, [Schweiger et al., 2011].

During the years 1979-2021, the ice volume decreased with 265 km^3yr^{-1} (-0.9% per year) in March (similar in April), 322 km^3yr^{-1} (-2.23% per year) in September and the fastest absolute decline is shown in July with 358 km^3yr^{-1} (-1.7% per year) (Data: PIOMAS ice volume time series, Schweiger et al. [2011]). Figure 2.6 shows the decadal trends for ice volume, and the trends indicate a similar behaviour as for ice area and extent, as shown in Figure 2.4. Similar to ice extent, the winter and spring months after 2012 suggest hitting a new minimal record in September. However, between June and August the course is interrupted. Zhang [2021] mentioned a stabilization of the ice volume decline during the years 2010-2020, similar to the findings by Francis & Wu [2020] for ice extent. However, they do not refer to similar causes. Zhang [2021] explains the stabilisation with trends in ice volume, ice velocity and ice export. First of all, the export (predominantly through Fram Strait) is decreasing as a result of the thinning of the Arctic. As the ice thickness decreases, less ice is available for export through Fram Strait [Wang et al., 2021; Zhang et al., 2012]. Secondly, the trends of ice volume, ice velocity and ice export act as a negative response system. When the volume decreases more than the velocity increases, the export decreases. This occurred during the period 2007-2020 resulting in a stabilization of the ice volume [Zhang, 2021]. It should be kept in mind, that increasing the ice cover might reverse this process and counter the stabilisation to a certain extent.

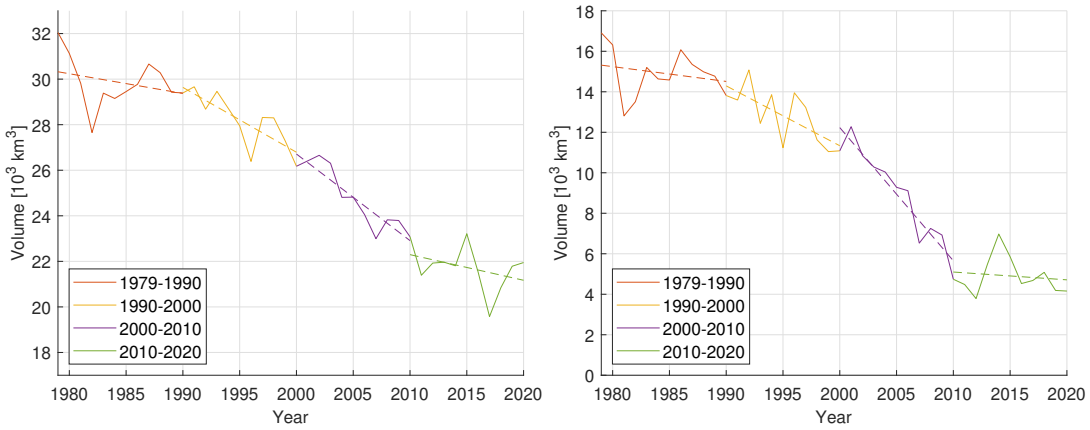

(a) Arctic sea ice volume - March 1979-2020

(b) Arctic sea ice volume - September 1979-2020

Figure 2.6: The decadal trends for ice volume during 1979-2020. Data: PIOMAS Ice volume time series provided by Polar Science Center, [Schweiger et al., 2011].

Ice thickness

The ice thickness is not a parameter often used to describe ice trends. Nevertheless, it has a fundamental role in describing the ice present. The trends in ice area and extent only account for ice completely disappearing, while research shows a decrease in ice thickness over the entire ice cover.

Research about ice thickness is often linked to ice age: First-year ice (FYI), multi-year ice (MYI) and perennial ice. The perennial ice cover consists of ice which has survived the summer and may include ridged first-year ice. Multi-year ice, as defined by the World Meteorological Organization, is all ice which has survived at least two summers and represents the thick part of the perennial ice cover. The perennial ice cover is decreasing and two main causes can be identified. First of all, more ice melts during the summer than grows during the winter. Secondly, multi-year ice exported through Fram Strait flows into the Greenland Sea and melts [Zwally & Gloersen, 2008]. Nowadays, the melted multi-year ice is not fully replaced, leaving an increased fraction of the ice cover with thinner first-year ice, and a larger vulnerable part of the ice cover at the start of the subsequent summer [Serreze & Meier, 2019]. Data up to and including 2011 revealed a faster decline of multi-year ice than perennial ice. This shows that the average ice thickness of the ice cover is decreasing [Comiso, 2012]. Already in 2002, it was expected that the multi-year ice layer would disappear within this century [Comiso, 2002].

Determining the mean ice thickness and the decrease in ice thickness shows its challenges as different observation techniques show different results. Lindsay & Schweiger [2015] conclude that the annual mean ice thickness in the Artic Basin has reduced with 0.58 ± 0.07 m per decade during the years 2000-2012. This is determined using the Ice Thickness Regression Procedure (ITRP) on eight different data sets for ice thickness observations.

2.3. Discussion: Determining the AIM target

Our aim for AIM implementation is to counteract the annual Arctic sea ice loss. As discussed in this chapter, there is not one definition for the annual ice loss and up to date data is fundamental. There are annual and seasonal values for both ice extent, ice area, ice thickness and ice volume. A summary of these parameters, except ice thickness, is given in Table 2.2.

Table 2.2: Trends for ice extent, area and volume calculated for 1979-2020. The maximum relative trend for each parameter is written in bold. Data: Extent and area by NSIDC [Fetterer et al., 2017], volume by PIOMAS [Schweiger et al., 2011].

	Extent km^2yr^{-1}	Area km^2yr^{-1}	Volume km^3yr^{-1}
March	-40 600 (-0.26%)	-3 800 (-0.03%)	-265 (-0.9%)
September	-83 400 **(-1.19%)**	-49 200 **(-1.03%)**	-322 **(-2.23%)**
October	-84 300 (-0.95%)	-56 600 (-0.83%)	-327 (-2.09%)
July	-70 800 (-0.71%)	-37 400 (-0.56%)	-358 (-1.7%)

To counteract the annual sea ice decline, a target value is determined in Section 2.3.1. Additionally, the best case scenario is a self maintaining ice cover after AIM. The possibilities for this scenario are discussed in Section 2.3.2 using simplified calculations.

2.3.1. AIM target

Ideally, the entire ice cover is increased with an additional layer of ice. However, this is not considered feasible. The area is too large and operating in thick MYI comes with its challenges. Instead, partly increasing the FYI cover with a thicker layer of ice is considered. An enlarged ice cover increases the overall surface albedo and hence reflects more radiation (SRM). For the Arctic region, this is effective after the vernal equinox and until the autumnal equinox (Northern Hemisphere). Therefore, to have a positive effect on the albedo factor, increasing the summer ice cover is considered most effective. Additionally, the maximum relative decline is chosen as a target value, which occurs in September for all three parameters.

Either ice extent, ice area or ice volume has to define the target for the AIM installation. Ice extent (as used for the AIM feasibility study by Desch et al. [2017]), partly includes open ocean. Increasing this value can be done by increasing the ice cover, but also by distributing the ice cover, which can be misleading and for the same reasons validation of the AIM system can be difficult. More logically is to use the ice area. Nevertheless, the main downside of this parameter is the possible inaccuracy due to melt ponds. Additionally, for both extent and area applies that the overall thickness decline is not taken into account. Ice volume accounts for both areal decline and overall reduced thickness. For this reason, ice volume is considered the most suitable parameter and our aim is set to compensate 322 km^3yr^{-1}.

There are several possibilities to counteract annual decline in ice volume. To increase the ice coverage, adding area by increasing the thickness of FYI is considered. Besides a direct increase in ice volume, this increases the summer surface albedo contributing to SRM. The required thickness depends on the regional survival thickness and is discussed in Chapter 4.

2.3.2. Long term target

Different climate models have analysed the effect of diminishing insolation to mitigate global warming due to CO_2. Models often compare various CO_2 scenarios to the pre-industrial CO_2 levels of 280 ppm. Last year (2021), the CO_2 levels reached a new maximum of 414 ppm. However, it should be kept in mind that CO_2 is not the only greenhouse gas contributing to global warming. Caldeira & Wood [2008] used the NCAR CCM3 atmospheric general circulation model and they compared a control climate with 280 ppm of CO_2 to climate simulations with doubled CO_2 concentration (560 ppm) with varying percentages of insolation reduction (SRM). The insolation reduction is applied on either global or regional scale (61°N-90°N or 71°N-90°N) and all scenarios were simulated for 70 years. Some interesting observations are that a 1.8% global reduction of insolation applied over the entire Earth is necessary to keep the global temperature increase at 0.11 K. A similar result is obtained by Govindasamy & Caldeira [2000] using the NCAR CCM3 model over 40 years. However, this would still increase the Arctic temperature with 0.83 K and decrease the ice fraction with 1.3%. A similar reduction in global insolation can be achieved by a regional reduction of 50% over 61°N-90°N. This would limit

the global warming to 0.15 K and would decrease the Arctic temperature with 11.2 K. These models emphasise the different effects of globally or regionally modifying the insolation. This difference is also concluded by Zampieri & Goessling [2019], who model the RCP8.5 scenario using the Alfred Wegener Institute Climate Model. By using the AIM principle as introduced by Desch et al. [2017], Zampieri & Goessling [2019] state an ice free Arctic summer can be delayed. However, the effect on global warming is small.

Caldeira & Wood [2008] suggest a necessary reduction of solar insolation of 21% over 71°N-90°N to restore the summer ice extent in a climate with 560 ppm CO_2. In the same paper the closest reduction elaborated is 25% (71°N-90°N). This results in a regional temperature change of -0.28 K, an ice fraction increase of 3.5%, but still a global temperature change of 1.83 K. In first place, the purpose of AIM is to stabilise the Arctic ice cover. To maintain the Arctic ice cover, the regional temperature change is an important factor. The results by Caldeira & Wood [2008] suggest a 21% reduction of regional solar insolation is necessary to counterbalance the regional temperature increase in a 560 ppm CO_2 scenario relative to the pre-industrial state (280 ppm).

The possibility of reducing insolation using AIM is simplified by defining solar insolation in terms of energy reflected and energy absorbed. The following formulae are used:

$$E_{reflected} = S \cdot sin(\delta) \cdot (1 - f) \cdot A \cdot a \tag{2.1}$$

$$E_{absorbed} = S \cdot (\delta) \cdot (1 - f) \cdot A_{Arctic} - \sum E_{reflected} \tag{2.2}$$

'S' is the solar constant (power per unit area) and is approximately 1366 Wm^{-2}. 'δ' is the solar declination and is averaged between the Autumn Equinox (around September 23) and the Spring equinox (around March 20) and the average declination angle over the Arctic region is approximately 9° [Hartmann, 2016]. Furthermore, an average cloud fraction 'f' of 85% is assumed over the summer months. Using a simple calculation and these estimated values results in 84.4 Wm^{-2} of solar insolation approaching the Earth's surface ($K_s \cdot \delta \cdot (1-f)$). This is in similar range to measurements by Vowinckel & Orvig [1962] and Herman & Curry [1984] and therefore considered plausible. To calculate the reflected and absorbed energy the area 'A' of ice, ocean and land is used in combination with the albedo factor. The Arctic circle contains an area of approximately 16.5·10^6 km^2 of which 2.4·10^6 km^2 is land. The remaining area is a combination of open ocean and ice. The ocean and land albedo are considered constant at 0.06 and 0.78 [Box et al., 2012] respectively. The ice albedo changes throughout the summer as snow melts and melt ponds form and deepen. Based on observations near Barrow, Alaska, Perovich & Polashenski [2012] find the variation of ice albedo as shown in Figure 2.7.

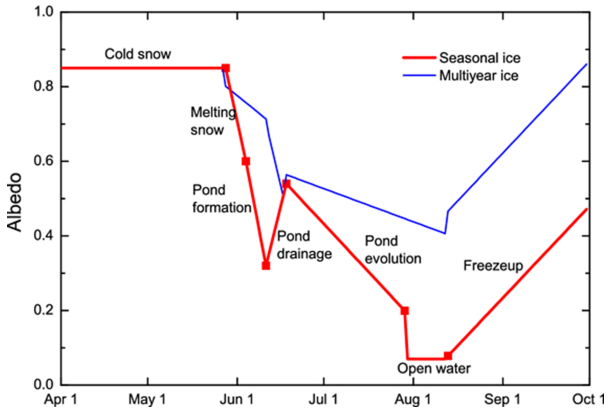

Figure 2.7: Changes in the sea ice albedo over the summer season. Figure as given by Perovich & Polashenski [2012], including the variation of multi-year ice albedo is by Perovich et al. [2007].

Considering the NCAR CCM3 model 21% of local (71°N-90°N) sunlight deflection is necessary to achieve a regional equilibrium in a 560 ppm CO_2 scenario. Instead of reducing the insolation (by for example aerosol injection in the stratosphere [Berdahl et al., 2014]), the ice area can be enlarged to increase the energy reflected. An indication of the necessary ice increase can be determined using Equations 2.1 and 2.2 for the present scenario (considering the average summer ice area during the period 2015-2020 of 7.23·10^6 km^2) compared to a scenario with an increased ice cover. As shown in

Figure 2.7, the ice albedo varies during the season and, therefore the ice increase is determined for an ice albedo of 0.75 and 0.4. An average ice albedo of 0.75 results in a necessary ice increase of $2.7 \cdot 10^6$ km^2 and using an average ice albedo of 0.4 results in $7.0 \cdot 10^6$ km^2 over the April-September average. An indication of the total average summer ice area necessary ranges from $9.9 \cdot 10^6$ km^2 to $14.2 \cdot 10^6$ km^2. The lower bound gives an ice area which already exceeds the average summer ice area at the beginning of satellite records starting in 1979 and the upper bound exceeds the area available in the Arctic circle. For this reason it is questionable if AIM alone can have sufficient regional effect in a 560 PPM CO_2 climate to restore regional temperatures. However, different CO_2 scenarios will influence the results and different solar radiation management techniques and/or negative emission technologies combined can increase the effect.

The desirable effect of AIM is in first place to stabilise and possibly restore (part of) the Arctic ice cover. Based on these simplified calculations and the conclusions made by Zampieri & Goessling [2019], AIM has to stay operable to maintain the ice cover. Otherwise, additional measurements are necessary to maintain the ice cover naturally. Ideally, the future effects of The Paris Agreement can sufficiently contribute to maintaining the ice cover without AIM.

3
The drift of sea ice

Except for ice which is attached to land (known as landfast or fast ice), all ice in the Arctic is in constant motion [Barry et al., 1993]. Whenever the ice is increased using AIM, the natural ice drift can enhance or diminish the effect of AIM. Ice drift can be described by a momentum balance (Section 3.1), but is more generally expressed relative to the geostrophic wind (Section 3.2). Furthermore, there is a remarkable difference when considering short term or long term ice motions. Over the long term, the Arctic knows two main circulation patterns for ice drift, these are described in Section 3.3. Additionally, the phenomena ice export and Atlantification are elaborated in Section 3.4. Finally, the possible effects of ice drift, ice export and Atlantification are discussed in Section 3.5.

3.1. Momentum balance for ice drift

The drift of sea ice can be described by a momentum balance including forces due to air and water stresses, Coriolis force, internal ice stresses, long term geostrophic current effects (often included in the formulation of water stresses) and surface tilt effects [Hibler, 1979].

$$m\frac{D\underline{\mathrm{u}}}{Dt} = -mf\underline{\mathrm{k}} \times \underline{\mathrm{u}} + \tau_a + \tau_w + F - mg\Delta H \tag{3.1}$$

Here 'm' is the mass per unit area, '$\underline{\mathrm{u}}$' is the ice velocity, 'f' the Coriolis parameter, '$\underline{\mathrm{k}}$' a unit vector normal to the ice surface, 'τ_a' the force due to air stress, 'τ_w' the force due to water stress, 'F' denotes the force due to internal ice stresses, 'g' the acceleration due to gravity and 'ΔH' is the sea surface tilt (which can be due to both pressure variations and the geostrophic current [Maykut, 1986]).

The Coriolis force depends on the mass and velocity of the ice floe. In the Northern Hemisphere (NH) the Coriolis acceleration acts 90° (i.e. perpendicular) to the right of the ice motion. The contribution of the Coriolis force is relatively small compared to air and wind stresses and internal friction. The sea surface tilt and possible other accelerations acting on the ice cover are on their turn small compared to the Coriolis force [Leppäranta, 2011]. The internal ice stresses are a result of ice interaction and have a high spatial and temporal dependency. The case of no (or minimal) internal ice stresses is known as 'free drift' [Mcphee, 1980], which is a good approximation for ice fields with low (< 0.8) compactness [Leppäranta, 2011]. A schematic representation of the different forces acting on the ice is shown in Figure 3.1.

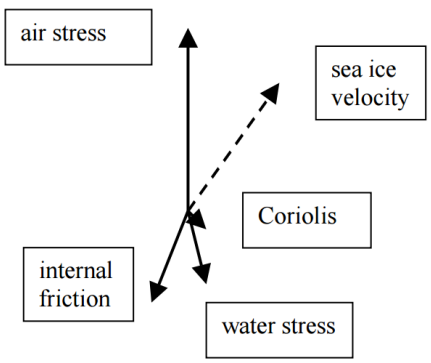

Figure 3.1: A schematic representation of the main forces resulting in ice drift in the Northern Hemisphere [Leppäranta, 2011]

On the time scale of a few days the current effects (in the momentum balance included in the water stresses) are of minor importance. However, when considering the ice drift over a few years, these effects become more significant. This is because the current effects are relatively small, but steady over a long time. While the wind highly fluctuates and averages out in a small mean value over a longer period [Hibler & Tucker, 1979]. Data of the First Global GARP Experiment in 1979 and 1980 shows similar effects. For a short time scale 70% of the ice movement can be explained by the geostrophic wind. For long term scale both the average geostrophic wind and geostrophic current count for half of the ice movement [Thorndike & Colony, 1982].

3.2. Rotation angle and wind factor

Instead of describing the ice motion using the momentum balance, the motion is often expressed relative to wind. During the Fram expedition (1893-1896), it was first noticed that the ice moved approximately 20° to 40° to the right of the surface wind. This phenomenon was explained by Fridtjof Nansen as a result of the rotation of the Earth. Wind affects the surface layer and the surface layer sets the layer below in motion (which is somewhat later than the initial motion of the surface layer it self) and this continues. The deviation increases and causes a spiral formed layer of approximately 100 meter in depth. This phenomena was mathematically confirmed by Ekman [1905] and is now known as the Ekman spiral. The spiral staircase results in a net water transport (Ekman transport) perpendicular to the surface wind velocity. This process is shown schematically in Figure 3.2. As shown in the figure, the surface velocity (surface current) is rotated clockwise (NH) relative to the surface wind. Note here, the geostrophic wind is also rotated clockwise (NH) compared to the surface wind, i.e. theoretically the surface current and geostrophic wind have similar direction. The angle of 45° in Figure 3.2 is mathematically determined under several assumptions, for example: uniform depth, no salinity and density differences creating water motion, no interaction with other ocean-currents and uniform wind direction and speed [Ekman, 1905]. In reality, all assumptions above and others do influence the motion and the angle observed is often found smaller. Nowadays, the ice movement is generally expressed relative to the geostrophic wind (and not the surface wind). The rotation or turning angle is measured clockwise to the geostrophic wind direction. Data shows a rotation angle which is larger in summer than in winter. The angles range between 10° to 20° and -10° to 5° respectively [Maeda et al., 2020; Serreze et al., 1989; Thorndike & Colony, 1982].

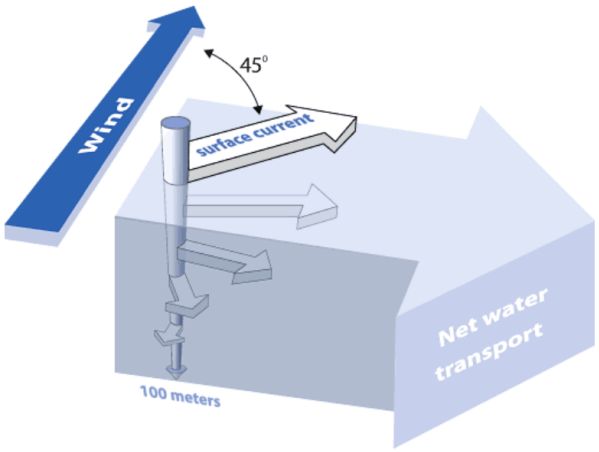

Figure 3.2: The Ekman spiral as a result of the coriolis effect [US Department of Commerce & Administration]

Also the ice velocity is often expressed as a fraction of the geostrophic wind velocity, referred to as the wind factor. Similar to the rotation angle, the wind factor is known to be slightly larger in summer than in winter. The values for the wind factor obtained from in-situ data lie around 1.1% in summer and 0.8% in winter [Serreze et al., 1989; Thorndike & Colony, 1982]. These values are somewhat smaller than the often used 2% rule [Mcphee, 1980], and the obtained range of 1.5 to 2% by Park & Stewart [2016] in an analytical model. Differences are also distinguished by Maeda et al. [2020], who expresses the difference in wind factor for seasonal ice areas (1.5 to 2%) and the central Arctic

(<0.7%). The seasonal and regional differences are expected to be the result of seasonal variation in the atmospheric boundary layer [Thorndike & Colony, 1982] and differences in internal ice stresses, as a result of ice concentration [Park & Stewart, 2016], the effect of the coastline [Thorndike & Colony, 1982] and ice thickness [J. E. Overland & Pease, 1988].

The responsiveness of ice to the wind is increasing, due to the thinning of the ice cover [Kwok et al., 2013; Rampal et al., 2009; Zhang et al., 2012]. More precisely, the changes in ice concentration are the main driver for variations in drift speed during summer and fall (lower concentrations). During winter and the start of Spring, the variations in drift speed are mainly due to ice thickness. April and May do not show a clear correlation between either factor and the variations in drift speed [Olason & Notz, 2014]. Data of the International Arctic Buoy Program shows drift speeds ranging from 9 to 5 km day^{-1} for thicknesses of 2.5 to 3.5 m respectively [Docquier et al., 2017], but no clear trend is presented. In the paper the low spatial variability of the data is expressed, as the speed varies over the Arctic region. Based on the same program, Rampal et al. [2009] shows an increase in the mean speed of the buoys from approximately 6 to 7.5 km day^{-1} for the Central Arctic (1979-2007). Regional variations mainly show an increase in ice speed, when ice approaches Fram Strait with velocities in the range of 4 to 13 km day^{-1} [Emery et al., 1997].

3.3. Main circulation patterns

Over the long term, there are two main wind driven circulation patterns in the Arctic, the Beaufort Gyre and the Transpolar Drift, which are shown in Figure 3.3 [Timmermans & Marshall, 2020]. The Transpolar Drift starts at the Siberian Shelf, flows across the Arctic Basin and through the west side of Fram Strait southwards. The Beaufort Gyre is a rotating motion North of the Canadian coast. Because of this circular flow, the ice can circle within this region for many years. Based on a mean drift speed of 1 to 3 cm s^{-1} (0.9 to 2.5 km day^{-1}), it takes about 5 years to make one round [Thorndike, 1986]. This speed is significantly lower than the previously mentioned speed observed by Rampal et al. [2009], but comparable to the statements by Colony & Thorndike [1985]. This difference might be the effect of thinner ice having an increased response to winds and currents and or enlarged open area increasing the ice motion. The two main currents meet in the Arctic Basin where ice floes mix [Leppäranta, 2011]. Seasonal trends show a stronger Beaufort Gyre during the winter, while in summer the Beaufort Gyre partly occurs over land and an anti-clockwise motion is visible in the Eastern Arctic (not shown) [Rigor et al., 2002].

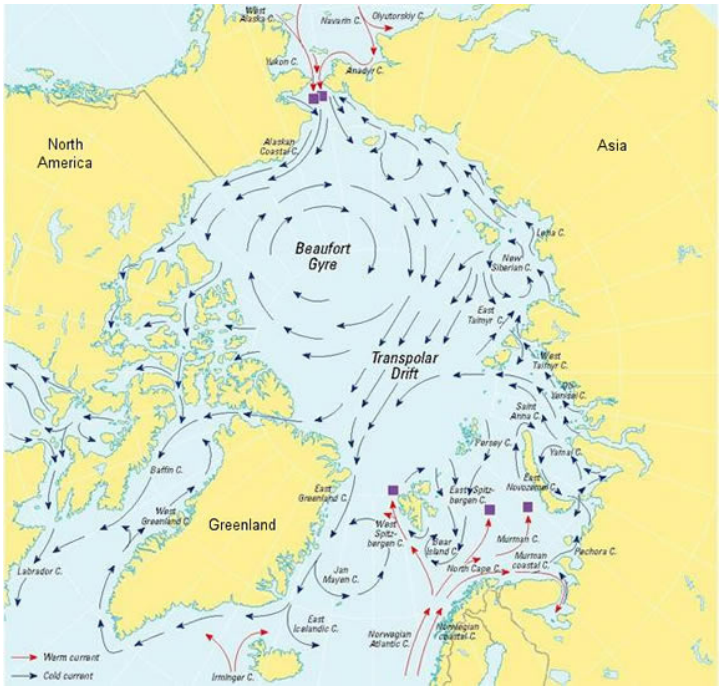

Figure 3.3: Main circulation patterns in the Arctic region [Arctic Monitoring and Assessment Programme (AMAP), 1998]

The Arctic atmospheric circulation is affected by changes in pressure between the Arctic and mid-latitudes known as Arctic Oscillation (AO) [Stockdale et al., 2015; Thompson & Wallace, 1998]. The AO knows two alternating phases, the positive and negative phase as shown in Figure 3.4. In case of a positive phase there is a lower than normal pressure in the Arctic region and a higher than normal pressure in the mid latitudes, creating a large pressure difference. This results in strong westerly winds, and locking the cold air in the Arctic region. In case of the negative phase there is a higher than normal pressure in the Arctic and a lower than normal pressure in the mid-latitudes. The difference between the high and low pressure areas is smaller, resulting in weaker winds and the cold air from the Arctic moves further south [National Snow and Ice Data Center; NOAA Climate.gov]. The alternating frequency for the daily AO index varies between a few days to weeks, while the monthly average AO alternation can be up to several months. This is also visible in data provided by The Climate Prediction Center.

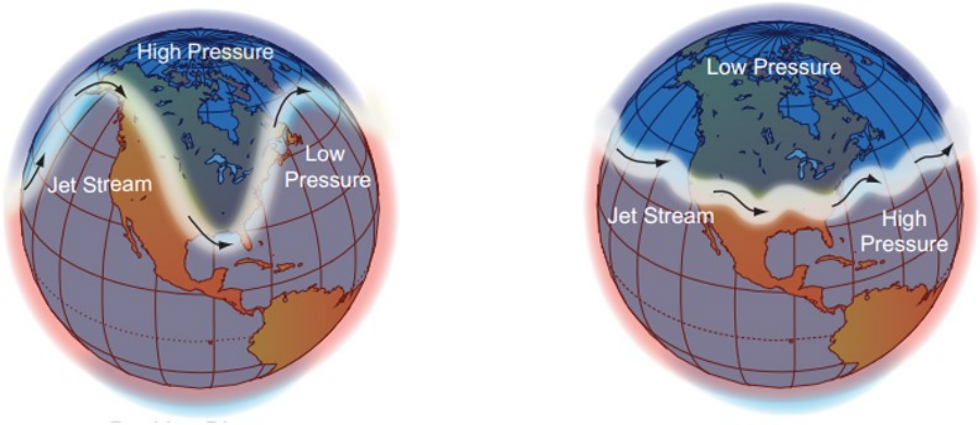

(a) Negative phase **(b)** Positive phase

Figure 3.4: Schematic representation of the Arctic Oscilattion phases [Freeman et al., 2011] (Note: high and low refer to higher and lower than average)

The Beaufort Gyre and Transpolar Drift vary as a result of the AO, as shown in Figure 3.5. The weaker winds during the negative phase (Figure 3.5a), reduce the overall ice motion and strengthen the Beaufort Gyre. The ice leaving through Fram Strait originates from the Beaufort Gyre and is often thick multi-year ice. A positive AO enlarges the Transpolar drift (Figure 3.5b), resulting in more ice leaving the Arctic through Fram Strait. However, most of this ice is young or thin multi-year ice [Hole & Macias-Fauria, 2017; Rigor et al., 2002].

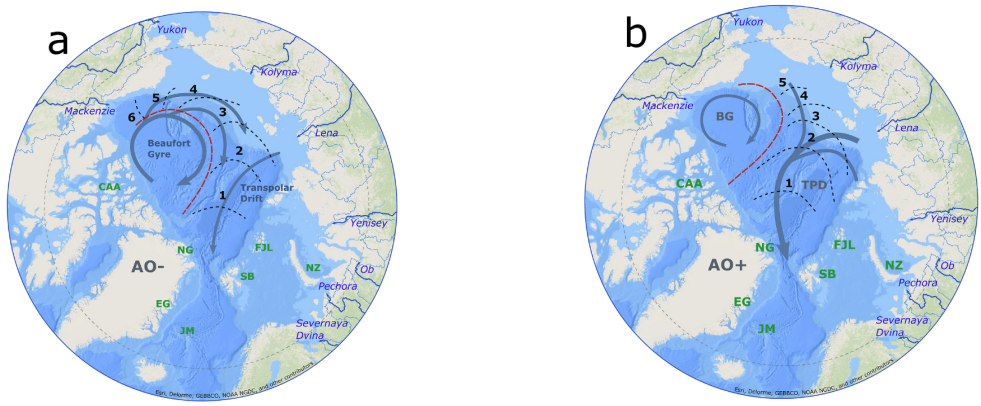

(a) Negative phase **(b)** Positive phase

Figure 3.5: Winter circulations patterns as a result of a negative Arctic oscillation (a) and a positive Arctic oscillation (b). The values indicate the number of years it takes for the ice at a specific location to leave the Arctic through Fram Strait and the red line indicates the region of recirculation in the Beaufort Gyre. (Figure as given by Hole & Macias-Fauria [2017], modified from Rigor et al. [2002].)

The circulation patterns for the Beaufort Gyre and Transpolar Drift shown in Figure 3.5 are long-term flows. When considering daily variations, the surface currents can reverse direction within a few days. This can be seen by data obtained from EUMETSAT SAFs and National Snow and Ice Data Center. The mean daily motion is known to experience large deviations [Colony & Thorndike, 1984]. This fluctuating behaviour can be described as random trajectories and has been modelled using a Markov process by Colony & Thorndike [1985]. The model includes thermodynamic ice decay and ice export through Fram Strait and reproduces or predicts ice particle behaviour. The initial purpose for this model was predicting pollutant transportation routes. However, it offers an opportunity for AIM as well. Possibly in combination with or parallel to ice models, which are discussed in Chapter 5.2.

3.4. Ice export and Atlantification

Every year approximately 10% (average 883 000 km^2 during the period 1935-2014) of the ice cover is exported through Fram Strait into the Greenland Sea [Kwok & Untersteiner, 2011; Smedsrud et al., 2017]. The export through other openings is less significant [Kwok et al., 2009]. Over the years 1979-2014, Smedsrud et al. [2017] found an increase in export of 6% per decade, with some of the later years exceeding 1 million km^2. Again a seasonal trend is distinguished. The summer ice export increases with 11% per decade compared to 2.6% during the winter. However, this increase is in contrast with findings by Spreen et al. [2020] (1992-2014) and Kwok et al. [2013] (1982-2009), who both do not find such an increase in areal export. Spreen et al. [2020] even finds a 27% decrease in ice volume export per decade (average 2 400 km^3). Here, the decreasing ice thickness is an important factor, but not enough to account for the suggested exported areal increase. A possible reason for the difference can be the methods used. The findings by Spreen et al. [2020] are in line with conclusions by Zhang [2021] (earlier mentioned in Chapter 2.2), who found a decrease in volume export of 20% for the 2007-2020 average compared to the 1979-2006 average.

On the same side of the Arctic region, the inflow of warmer (and saltier) currents into the Barents Sea (the Atlantic inflow) are both increasing in strength and temperature, which causes the ”Atlantification” of the Barents Sea [Årthun et al., 2012]. Data show increased penetration of the Atlantic inflow towards the central Arctic [Tesi et al., 2021]. The Atlantification contributes to sea ice decline and reduces ice formation not only in the Barents Sea, but in the Eurasian Basin in general [Polyakov et al., 2017].

3.5. Discussion: Effect of ice drift on AIM

Considering the available literature, sea ice drift is expected to have a significant influence on the location selection and success of AIM. Ice drifting in the Arctic region follows two main circulation patterns: The Beaufort Gyre and the Transpolar Drift. Ice located in the Beaufort Sea follows the Beaufort Gyre for a certain duration and is expected to remain in the Arctic for approximately five to six years. In contrast to ice drifting with the Transpolar Drift, which is generally exported within one to two years. Ideally, the increased ice is transported into the Beaufort Gyre, where it can follow the circular motion for a few years. For similar reasons, the South of the Transpolar Drift near Greenland (Fram Strait) is preferably avoided for AIM implementation. It should be considered that the thinner ice cover can increase the drifting speed and reduce the duration of ice in the Arctic. At the same time, increasing the ice thickness and ice availability can decrease drifting speeds. This reversed phenomena might also occur for ice export. Data has shown a decrease in ice volume export through Fram Strait, increasing the ice thickness might increase the absolute ice volume export as well.

Furthermore, the Barents Sea and possibly regions further into the central Arctic are influenced by Atlantification, which can decrease the effect of AIM. This also indicates the possible negative effects of locations South in the Transpolar Drift.

For exact location selection, the simulation of ice drift including circulation patterns, ice export and warm water inflow is recommended. For this research these aspects are considered, but no simulations on ice drift are included. These simulations are recommended for future work.

4

Survival ice thickness

AIM should increase the ice thickness to a height which is sufficient to withstand the melting season. To determine this survival ice thickness, the ice decay during the melting season should be estimated. Ice decay models are not frequently derived. The existing methods are described in Section 4.1 and based on these methods, ice decay is analysed using an analytical approach in Section 4.2. Furthermore, calculating ice decay using a location dependent empirical approach is discussed in Section 4.3. Finally, Section 4.4 combines these findings to determine regional survival ice thicknesses.

4.1. Existing methods for ice decay

It is possible to define an analytical relation for ice decay by looking at the surface heat balance. The balance of the upper boundary is defined by incoming and outgoing energy fluxes and determines if ice is either growing or melting. The energy balance as derived by Maykut & Untersteiner [1971] is used. They define the main energy fluxes as incoming long-wave radiation 'F_L', incoming short-wave radiation 'F_r' (minus the fraction reflected by the ice/snow cover, which is defined by the albedo coefficient 'a') and outgoing long-wave radiation '$\epsilon_L \sigma T_s^4$'. Also contributing, but of smaller importance, are sensible heat 'F_s', latent heat 'F_l', heat conduction in the ice (or snow) as a function of the thermal conductivity 'k_i' and radiative energy penetrating into the ice 'I_o'. The sum of these energy fluxes is either zero during ice growth or non-zero during ice decay. In the latter, the surplus of energy to the surface is used to melt the ice at the upper boundary. To account for this, they include an additional term defining the heat absorbed due to melting resulting in an upper boundary balance equation:

$$\begin{aligned}(1-a)F_r - I_o + F_{L,in} - F_{L,out} + F_s + F_l + k_i \cdot (\frac{\delta T}{\delta z})_o = 0 \text{ if } T_o < 0\ ^\circ\text{C} \\ = -[\rho_i l_i \frac{d}{dt}(h+H)]_o \text{ if } T_o = 0\ ^\circ\text{C}\end{aligned} \tag{4.1}$$

The decrease in ice thickness due to the surplus of energy is determined as a function of the ice density 'ρ_i' and the latent heat of ice 'l_i'. Furthermore, the outgoing longwave radiation exceeds the incoming longwave radiation throughout the year. This causes the net longwave radiation to extract energy from the ice. During the summer, the net longwave losses are at a minimum, because the radiative temperature of the atmosphere and the ice surface are similar. For this reason, shortwave radiation dominates the energy balance [Maykut, 1986].

A different approach is used for the analytical relation introduced by Desch et al. [2017]. Instead of using shortwave and longwave radiation, Desch et al. [2017] defines ice decay as a result of insolation and contact with warm air:

$$-\rho_i l_i \frac{\Delta h}{\Delta t} = S_i(1-a)(1-f) + C_t(T - 273K) \tag{4.2}$$

The insolation 'S_i' depends on both local latitude and declination of the sun and is comparable to the shortwave radiation used by Maykut & Untersteiner [1971]. Included in the formula is the cloud coverage 'f' and reflected insolation due to the surface albedo 'a'. The changing albedo is accounted for, but is simplified to an abrupt change from 0.75 to 0.30 at the end of June. Furthermore, the heat exchange between the surface and atmosphere is included using a heat transfer coefficient 'C_t'. Desch et al. [2017] state the ice decay is dominated by insolation over air temperature, which is similar to the statement by Maykut [1986]. However, the order difference is not enough to eliminate air temperature

from the balance. Interesting are the regression analysis by Bilello [1980] (lake and sea ice) and derivation by Ashton [1983] (lake ice), who define the air temperature as a better independent variable to define ice decay than incoming solar radiation. Bilello [1980] mentions a possible improvement when both insolation and air temperatures are included in a regression analysis, but due to a lack of data this method was insufficient for conclusions.

Besides the upper boundary equation, there is a balance at the bottom of the ice cover. Bottom accretion or ablation is defined as a balance between conductive heat flux and the oceanic heat flux [Maykut & Untersteiner, 1971]. In analytical ice growth expressions, the oceanic heat flux is often neglected. However, for ice decay, Lin & Zhao [2019] have analyzed data of ice mass balance (IMB) buoys over 2004-2013 and concluded the oceanic heat flux was responsible for an average bottom melt of 0.4 m over the Summer. During the melting season the oceanic heat flux is mainly caused by insolation reaching open water. This indicates the oceanic heat flux might have an important contribution to ice decay.

Alternatively, an empirical fit can provide insights in the process of melting ice. However, melting ice is not often analysed. One empirical fit by Bilello [1961] gives

$$\Delta h = 0.55TDD \tag{4.3}$$

Where, 'Δh' is the decrease in thickness given in centimeters and 'TDD' (Thawing Degree Days) are the accumulated degree days above the freezing temperature. As explained by Maykut [1986], this fit is based on near shore data and it is unsure if this relation is applicable for further offshore ice decay.

Due to this uncertainty, the empirical fit by Bilello [1961] is not considered to calculate ice decay. The analytical formula based on the surface heat balance as shown in Equations 4.1 and 4.2 contain both air temperature and insolation, which is necessary for adequate results. The derivation by Maykut [1986] includes all heat fluxes and will be used for further analysis. The derivations highly depends on several variables (depending on time, location, weather conditions and ice conditions) and Desch et al. [2017] tunes the derivation for one specific location. To analyse the optimal location for AIM, location specific results are of interest and the many variables can make this time consuming. Therefore, it is of interest if the balance by Maykut [1986] can be simplified to reduce the number of variables. Additionally, including the effect of the oceanic heat flux should be considered.

4.2. Ice decay using the energy balance method

Before analysing the possibility to simplify the energy balance, the surface heat balance as derived by Maykut & Untersteiner [1971] should be validated with available data. Equation 4.1 is simplified to the main energy fluxes and is only considered for temperatures above the melting temperature. Since most of the brine is rejected from the ice, the melting temperature is assumed to be similar to the melting temperature of fresh ice (0 °C). The following simplified formula is considered for ice decay:

$$(1-a)\cdot F_r + F_{L,in} - F_{L,out} = -\left[\rho_i l_i \frac{d}{dt}(h+H)\right]_o \tag{4.4}$$

The paper written by Maykut & Untersteiner [1971] uses observational data of long- and shortwave radiation by Fletcher [1965] in combination with Equation 4.1 to estimate ice decay and this results in accurate predictions. In this paper the energy fluxes are calculated using common data (air temperature, ice thickness and snow thickness) obtained by '*The CRREL-Dartmouth Mass Balance Buoy Program*' (IMB buoy program).

Shortwave radiation: The incoming shortwave radiation is determined by insolation and is a function of the solar constant 'S', cloud fraction 'f', vapour content 'e_{air}' and zenith angle 'Z' (subsequently a function of latitude 'ϕ', solar declination 'δ' and day of year 'd'). Truly, the zenith angle also has a contribution dependent on the hour angle '$cos(hr)$'. Since the time interval considered for ice decay is a few months and the contribution of the hour angle averages out over 24 hours, this term is neglected. The incoming shortwave radiation is calculated using the following formulae:

$$\delta = -23.45 \cdot cos\left(\frac{360}{365.25}\cdot(d+10)\right) \tag{4.5}$$

$$cos(Z) = sin(\delta)sin(\phi) \tag{4.6}$$

$$F_r = \frac{S \cdot cos(Z)^2}{1.085 \cdot cos(Z) + (2.7 + cos(Z)) \cdot e_{air} \cdot 10^{-3} + 0.1} \tag{4.7}$$

To obtain the shortwave radiation, the day of year and latitude are obtained from the IMB program and vary with each measurement. Constant values are used for the other variables. An overview of the input values is shown in Table 4.1.

Not all of the shortwave radiation contributes to the surface energy balance. First of all, the presence of clouds prevents part of the shortwave radiation from reaching the ice surface. The reflectivity (cloud albedo) is estimated at '$0.6f^3$' as suggested by Laevastu [1960] and calculated to be within 10% of observed data at latitudes between 70 to 90°N for the months May-September [Maykut, 1986]. Secondly, part of the shortwave radiation which reaches the ice surface is reflected. The proportion reflected is determined by the albedo coefficient, which changes during the summer season. To determine the reflected shortwave radiation, the albedo evolution as shown in Figure 2.7 is included. This results in the following formula to calculate the incoming shortwave radiation contributing to the energy balance:

$$F_{r,in} = F_r \cdot (1 - 0.6f^3)(1 - a) \tag{4.8}$$

Longwave radiation: Both incoming and outgoing longwave radiation express the radiative energy of the atmosphere and ice surface respectively. The longwave radiation can be calculated as a function of the Stefan-Boltzman constant 'σ', emissivity 'ϵ' and temperature 'T' of the concerning material in °C. The radiative energy is obtained by the following formula:

$$F_L = \epsilon \cdot \sigma \cdot (T + 273)^4 \tag{4.9}$$

The incoming longwave radiation is determined by the properties of the atmosphere. The emissivity is a function of the cloud fraction and can be calculated as $\epsilon = 0.7855 \cdot (1 + 0.2232 \cdot f^{2.75})$. The temperature used to calculate the longwave radiation is the air temperature (generally measured at a height of 2 m). For the outgoing longwave radiation, the properties of the ice surface are used. Ice has an emissivity close to one and the ice surface temperature is assumed to equal the melting temperature during the melting process. Before the melting process starts, the surface temperature is obtained from the IMB buoy program as the temperature measured at 0 m, which is positioned at the original ice surface.

Oceanic heat flux: Besides the upper boundary balance, there is a boundary balance at the ice-ocean interface where the oceanic heat flux causes bottom ablation. For the calculations of ice decay, the oceanic heat flux is included according to the values derived by Lin & Zhao [2019]: $F_w = 16.8$ W m^{-2} in the Beaufort Sea and $F_w = 7.7$ W m^{-2} in the Transpolar Drift.

Table 4.1: Input parameters for analytical ice decay calculations

Parameter	Symbol	Value
Density ice	ρ_i	917 kg m^{-3}
Latent heat ice	l_i	3.34· 10^5 J kg^{-1}
Day of year	d	Obtained from IMB
Latitude	ϕ	Obtained from IMB
Solar constant	S	1366 W m^{-2}
Vapour content	e_{air}	1.5 mb
Cloud fraction	f	[0.75-0.95]
Temperature air	T_a	Obtained from IMB
Temperature ice surface	T_o	Obtained from IMB if $T_o > 0$ °C 0 °C otherwise
Emissivity air	ϵ_{air}	0.7855· (1+0.2232· f$^{2.75}$)
Emissivity ice	ϵ_{ice}	[0.95 1]
Stefan-Boltzman constant	σ	5.670· 10^{-8} W m^{-2}K^{-4}

The data indicate the ice starts to melt when the snow layer has melted. For this reason, a 'snow buffer' of 2 cm, which results in the best fit, is included in the calculations. The ice surface is assumed to start melting once the energy balance results in a surplus of energy and the thickness of the snow layer is below the snow buffer. Furthermore, when the atmospheric temperature exceeds the melting temperature, ice bottom ablation is accounted for. The energy balance is used to calculate the ice decay and this is compared to data obtained by the IMB buoy program. At first, all available data sets covering ice melt and defined as FYI are assembled. Implementing the data of each buoy and parameters as defined in Table 4.1 in Equation 4.1 results in Figure 4.1. The figure shows resemblance for the measurements and calculated ice decay in Figures 4.1b, 4.1d and 4.1e. For Figures 4.1a and 4.1c, the calculated ice decay overestimates the actual ice decay. However, the course of the ice decay is similar for the data and calculated decay.

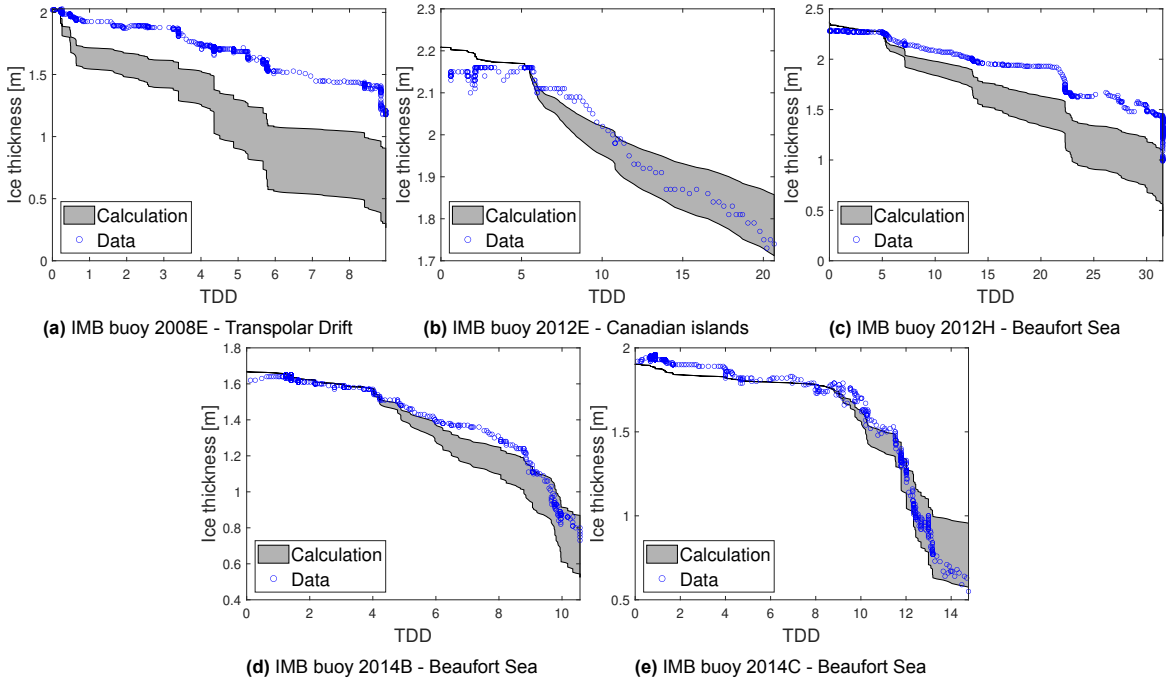

(a) IMB buoy 2008E - Transpolar Drift **(b)** IMB buoy 2012E - Canadian islands **(c)** IMB buoy 2012H - Beaufort Sea

(d) IMB buoy 2014B - Beaufort Sea **(e)** IMB buoy 2014C - Beaufort Sea

Figure 4.1: Ice decay based on the upper boundary energy balance for FYI

To explore if there is a relation between the ice location and ice decay, additional data sets defined as MYI for both locations are analysed. Figure 4.2 shows the selected buoys in the Beaufort Sea. The simulations show accurate results with the measurements for each buoy. This in contrast with Figure 4.3, which represents buoys moving with the Transpolar Drift from the central Arctic south towards Fram Strait. This suggests the energy balance method can estimate the ice decay in the Beaufort Sea, but generally overestimates the ice decay in the Transpolar Drift. A possible reason for the overestimation for ice in the Transpolar Drift is the varying snow conditions. The ice in the Beaufort Sea generally melts under snow free conditions, whereas data show increased snow conditions for the ice in the Transpolar Drift. The calculations only include the snow conditions to define initial ice melt, but snow fall during the summer season is not accounted for. Snow fall during the summer can result in an increase in cloud fraction and a fresh protective layer on top of the ice, which is expected to slow down the ice melt. However, to what extent it slows down the melt is unclear.

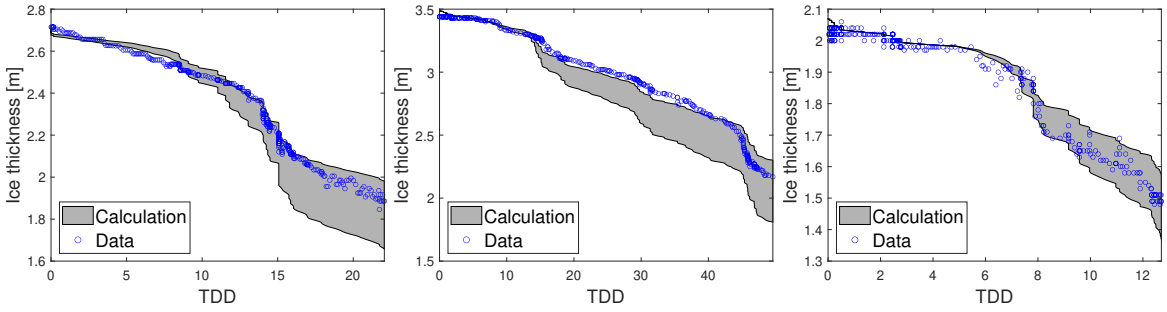

(a) IMB buoy 2007B **(b)** IMB buoy 2012L **(c)** IMB buoy 2015F

Figure 4.2: Ice decay based on the upper boundary energy balance for MYI in the Beaufort Sea

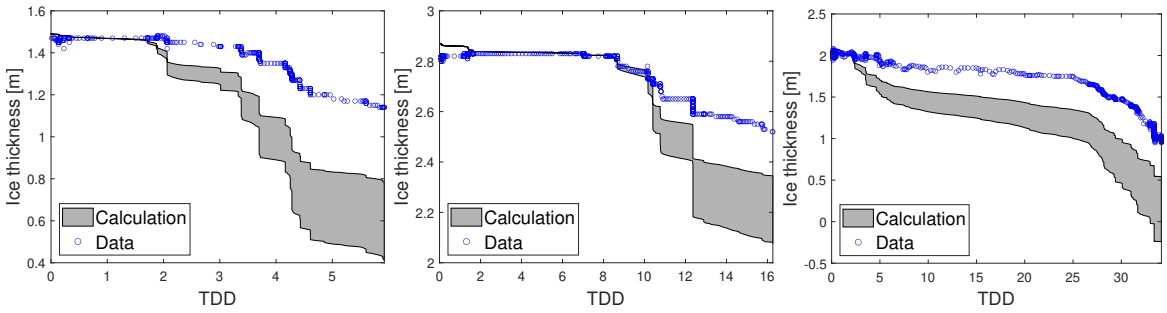

(a) IMB buoy 2007D **(b)** IMB buoy 2008C **(c)** IMB buoy 2015D

Figure 4.3: Ice decay based on the upper boundary energy balance for MYI in the Transpolar Drift

Figures 4.1, 4.2 and 4.3 indicate that the course of ice decay can be predicted using the energy balance method. However, the prediction of the exact ice decay is only representative in the Beaufort Sea. Furthermore, the main downside for this method is the data required for the calculations. The ice decay is defined using thawing degree days, but the simulations do not show a clear trend among the buoys in the Beaufort Sea. This indicates a precise prediction of the air temperature and snow conditions for each individual day during the melting season is required to make a representative prediction for the ice decay. For this reason the accuracy is questioned, and an empirical approach without the need for precise weather predictions is analysed in Section 4.3.

4.3. Ice decay using an empirical approach

Maykut & Untersteiner [1971] and Desch et al. [2017] suggest that ice decay is dominated by insolation (shortwave radiation). In that case, the position of the sun relative to the desired location has a fundamental role in determining the ice decay. Equation 4.6 shows the relative position of the sun subsequently depends on the day of year and latitude of the required location. Again, the IMB Program is used and all usable data sets between 2006 and 2016 are included to examine if there is a clear relation between the latitude and ice decay.

First of all, the start of the ice melt is determined. When considering the available data sets, there is not one general moment when ice starts to melt. The main factors influencing the initial melt are insolation, air temperature and snow depth. First the snow layer melts away, after which the ice layer starts to decrease at the upper boundary. For this reason, ice decay is considered to occur when the snow layer has disappeared. Comparing this to the data gives accurate resemblance except for buoys 2012G, 2012J, 2013A, 2013F and 2015E. For these buoys, the snow layer does not entirely disappear over the summer. To include these buoys in the analysis, the initial ice decay is determined by examining the plotted ice decay data and initial melt is inserted manually. Secondly, the end of ice melt needs to be included. The end of the melting period can be recognized by the ice thickness not decreasing any longer. However, most of the available data sets do not reach this point, instead the measurements stop somewhere during the melting process. For the data sets that do exceed the melting period, the final measurements that are within two centimeters from the minimum measured

ice thickness are removed. This limit is chosen to account for minor variations in the measurements and is only applied on data sets exceeding the melting duration. To indicate the locations during the measurements, the track of each buoy during the melting season is illustrated in Figure 4.4.

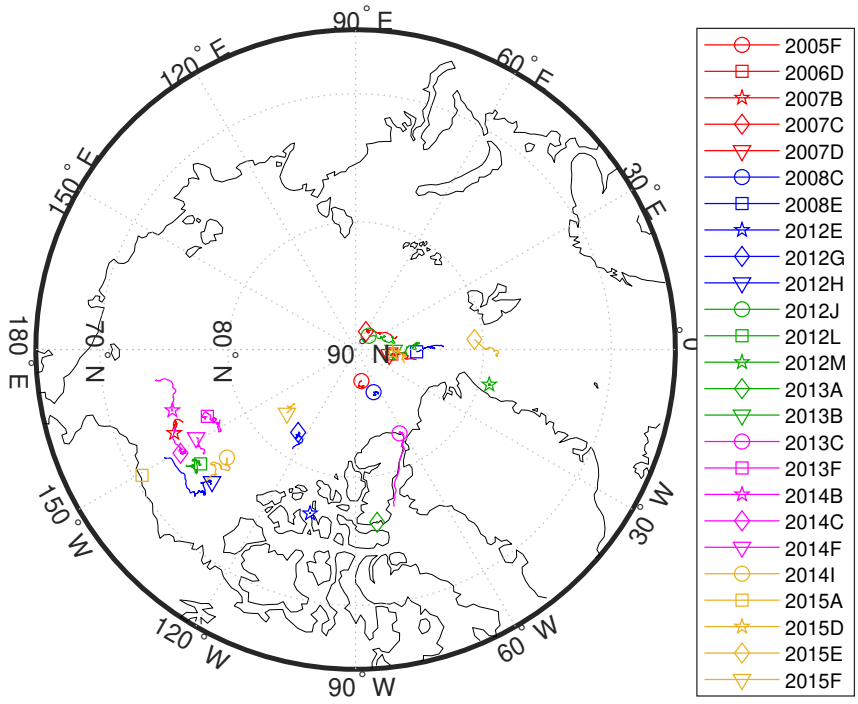

Figure 4.4: The movement of each buoy during the recorded melting data

For the analyses of ice decay, two locations are considered: The Beaufort Sea and the Transpolar Drift. To investigate the possible relation with latitude, the figure shows the movements during the melting process. Buoys 2012E, 2012M, 2013A, 2013C and 2015A are not included in the analyses, because they are either too close to land or not within the region of interest.

In contrast to Section 4.2, the ice decay is now evaluated relative to the day of year instead of TDD. The data set for buoys 2013B and 2006D contain deviating measurements and are eliminated for further calculations. The ice thicknesses for the Beaufort Sea and Transpolar Drift are shown in Figure 4.5a and 4.5b respectively. The figures also include the development of the ice thickness prior to melting and enlarged markers indicate the initial and final moment of ice decay. For each buoy the duration of ice decay is retained and a linear trend line based on the least-squares method is fitted through the data points, resulting in Figures 4.6a and 4.7a. To compare the ice decay, the trend lines are combined in Figures 4.6b and 4.7b for the Beaufort Sea and Transpolar drift respectively.

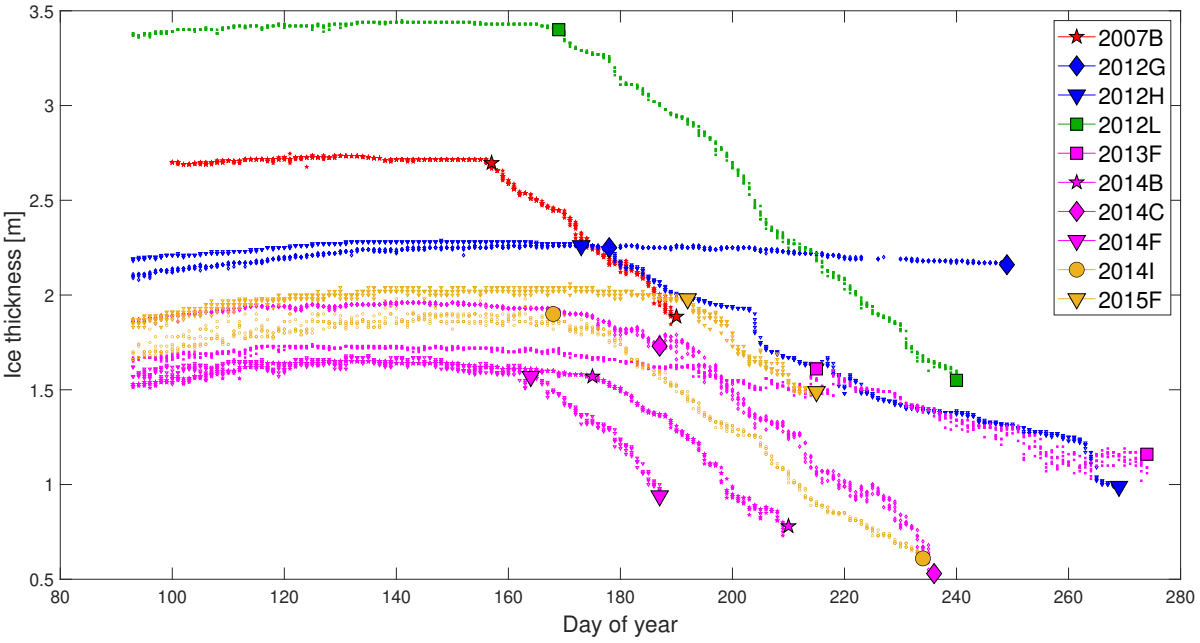

(a) Ice decay in the Beaufort Sea

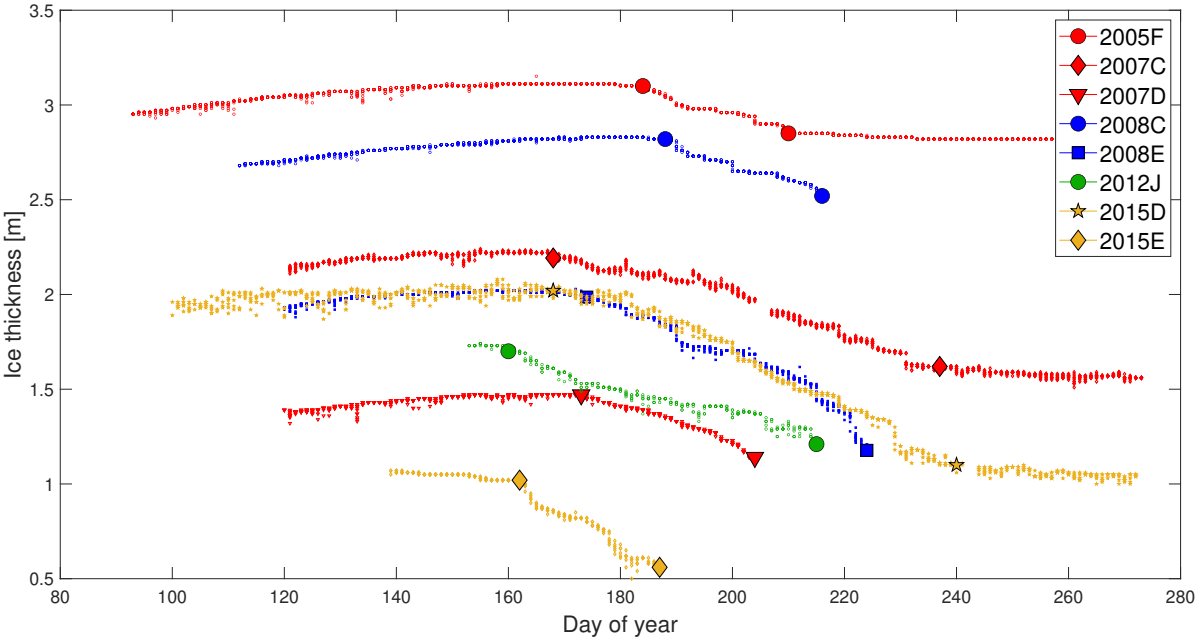

(b) Ice decay in the Transpolar Drift

Figure 4.5: Raw data of the ice decay relative to the day of year

When comparing the ice decay processes in the Beaufort Sea a trend is recognisable. Figure 4.6b shows comparable trends with a gradient between -2.1 and -2.7 cm day^{-1}. The data indicates that only three buoys do not match this resemblance: 2012G, 2012H, 2013F. As mentioned earlier, the snow layers for 2012G and 2013F do not fully disappear and a snow layer between approximately 0.05 m and 0.1 m remains throughout the melting process. For 2012H, the beginning of ice decay is defined for a snow layer reaching 0 m. However, the second half of the melting process shows the formation of a new snow layer. When analysing only the ice decay section without a snow layer, the gradient increases slightly to -1.6 cm day^{-1}, which still deviates from the general trend. Besides the snowfall, the course of the ice decay behaves differently compared to the course of other buoys, which might cause the ice decay gradient to be more gradual. Based on these findings, a gradient between -2.1 and -2.7 cm day^{-1} is considered a valid approximation for ice decay in the Beaufort Sea.

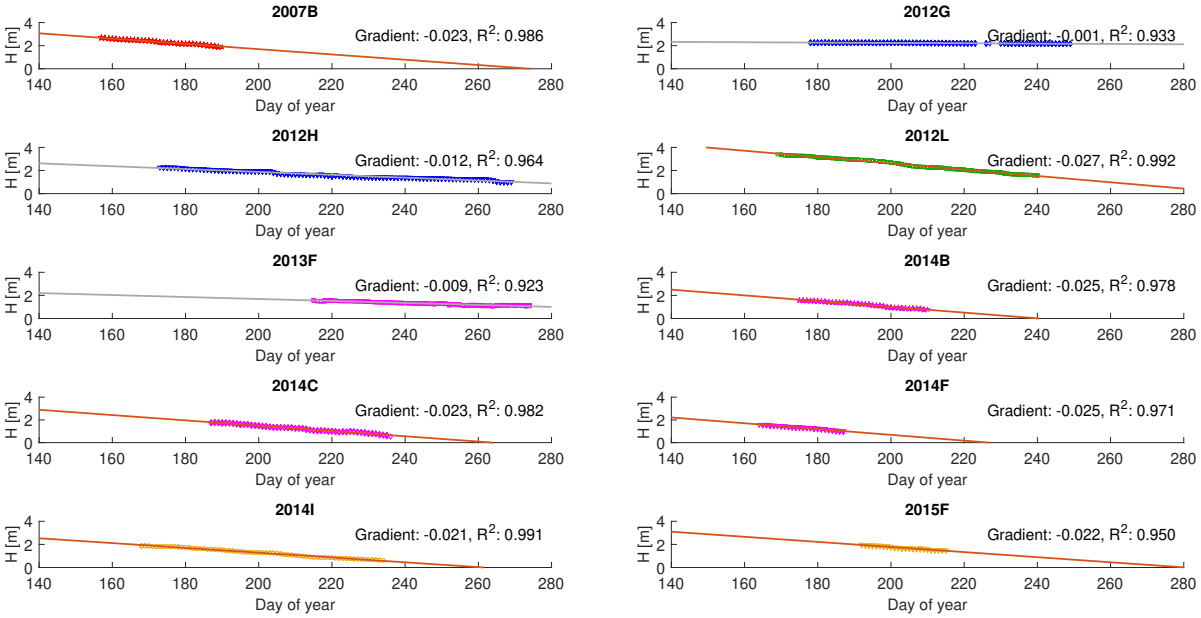

(a) Ice decay data with trendlines

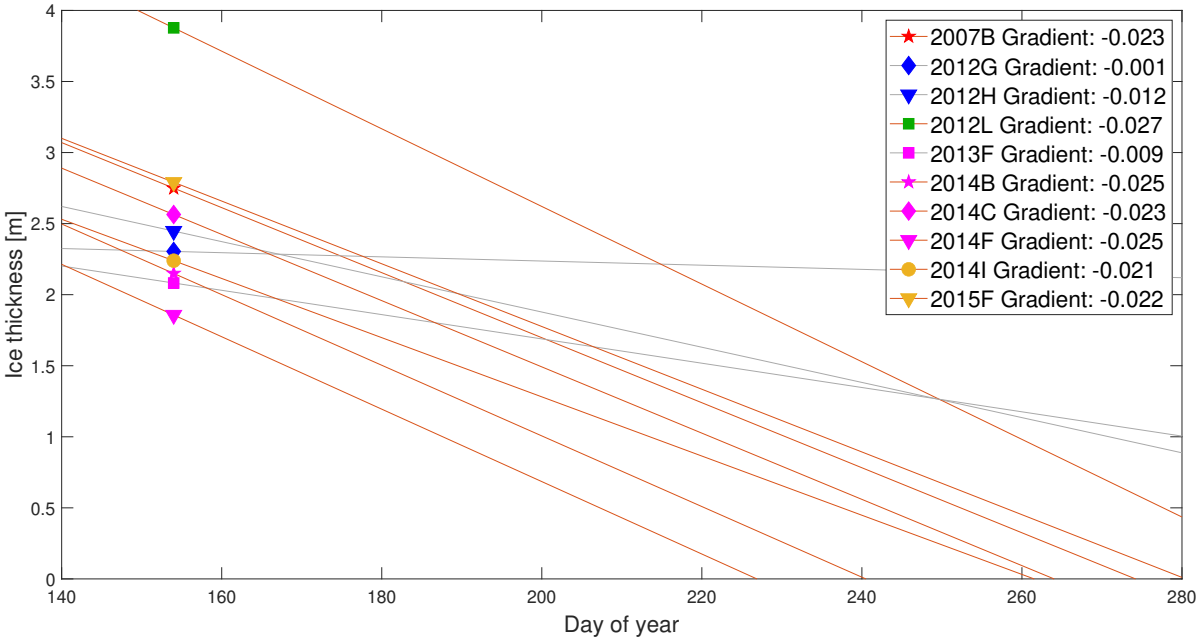

(b) Comparison between trendlines

Figure 4.6: Ice decay analysis for the Beaufort Sea

Similarly, Figure 4.7 indicates a trend for ice in the Transpolar Drift. At first sight, there are three buoys following a slightly steeper trend: 2008E, 2015D and 2015E. Buoy 2015E is relatively far south compared to the other buoys in this region, which can be an explanation for the increased ice decay. For buoys 2008E and 2015D, the data examined does not show a clear explanation for the steeper trend. In contrast to the buoys in the Beaufort Sea, the snow conditions for the buoys in the Transpolar Drift vary throughout the summer. As mentioned earlier, buoy 2015E and 2012J have a continuous snow layer throughout the measurements. For buoys 2005F, 2008C and 2008E, the snow layer disappears, but there is snow fall during the melting process. The three remaining buoys, 2007C, 2007D and 2015D experience ice decay under snow free conditions. These various conditions do not show proportionate effects on the ice decay and the trend shows good resemblance for all conditions. The largest deviating circumstances occur for 2015E due to its latitude and 2012J due to a minimum snow thickness of 0.15 m. Eliminating these buoys results in an expected ice decay gradient between -0.8 and -1.4 cm day^{-1}.

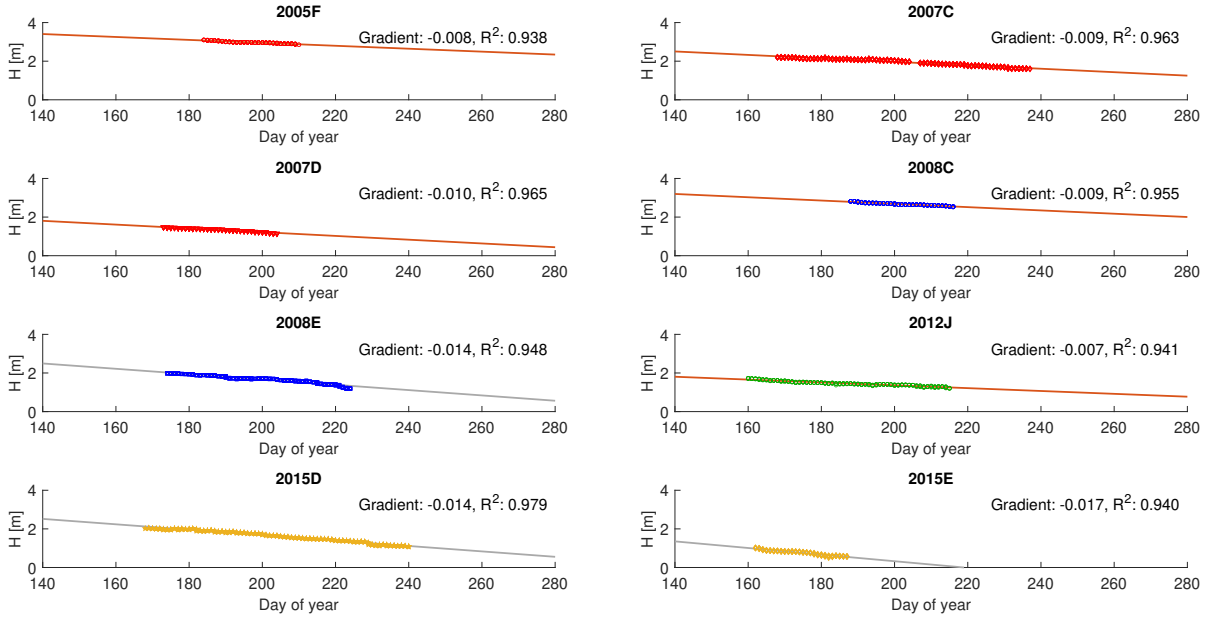

(a) Ice decay data with trendlines

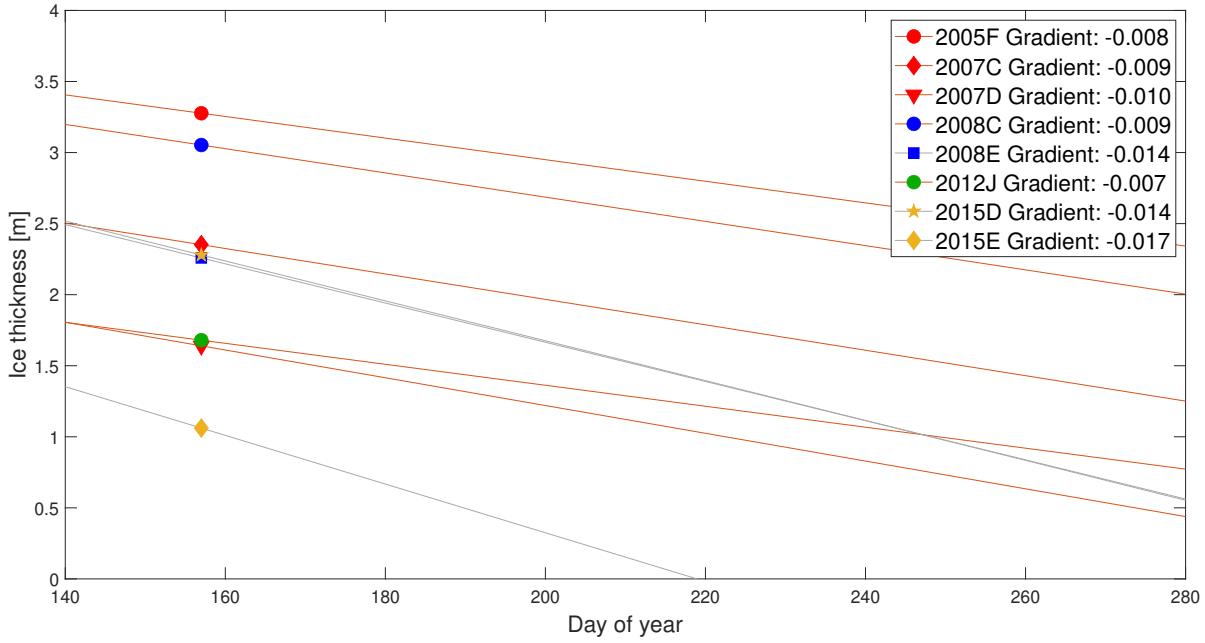

(b) Comparison between trendlines

Figure 4.7: Ice decay analysis for the Transpolar Drift

Comparing both regions, the buoys positioned in the Beaufort Sea experience faster ice decay (-2.1 to -2.7 cm day^{-1}) than the buoys located in the Transpolar Drift (-0.8 to -1.4 cm day^{-1}). Three possible reasons for this are the latitude, oceanic heat flux and snow conditions. First of all, the buoys analysed in the Transpolar Drift are between 85 and 90 °N, while the buoys in the Beaufort Sea are further South (on average approximately 75°N). Ice located southward experiences more insolation, resulting in increased ice decay. Secondly, the oceanic heat flux is different for both regions. Based on the IMB data, Lin & Zhao [2019] determined an average oceanic heat flux of 16.8 W m^2 for the Beaufort Sea and 7.7 W m^2 for the Transpolar Drift. This indicates the bottom melt in the Beaufort Sea exceeds the bottom melt in the Transpolar Drift. At last, the varying but generally increased snow conditions in the Transpolar Drift can result in less ice decay compared to the Beaufort Sea.

4.4. Discussion: Determining the survival ice thickness

The energy balance method has shown accurate results for ice decay in the Beaufort Sea. However, the method overestimates ice decay in the Transpolar Drift. Additionally, the number of detailed parameters needed to use this method question the usefulness for predictions in the future.

Instead, an empirical fit based on the day of year, and consequently insolation, shows presentable ice decay trends and a clear difference for ice decay in the Beaufort Sea (-2.1 to -2.7 cm day^{-1}) and the Transpolar Drift (-0.8 to -1.4 cm day^{-1}). Considering this, the only required parameter to determine the survival ice thickness is the number of expected melting days. These trends are considered reliable for ice thicknesses of 0.5 m and above. The trends can suit thinner ice, however, this can not be confirmed as data of ice thicknesses below 0.5 m are not available in the database.

Considering the trend obtained and insolation being the dominating factor, the maximum days of ice decay depends on the solar equinox. The vernal or spring equinox takes places around March 20 (79^{th} day of the year) and the autumnal or fall equinox occurs around September 23 (266^{th} day of the year). This results in a maximum of 187 melting days. However, Figure 4.5 shows the earliest ice decay is reported on the 157^{th} day of the year (buoy 2007B) and on average the ice decay starts on day 175. The data suggests the ice in the Transpolar Drift starts slightly earlier, but no significant difference is shown and the average of 175 days is considered for both locations. Since most of the data sets do not cover the complete melting season, the final day of ice decay cannot be obtained from the data. For this reason, the autumnal equinox is considered as the final day of ice decay. The few buoys that do cover the entire melting season, generally stop a few days earlier. For this reason, this assumption might overestimate the number melting days. Using the earliest measurement of ice decay results in a maximum of 109 melting days and based on the average initial ice decay there are 91 melting days. The average initial ice decay is considered for further calculations, which results in a survival ice thickness between 1.91 and 2.46 m for the Beaufort Sea and between 0.73 and 1.27 m for the Transpolar Drift.

5
Natural sea ice growth

The necessity and requirements of AIM depend on the natural ice growth. First of all, the theory of natural ice growth and existing models are discussed in Section 5.1. This is followed by the current ice availability in Section 5.2. Finally, the effect of the natural ice growth process on AIM is discussed in Section 5.3.

5.1. Ice growth models

The theory describing ice growth was developed as early as 1891 by Stefan [1891] and is still widely used as the basis for developing analytical ice growth models. Section 5.1.1 discusses this theory and compares several existing models. Secondly, ice growth is not linear over time and the effective increase of AIM is expected to depend on the initial ice conditions. For this reason the ice growth rate is discussed in Section 5.1.2. Finally, to determine the need for AIM depends on the feasible ice growth during one winter and this is discussed in Section 5.1.3.

5.1.1. Stefan's law

When the air temperature is below the freezing point of water (values between -1.6 to -1.8 °C are generally used for sea water) ice starts to form at the ocean surface. After the initial ice formation, the upper surface of the ice layer is colder than the ice at the ice-water interface. This results in upward heat conduction. Heat is extracted from the water underneath the ice and freezes, the heat is transported through the ice and released at the ice-atmosphere interface. This is the principle behind Stefan's law, which is a simple one-dimensional model to estimate the ice thickness based on air temperatures. Stefan's law uses several assumptions, of which the mostly discussed are:

1. No snow on top of the ice
2. No heat flux from the ocean ($q_{ocean} = 0$)
3. The ice surface temperature equals the atmospheric temperature ($T_o = T_a$)
4. A linear temperature profile through the ice
5. The latent heat equals the heat flux through the ice and atmosphere ($q_{lat} = q_{ice} = q_{surface}$)

The model and the assumptions are visualised in Figure 5.1. In adapted ice growth models, some of these assumptions are included and others remain assumed.

In Stefan's law the heat conduction and latent heat are balanced. The heat conduction through the ice can be described using Fourier's law:

$$q_x = -k\frac{dT}{dx} \tag{5.1}$$

When considering thin ice, the temperature gradient in the ice cover is expected to be linear (Assumption 4). Using Fourier's law, this gives the following equation for the thermal heat conduction:

$$q_c = \frac{k_i}{h}(T_o - T_f) \tag{5.2}$$

Where 'h' is the ice thickness, 'T_o' is the surface temperature and 'T_f' is the freezing temperature of sea water. When ice grows, latent heat is released and transported to the surface. The latent heat balances the heat flux from the ocean and the heat conducted through the ice (Assumption 5):

$$-\rho_i l_i \frac{dh}{dt} = q_c + q_{ocean} \tag{5.3}$$

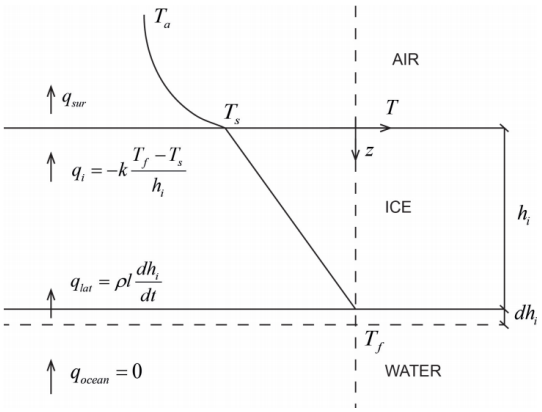

Figure 5.1: Illustration of the assumptions behind Stefan's law [Høyland, 2021]

Considering the other assumptions made in Stefan's law: First, the oceanic heat flux is considered negligible (Assumption 2). Secondly, it is assumed that the surface temperature (as mentioned in Equation 5.2) is equal to the atmospheric temperature 'T_a' (Assumption 3). This results in the following expression for ice thickness:

$$H = \sqrt{\frac{2k_i}{\rho_i l_i}\alpha FDD} \tag{5.4}$$

'FDD' refers to Freezing Degree Days, which is the cumulative sum of the degree days below the freezing temperature over a certain period of time ($FDD = \int_0^t (T_s - T_f)dt$). To convert FDD from days to seconds the factor $\alpha = 86400$ is used.

It is unrealistic to assume the surface temperature equal to the atmospheric temperature. The surface temperature can be warmer than the atmospheric temperature and a heat transfer coefficient is used to take this into account.

$$q_t = C_t(T_a - T_o) \tag{5.5}$$

'C_t' describes both sensible heat exchange and latent heat exchange. Substituting this expression for 'T_o' and solving Equation 5.3 gives the following expression for the ice thickness:

$$H^2 + \frac{2k_i}{C_t}H = \frac{2k_i}{\rho_i l_i}FDD \tag{5.6}$$

The actual ice growth will be slower than expressed in Equation 5.6, one of the reasons for this is a snow cover on top of the ice. Snow insulates the ice, which decreases the ice growth. A snow layer 'h_s' can be included in the analytical expression mentioned above:

$$H^2 + \left(\frac{2k_i}{k_s}h_s + \frac{2k_i}{C_t}\right)H = \frac{2k_i}{\rho_i l_i}FDD \tag{5.7}$$

Maykut [1986] compares this analytical derivation to empirical relations between ice thickness and FDD by Anderson [1961] and Lebedev [1938]. He concludes a 5 cm snow thickness results in the best fit.

Based on the same principle Desch et al. [2017] derived a formula for the ice thickness with the purpose to easily determine the additional ice thickness after AIM. A modification is made concerning the thermal conductivity of ice. In this derivation the thermal conductivity depends on the ice thickness as described by Trodahl et al. [2001]. Different thermal conductivities are used for ice above and below $x_0 = 0.5$ m. In this derivation Desch et al. [2017] assumes the surface temperature equals the atmospheric temperature and chooses the snow thickness to match the earlier mentioned empirical formula by Lebedev [1938]. This coincides with a snow layer of approximately 8 mm and results in the following expression:

$$H(FDD) = -0.533 + 0.5\left(\frac{FDD}{221.2} + 1.364\right)^{1/2} \tag{5.8}$$

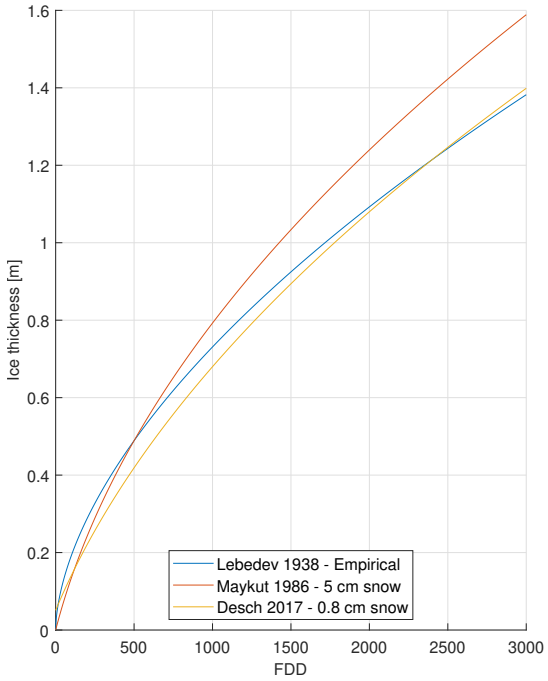

Figure 5.2: Relation for ice thickness as given by Lebedev [1938], Maykut [1986] and Desch et al. [2017]

The formulae as proposed by Maykut [1986] and Desch et al. [2017] compared to the formula by Lebedev [1938] are shown in Figure 5.2. All formulae give comparable results, however, the large difference in snow thickness is remarkable. When taking a closer look at the input values used by Maykut [1986] and Desch et al. [2017], the parameters concerning ice are very similar. This is in contrast to the snow parameters. Both bodies of research include a certain thermal conductivity for snow, and the snow thickness is adapted to match the empirical formula by Lebedev [1938]. Desch et al. [2017] uses $\rho_s = 100$ kg m^{-3} and corresponding $k_s = 0.045$ W m^{-1}K^{-1} as given by Pomeroy & Brun [2001], who have identified these values for dry snow. While in the research by Maykut [1986] a commonly applied value for the snow conductivity of $k_s = 0.31$ W m^{-1} K^{-1} is used. This value is a result of the snow density-conductivity relation defined by Abels [1892], for a snow density of $\rho_s = 330$ kg m^{-3}. In more ice growth models the thermal conductivity of snow is taken as $k_s = 0.31$ W m^{-1}K^{-1} [Ledley, 1991; Maykut & Untersteiner, 1969; Semtner, 1976]. Other papers give the thermal conductivity as a function of the density [Sturm et al., 1997; Yen, 1981], taking into account the seasonal variation of snow density [Warren et al., 1999]. Merkouriadi et al. [2017] measure the spatial and temporal variations of snow properties during the winter (January-March 2015). For first-year ice, the measured snow's thermal conductivity ranges from $k_s = 0.13$ to $k_s = 0.32$ W m^{-1}K^{-1}. Large differences in thermal conductivity have been analysed before. Sturm et al. [2002] compares the different ways of deducing the thermal conductivity (measured or deduced from ice growth). The gap is explained by the high complexity of the snow cover, as also mentioned by Wu et al. [1999] and by possible non conductive heat transfers. This suggests a thermal conductivity for snow of $k_s = 0.31$ W m^{-1}K^{-1} is not necessarily the true conductivity, but does correctly predict the ice growth by including possible other factors.

Additionally, the snow depth by Maykut [1986] (5 cm) is considered more plausible than the 8 mm given by Desch et al. [2017]. However, it is still on the lower side when comparing this to snow depths retrieved from satellite lidar and radar data for ice freeboards. Here, first-year ice is covered with 4 cm of snow in late October and 17 cm in April [Kwok et al., 2020]. Similar results are presented by Forsström et al. [2011] for specifically the Barents Sea and Fram Strait. The relatively low snow depth set by Maykut [1986] might be, but is not necessarily, an explanation for the increasing difference compared to Lebedev [1938] when the FDD increase (Figure 5.2).

Based on the models discussed, it is necessary to include an atmospheric heat transfer coefficient and a properly chosen snow thickness to Stefan's law. Furthermore, the impact of varying the thermal conductivity over the ice thickness as applied by Desch et al. [2017] should be analysed to determine if the increased complexity is worthwhile.

5.1.2. Ice growth rate

There is no general analytical expression for ice growth rate. Some relations have been derived as a function of the ice thickness, based on measurements [Nakawo & Sinha, 2022; Smith et al., 2012; Turner et al., 2017]. Alternatively, Maykut [1986] shows the ice growth rate as a function of the ice thickness and air temperatures based on Equation 5.7 and the data by Anderson [1961]. The relation is shown in Figure 5.3. The figure is based on the empirical fit by Anderson [1961] and not directly on the measurements. Growth rate relations directly derived from data points are less smooth, but similar trends can be recognized.

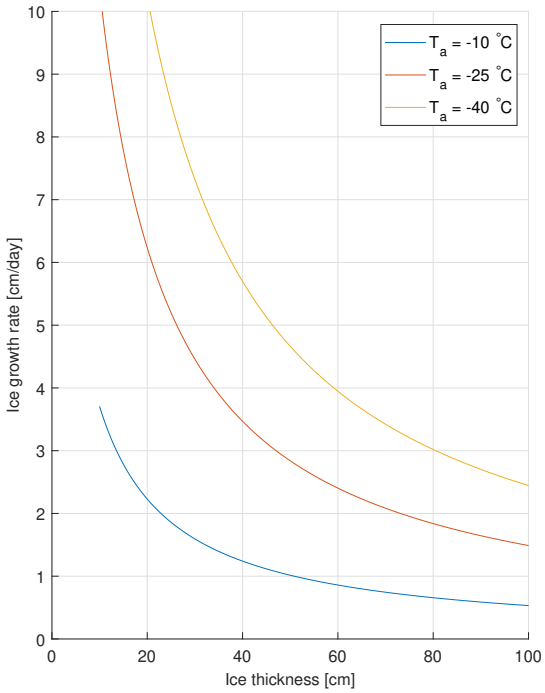

Figure 5.3: The growth rate of young sea ice for different air temperatures (based on the figure by Maykut [1986])

The relation between growth rate and ice thickness indicates a fast initial growth, after which the growth rate decreases. At approximately 0.6 to 0.8 m, the fast initial growth has decreased for most atmospheric temperatures. Additionally, Figure 5.3 shows an asymptotic behaviour for the growth rate indicating linear growth. This indicates that the initial ice thickness prior to AIM is important for the effect AIM has on the natural ice growth. Furthermore, the natural ice growth is not unlimited, but is restricted to a so-called thermodynamic equilibrium thickness. For this thickness, heat is no longer conducted through the ice and the ice growth at the ice-ocean interface stops. In the Arctic this equilibrium is reached at approximately 3 m [National Snow and Ice Data Center]. In combination with natural and increased ice growth, this equilibrium thickness can define an upper limit for efficiently using AIM.

5.1.3. Naturally feasible ice thickness

The derivation by Maykut [1986] is used to evaluate the possible natural ice growth during one season. The monthly average temperature is obtained from the 2m height air temperature data between 60 to 90°North of the ECMWF European Reanalysis V5 (ERA5) [Dee & National Center for Atmospheric Research Staff (Eds)] and a freezing temperature of -1.65°C are considered to determine the number of FDD, which is shown in Figure 5.4. Based on recent years, 2500 to 3000 FDD are assumed to occur during a freezing season. This results in a maximum ice thickness of 1.5 to 1.7 m for FYI, assuming immediate ice formation and no insulating snow conditions throughout the growth process.

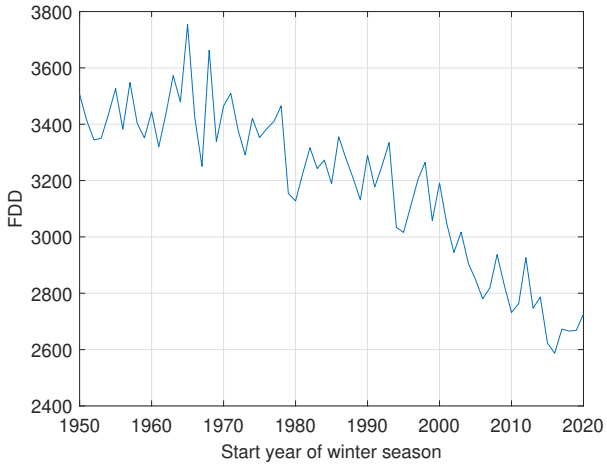

Figure 5.4: Freezing Degree Days during each winter based on 2m Temperature

5.2. Ice availability

The present ice conditions give an indication of interesting regions for AIM, by showing the current ice cover and thicknesses. The modelled ice thicknesses (HYCOM-CICE model [Danish Meteorological Institute]) for May and September (2000, 2020 and 2021), maximum and minimum sea ice volume, are shown in Figure 5.5. The figure illustrates the high annual variability (2020-2021), but also where the ice generally survives (2000-2021). The difference in ice present indicate the region of FYI, which can potentially be increased to survive the melting season.

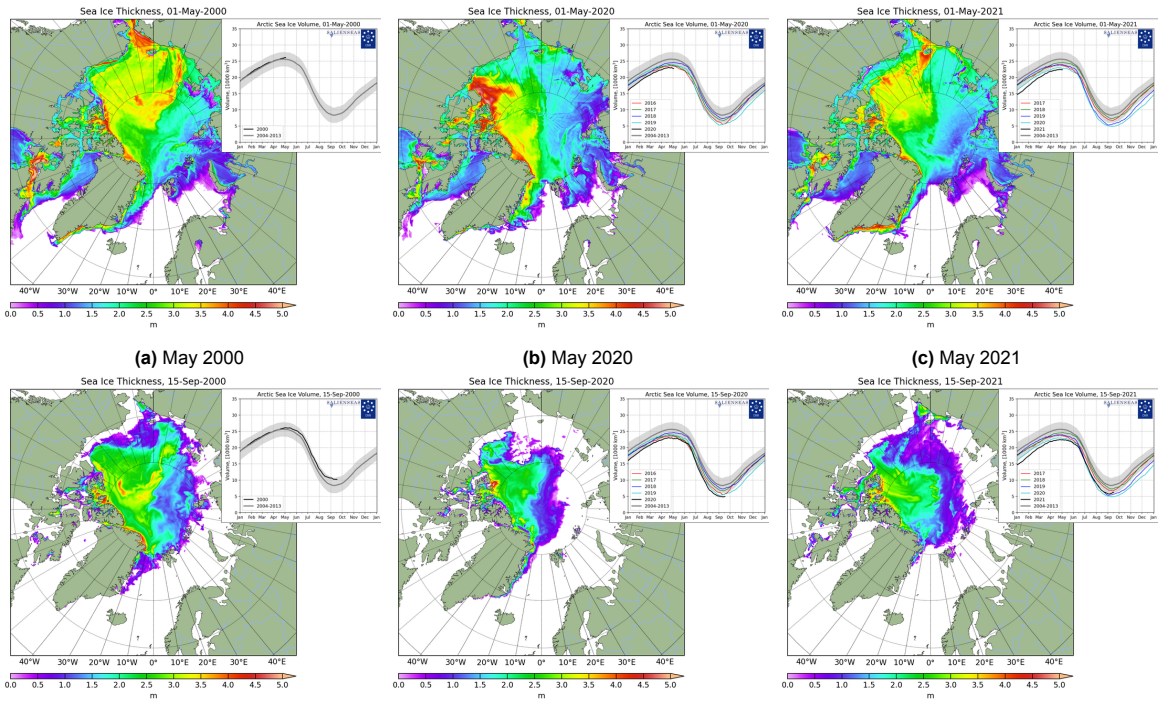

(a) May 2000 **(b)** May 2020 **(c)** May 2021

(d) September 2000 **(e)** September 2020 **(f)** September 2021

Figure 5.5: Modelled ice thickness in 2000, 2020 and 2021 for May and September. Credit: Danish Meteorological Institute.

The exact ice minimum is hard to determine, because the minimum extent varies regionally [Zwally & Gloersen, 2008]. Some places still encounter ice decay, while in other places the ice has started to grow again. Another complexity is the regional variability in ice loss or ice gain [Comiso, 2001]. Remote sensing (by for example satellite sensors or passive/active microwave sensors) provide meteorological data which are, in this case, used to determine the current ice thickness. For AIM it is, besides the

current situation, of interest to predict the Arctic climate on seasonal and interannual timescale. The predictability of several existing models is assessed in the Arctic Predictability and Prediction on Seasonal to Interannual Timescales (APPOSITE) project. The conclusions show predictability of winter ice extent for all models, more variation for the summer ice extent and better predictability for ice volume than ice extent [Day et al., 2016].

There are many models used for climate research with varying complexity. Several models are compared in the Coupled Model Intercomparison Project (CMIP), and the IPCC assessment reports feature these projects. These models couple included or implemented sub-models for the atmosphere, ocean and ice. A commonly used sea ice model is the Los Alamos sea ice model (CICE) [Flato et al., 2013]. CICE models ice including growth, decay and dynamics and can be used as a standalone model or implemented in a coupled model [Hunke et al., 2015]. Two main advantages of the CICE model are the high computational efficiency for modelling ice growth, ice decay and ice dynamics and the transparency of the model [Roberts et al., 2018]. Because of these advantages, CICE might contribute to AIM by indicating areas with potential sea ice loss. However, based on model comparisons with observed data [Hunke, 2010; Roberts et al., 2018], it is unsure if the accuracy of the currently existing models is sufficient for this purpose. Alternatively, Zampieri & Goessling [2019] already showed the possibility to simulate AIM in a climate model by adapting the surface heat and mass fluxes. If ice conditions including AIM can be implemented in ice models, the effect of AIM can be modelled and compared for different scenarios.

Besides considering the ice availability, the continental shelf division among several countries can influence the AIM possibilities due to, for example, political reasons. Figure 5.6 shows the claims of Canada, Denmark, Norway, Russia and the USA [1].

Figure 5.6: Boundaries in the Arctic region as presented by IBRU Durham University

5.3. Discussion: Effect of natural ice growth on AIM

The adapted Stefan's model including a snow layer can be used as the basis for developing an AIM model, which is expected to have a comparable insulating effect during the flooding process. This suggests a negative effect of AIM on the natural ice growth. To limit the disadvantageous effects, the ice growth rate should be considered. The growth rate suggests at least 0.6 m of initial ice thickness is required retain the fast initial growth for various atmospheric temperatures.

AIM should be applied according to the naturally feasible ice thickness. Based on 2500 to 3000 FDD, seasonal ice can grow up to a maximum of 1.5 to 1.7 m if initial ice formations starts immediately and without any insulating snow layer during the growth process. Depending on the desired ice thickness, AIM can be applied accordingly. However, also MYI can be increased by AIM. Ice conditions and availability are subject to change continuously, which complicates the planning of AIM.

[1] The claims shown in Figure 5.6 are explained in the notes presented at the following website: https://www.durham.ac.uk/research/institutes-and-centres/ibru-borders-research/maps-and-publications/maps/arctic-maps-series/.

6

Ice growth with AIM

An ice growth model including AIM is required to identify the necessary AIM implementation. First of all, the different processes occurring during AIM are elaborated in Section 6.1. These processes are combined to develop a theoretical AIM model in Section 6.2. The model is validated using small scale experiments in Section 6.3 and a COMSOL Multiphysics simulation is used to show the effect of AIM on the temperature profile in Section 6.4. Finally, Section 6.5 uses the AIM model to show how AIM can be optimised.

6.1. Ice growth including AIM

The height of water pumped onto the ice will not result in exactly the same increase in ice. This is has two main reasons. First of all, the surface temperature increases due to the release of the latent heat and this slows down the ice growth. Secondly, the extra ice layer creates a blanketing effect for natural ice growth at the ice-ocean interface. Desch et al. [2017] state that due to these effects the increased ice thickness is approximately 70% of the pumped water (i.e. pumping 1 m of water results in 0.7 m of effective ice increase). Desch et al. [2017] conclude the change in surface temperature due to AIM is minor. This is determined for adding an ice thickness gradually over the entire Arctic winter (6 months). The effect on the surface temperature when the time span is shortened is not discussed. The derivation could be adapted to other time intervals. However, the derivation used is questioned, because the thickness of the ice layer is missing in the term determining the heat conduction. For this reason the derivation as proposed by Desch et al. [2017] will not be used in this research to model ice growth including AIM.

A different analytical theory concerning the progress of flooded ice platforms was developed by Lozowski et al. [1991]. Despite the difference in purpose, the theory might satisfy the development of AIM. The model is based on the principle that "*if the ice onto which the layer is flooded is cold, the freezing process will proceed both from above due to convective heat transfer at the surface, and from below due to conduction of heat into the underlying ice*" [Lozowski et al., 1991]. The solution provided for ice growth at the bottom of the flooded layer is valid for $\frac{H}{2}\sqrt{\frac{k}{\rho c}t} > 1.8$, which coincides with a minimal ice thickness of 1.2 m. Based on the findings from ice growth rate (Section 5.1.2), AIM might be applied on thinner ice. Additionally, the paper shows interesting results for the changes in temperature profile when flooding ice formed using an EGADS dopant. The results by Lozowski et al. [1991] are shown in Figure 6.1 and illustrate an initial nearly linear temperature profile (Line 1), which bends due to flooding with warmer water (Line 2) and becomes nearly vertical (Lines 3 and 4) before approaching the initial linear shape again (Lines 5 and 6). It is expected that, depending on the ice thickness and thickness of the flooded layer, the temperature profile does or does not reach a vertical profile for a certain duration. In contrast to the paper by Desch et al. [2017], Lozowski et al. [1991] does not describe ice growth at the ice-ocean interface during or after flooding the ice. For these reasons, this model is not adapted, but the theory is used to develop a new AIM model.

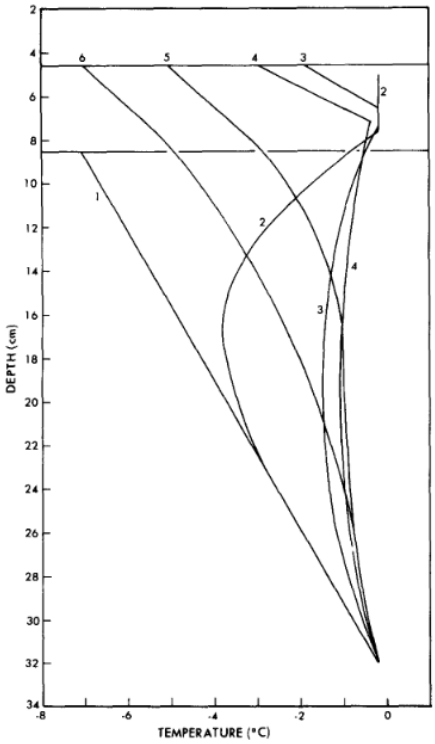

Figure 6.1: The effect of flooding on the temperature profile of an EGADS ice sheet. Figure as given by Lozowski et al. [1991].

6.2. Theoretical AIM model

To develop an AIM model, some assumptions about the ice growth at the different interfaces are necessary. When AIM is applied, the following successive layers are identified: Atmosphere, AIM, ice and ocean. Based on the experimental results by Lozowski et al. [1991], the temperature profile is expected to change, resulting in the following ice growth processes:

- Ice growth at the ice-ocean interface ‘d1’. Heat conduction upwards into the original ice, depending on the minimum temperature along the temperature profile.
- Ice growth at the AIM-ice interface ‘d2’. Heat conduction downwards into the original ice, depending on the minimum temperature along the temperature profile.
- Ice growth at the atmosphere-AIM interface ‘d3’. Convective heat transfer to the atmosphere and heat conduction after a thin ice layer has formed at the top of the flooded layer depending on the surface temperature.

The processes are illustrated on the left hand side of Figure 6.2. Before AIM is applied, the ice grows according to Stefan’s law (Step 1). When the ice is flooded, ice is growing according to ‘d1’, ‘d2’ and ‘d3’ simultaneously (Step 2). When the flooded layer is completely frozen, the ice is expected to behave as one section of ice and grows further according to Stefan’s law (Step 3).

The ice growth for Step 1 and Step 3 are straightforward, while the different ice growth processes during Step 2 require additional attention. As described in Chapter 5.1, the temperature difference over the ice sheet causes heat conduction. Normally, the minimal temperature over the ice thickness occurs at the ice surface and heat is conducted upwards. However, when the ice is flooded, the temperature profile changes. Now, the minimum temperature occurs at a currently unknown time dependent height between the top and bottom of the ice sheet. Based on the theory described, heat conduction occurs simultaneously upwards (at the ice-ocean interface) and downwards (at the AIM-ice interface). Resulting in ice growth downwards (at the ice-ocean interface) and upwards (at the AIM-ice interface). At the same time, convective heat transfer causes the flooded layer to cool, and ice growth is initiated at the atmosphere-AIM interface. The ice formation at the top of the flooded layer is expected to follow Stefan’s law.

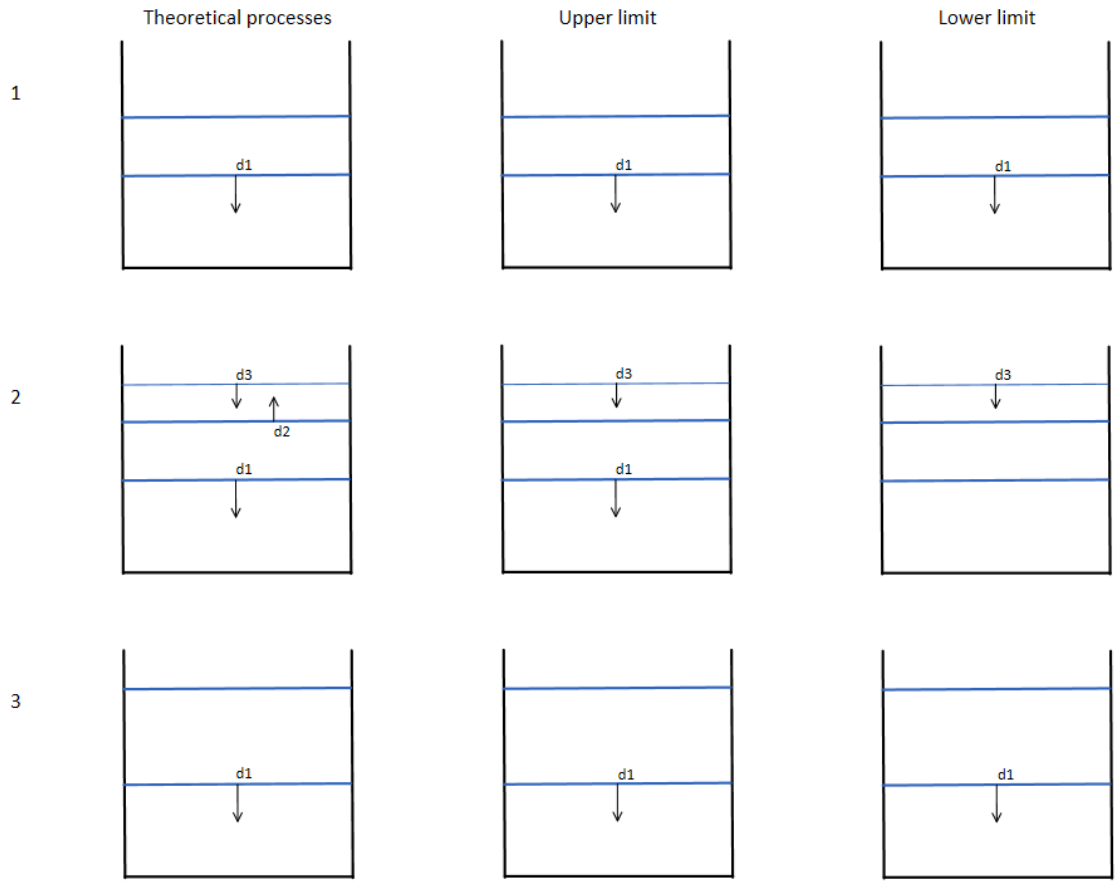

Figure 6.2: Ice growth processes as theoretically expected and as included to create an upper and lower limit

To create an AIM model, the effect of flooding on the temperature profile in the ice requires further understanding. Assuming only vertical heat transfer, the temperature profile might be approachable using an 1D problem analysis. However, due to flooding, the boundary condition at the generated AIM-ice interface experiences a sudden change. This complicates an analytical approach. Therefore, it is recommended to analyse the effect of flooding on the temperature profile using a software program like COMSOL Multiphysics.

To simulate the effects of AIM without software programs, the ice growth including AIM is modeled using an upper and lower limit scenario. Both situations are illustrated in Figure 6.2 and for both scenarios, the ice growth at the AIM-ice interface (d2) is excluded. For the upper limit scenario, the flooded layer is modeled similar to thin ice growth. The ice growth at the bottom of the original layer is modeled as if the ice is insulated by an ice and water mixture (similar to ice growth insulated with a snow layer, but using the time dependent properties of the flooded layer instead). This is expected to overestimate the ice thickness, because the change in temperature profile is expected to slow down or temporarily interrupt the ice growth ‘d1’. For the lower limit scenario, the ice growth at the bottom of the original layer stops until the flooded layer is completely frozen. This scenario is expected to underestimate the ice growth ‘d1’, because ice growth at the ice-ocean interface is expected to continue in some measure corresponding with the changed temperature profile. These scenarios can be generated for both instant and incremental flooding.

Figure 6.3a shows the upper and lower limit as derived for the AIM model compared to normal ice growth without AIM. Incremental flooding shows a slightly faster flooding phase than instant flooding, which can be explained by the faster growth rate of each sub layer in incremental flooding compared to a single thicker layer (Section 5.1). Furthermore, the lower limit scenario for both flooding processes has the same ice thickness at the end of the flooding phase. This is in contrast with the upper limit scenario, which clearly shows thicker ice at the end of the flooding phase for instant flooding. When flooding instantly, the ice growth of the original ice layer continues to grow according to the initial ice

thickness of the flooding phase, but insulated. However, when flooding incrementally, the ice thickness changes for every new layer added during the flooding phase, which has a negative effect on the growth rate of the original ice layer. For this reason, the difference should decrease for thicker initial ice and is indeed shown in Figure 6.3b, where different initial ice thicknesses are compared. Additionally, the difference between the upper and lower boundary for both flooding processes decreases for increasing initial ice thickness.

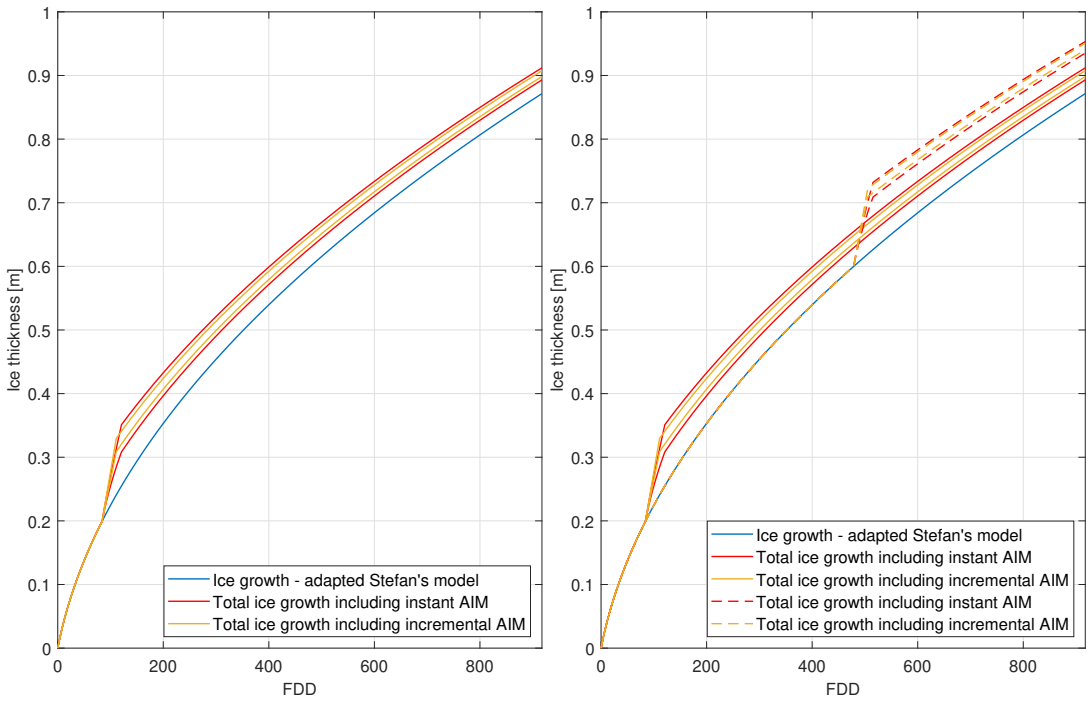

(a) The upper and lower limit as implemented in the AIM model **(b)** The upper and lower limit for different initial ice thicknesses

Figure 6.3: Results of the analytical AIM model

6.3. Validation: Small scale AIM experiments

To validate the upper and lower bound theory, experiments are conducted in a cold room at the Delft University of Technology. Three identical coolers are used with inside dimension of 458 x 396 x 325 mm (LxWxH). Each cooler is filled with 45 L of fresh water, which leaves enough margin for moving the coolers and flooding the ice. The tap water is mixed with Aquaforest Sea Salt to obtain a salinity of 30.5 ($\pm$ 0.5) psu. The salinity is measured using the Greisinger GMH 3431, which accounts for the water temperature. The coolers are placed in the cold room which is maintained at an average temperature of -20 $\pm$ 1.5°C. The temperature slightly fluctuates due to the defrost cycle of the cooling system. Throughout the experiment, the ice thickness is measured using a ruler and for this reason a margin of $\pm$1 mm is included in the results. Additionally, a Greisinger G1710 Thermometer is used to obtain the ice surface temperature and water temperature underneath the ice for each measurement. The accuracy of the surface temperatures measured using this thermometer is questioned and a thermistor array as used in the experiment by Lozowski et al. [1991] would be recommended instead. The experimental setup is shown in Figure 6.4a including the camera used to monitor initial ice formation and Figure 6.4b shows an ice sample and how the water temperature is measured. Some remarks on the ice growth are that the ice is left to grow to the sides of the cooler, which is necessary for flooding the ice. Furthermore, the grain structure is not accounted for, because the effects on the ice growth process are expected to be minor. Lastly, the coolers provide insulation at the sides and bottom to avoid cooling and ice formation. In practice, the ice would be flooded with water retrieved from underneath the ice. However, this is not possible for this experimental setup. Therefore, an additional cooler is prepared with saline water, which is cooled down to near freezing temperature (-1.65°C at 30 psu [Millero, 1978]).

(a) Test setup: Three coolers positioned in the ice lab **(b)** Example of water temperature measurements

Figure 6.4: AIM setup used for small scale experiments

First of all, a reference experiment is conducted, to compare the natural ice growth in the cold room with the analytical derivation by Maykut [1986] as discussed in Section 5.1. Two coolers are placed in the cold room and the ice thickness is measured for three consecutive mornings. Figure 6.5 shows the results for both coolers and the theoretical ice growth derivation. There is a significant effect when varying the heat transfer coefficient and several values are used in literature for theoretical models, for example: 24 W $m^{-2}K^{-1}$ [Maykut, 1986] and 30 W $m^{-2}K^{-1}$ [Desch et al., 2017]. However, Lozowski et al. [1991] derived a heat transfer coefficient based on a similar ice growth experiment and obtained a value of 15.2 W $m^{-2}K^{-1}$, which matches with our experimental measurements. Simulating ice growth for more FDD shows the difference in ice thickness due to various heat transfer coefficients decreases significantly over time. Noticeable was the ice surface which remained slightly wet throughout the experiment. This might be the result of water being pushed through the ice due to pressure build up underneath the ice as ice grows. This is not experienced when growing fresh water ice, so the sea ice might be more porous and/or brine channels allow the water to flow through the ice. Furthermore, the salinity of the water underneath the ice increases significantly due to salt rejection when the ice grows. This is the consequence of working with a finite volume and does not occur, to this extent, in the Arctic. The decreasing freezing temperature due to increasing salinity is included in the FDD calculations to account for this effect in the experimental results.

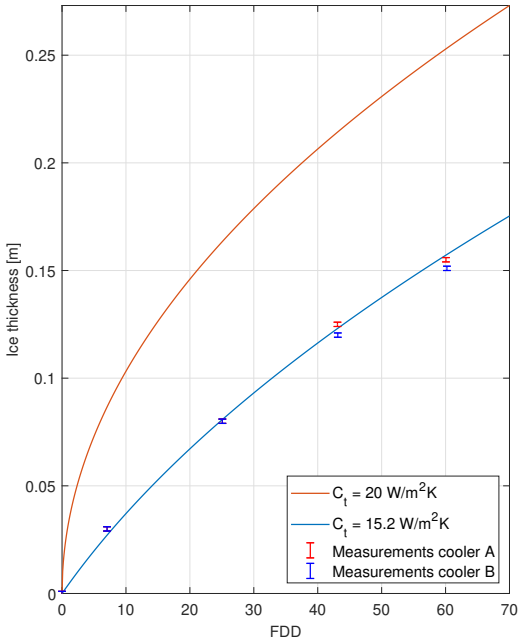

Figure 6.5: Measurements during reference experiment to test natural ice growth

Four different experiments are used to validate the AIM model. The ice is either flooded instantly or flooded incrementally and this is tested for two different initial ice thicknesses. The initial ice thickness depends the starting temperature of the water and the cooling time prior to flooding. For convenience, the cooling time prior to flooding is used as input parameter instead of the initial ice thickness. An overview of the experiments is shown in Table 6.1. After flooding, the ice clearly shows the AIM effect. This can be seen in Figure 6.6, which shows some ice samples after they have been drained. Figure 6.6a shows a single thick AIM layer, while in Figure 6.6b the thinner sub-layers can be defined. In both scenarios the AIM layer seems to be more white, this might be due to a salt difference between the original ice layer and the AIM layer or perhaps more air included in the ice. However, the exact reason is still unclear. If the difference remains on the long term, this can be beneficial for the albedo effect. However, to ensure this, the ice should be monitored for a longer period of time.

Table 6.1: Overview of experiments used to validate the AIM model

Experiment	Flooding phase	Cooling time prior to flooding
Test I	Instantly 2.5 cm (4.5 L)	24 h
Test II	Instantly 2.5 cm (4.5 L)	48 h
Test III	Incrementally 9x0.28 cm (9x0.5L)	24 h
Test IV	Incrementally 9x0.28 cm (9x0.5L)	48 h

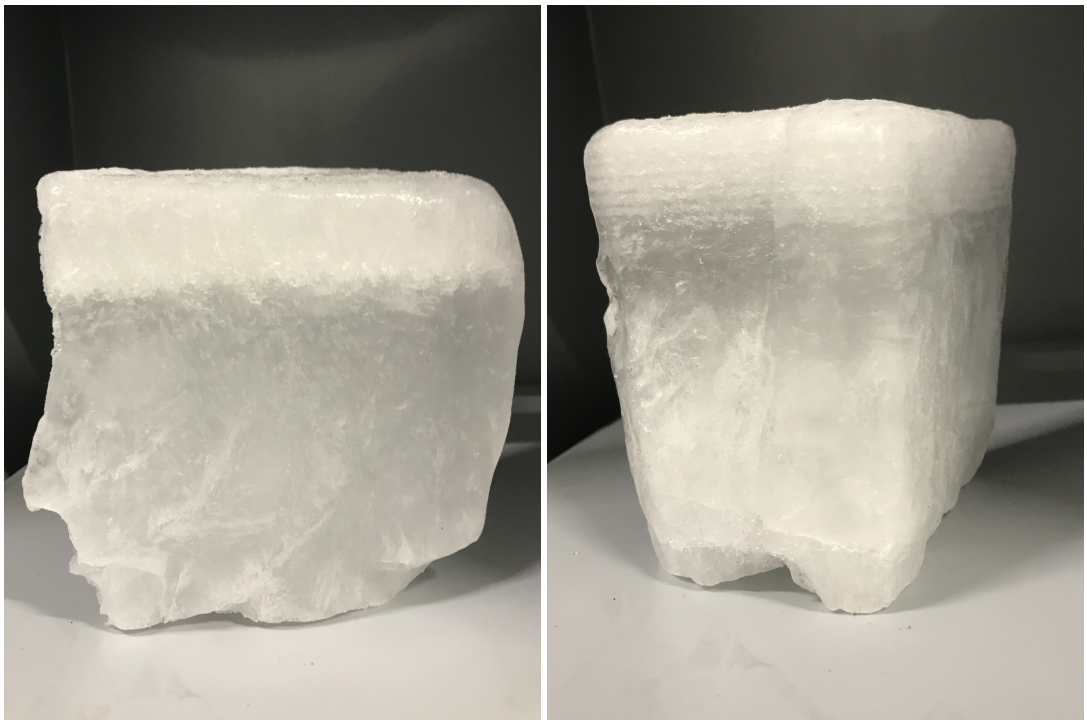

(a) The ice after instant flooding, showing one thick layer **(b)** The ice after incremental flooding, showing multiple thin layers

Figure 6.6: An example of how ice looks after flooding, when the ice has been drained

During each experiment, an additional cooler is used to monitor natural ice growth. If the reference cooler shows deviating measurements, there is a possibility that external factors have influenced the experiment and the results are considered invalid. Each test is replicated for reliability. However, the initial ice thickness for each duplicate is of similar height, but not equal due to a difference in water temperature prior to cooling. Figure 6.7 shows the results for each experiment. During each test the

reference cooler confirms ice growth as expected and therefore the results are considered valid. One exception is the fourth measurement during Test III, Figure 6.7c. This measurement shows deviating thicknesses and for this reason the last measurement was conducted at multiple locations of the cooler to ascertain the thickness. As the last measurement does confirm normal ice growth for the reference cooler and duplicate experiment does not indicate any deviations, the fourth measurement is considered a measurement error.

Furthermore, Figure 6.7 shows an ice thickness in between the upper and lower boundary at the end of the flooding phase for all test set-ups. However, when ice growth continues the ice thickness approaches the lower boundary estimation. Afterwards, the ice growth continues according to Stefan's law and, based on the number of measurements, the ice is expected to continue to do so. In case of thicker initial ice and/or incremental flooding, the ice thickness at the end of the flooding phase is further towards the upper boundary condition compared to the other scenarios. This suggests that the temperature profile in the original layer is affected less for thicker ice and for incremental flooding resulting in ice growth at the ice-ocean interface 'd1'. The replication of the study, as shown in Appendix B, confirms this trend.

The observations indicate a 'delay' between the flooding phase and continued ice growth according to Stefan's law. To ensure this delay is not the result of forces due to sawing through the ice, a fifth test is conducted for two coolers simultaneously. The ice thickness of each cooler including AIM is measured only once to eliminate influence of the sawing process. The results can be seen in Appendix B and are in line with the measurements in Figure 6.7. This ensures the cutting process has no significant impact on the ice growth and confirms a 'delay' occurs between the flooding phase and ice growth according to Stefan's law. Instead, the time it takes before the two layers are completely merged and/or the effect of AIM on the temperature profile in the ice (which is elaborated in Section 6.4) can be the cause for this 'delay'.

Analysing the effective ice thickness increase validates an enlargement for thicker initial ice for both flooding processes. Furthermore, as all results follow a similar trend, it is expected that the difference between the flooding processes indeed decreases for thicker initial ice. These results reveal the importance of the initial ice thickness on the effective ice thickness increase.

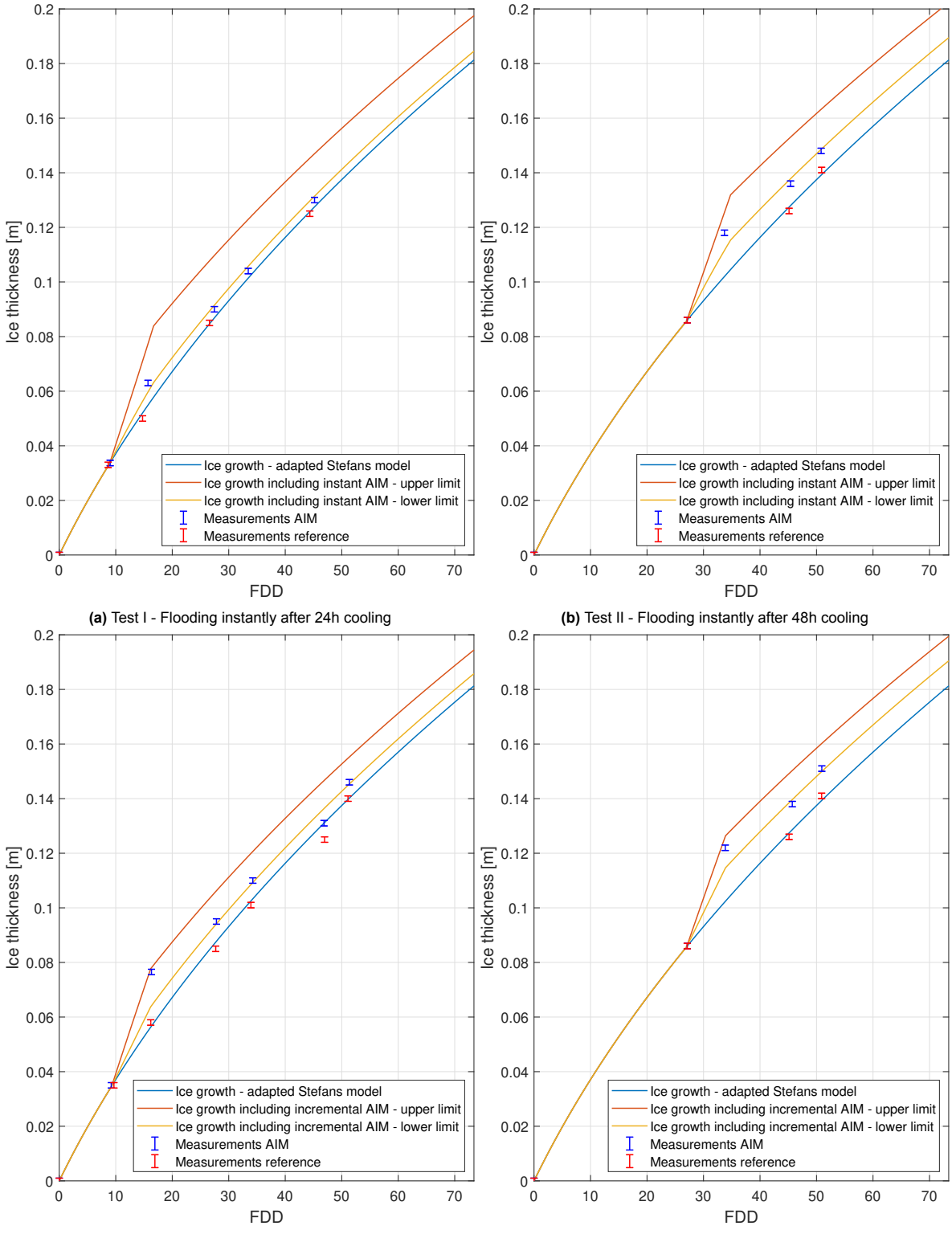

(a) Test I - Flooding instantly after 24h cooling

(b) Test II - Flooding instantly after 48h cooling

(c) Test III - Flooding incrementally after 24h cooling

(d) Test IV - Flooding incrementally after 48h cooling

Figure 6.7: Results of the AIM experiment

6.4. Verification: COMSOL Multiphysics simulations

To verify the AIM model and the observations made during the experiments, a COMSOL Multiphysics (hereafter referred to as COMSOL) model is created to research the time dependent effect of AIM on the temperature profile. First of all, natural ice growth is simulated to confirm ice growth according to Stefan's model. The model has an initial geometry of 2x2 m water at -1.65°C and uses a phase change material subnode to simulate ice formation. This subnode is applicable on boundaries between fluid and solid domains and allows movement of the interface as a result of phase change. However, no topology changes are permitted and for this reason an initial ice layer of 1 mm is added to the geometry. Furthermore, heat transfer at the atmosphere-ice interface is simulated using convective heat flux and all other outside boundaries are thermally insulated to prevent heat transfer. Figure 6.8 shows the geometry and how it changes due to ice formation. Material properties and input parameters used are shown in Table 6.2.

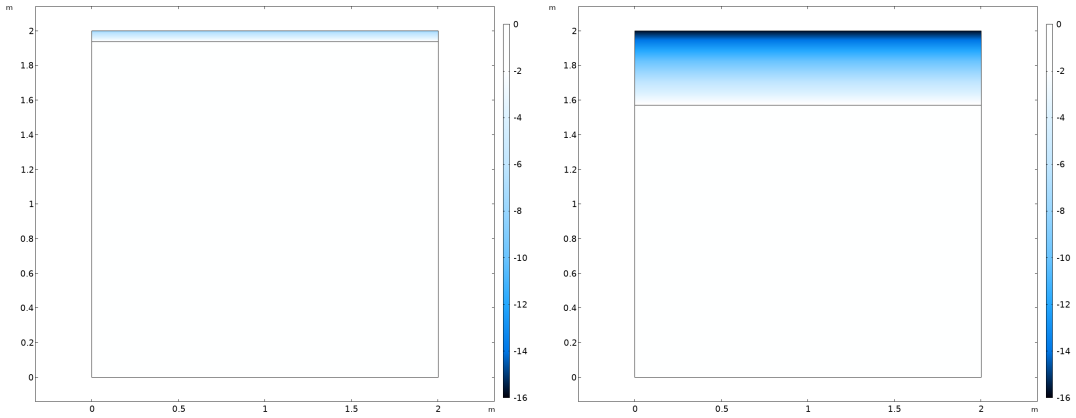

(a) Natural ice growth after 1 day **(b)** Natural ice growth after 15 days

Figure 6.8: COMSOL simulation for natural ice growth at T_a= -20°C

Table 6.2: Material properties and input parameters used during COMSOL simulation

Saline water [Sharqawy et al., 2010] [Nayar et al., 2016]	Thermal conductivity	k_w	0.57 W m^{-1} K^{-1}
	Density	ρ_w	1024 kg m^{-3}
	Heat capacity at constant pressure	$C_{P,w}$	4006 J kg^{-1} K^{-1}
Ice [Ono, 1967]	Thermal conductivity	k_i	1.9 W m^{-1} K^{-1}
	Density	ρ_i	917 kg m^{-3}
	Heat capacity at constant pressure	$C_{P,i}$	3000 J kg^{-1} K^{-1}
Input parameters	Initial ice thickness	H_i	0.001 m
	Initial water depth	D_i	2.0 m
	Initial temperature ice	$T_{i,i}$	-1.65 °C
	Initial temperature water	$T_{w,i}$	-1.65 °C
	Phase change temperature	T_p	-1.65 °C
	Latent heat	l_i	3.34·10^5 J kg^{-1}
	Heat transfer coefficient	C_t	15.2 W m^{-2} K^{-1}
	External temperature	T_o	-20 °C

The ice thickness obtained from the COMSOL simulation is compared to Stefan's model to confirm the natural ice growth is correctly simulated. Figure 6.9 shows the data obtained from COMSOL matches the Stefan's model. This indicates the model and input parameters can be used to simulate ice growth including AIM.

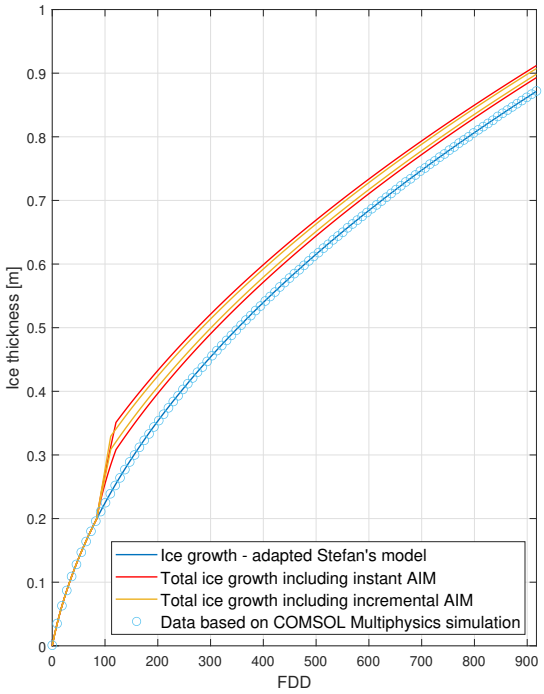

Figure 6.9: Ice growth model including COMSOL simulation for natural ice growth

To simulate AIM, an initial ice thickness geometry including temperature profile is exported from the natural ice growth model and a layer of 2, 5 or 10 cm water is added with an initial temperature of -1.65°C. To avoid topology changes, the AIM layer is modeled using a phase change material subnode. Furthermore, heat transfer is simulated at the AIM-atmosphere interface and other parameters and subnodes remain the same as for the natural ice growth model. Figure 6.10 indicates how AIM effects the temperature in the original ice layer and AIM layer. Directly after flooding, Figure 6.10a, there is a harsh temperature difference between the original ice and AIM layer. Figure 6.10b, 2hr after flooding, shows the AIM layer is cooling at the atmosphere-AIM interface and AIM-ice interface and the original ice layer is indeed warmed due to heat conduction into the original ice. After the AIM layer is completely frozen, the entire ice layer is cooled as shown in Figure 6.10c. Furthermore, Figure 6.10c clearly shows the increased ice thickness relative to Figures 6.10a and 6.10b. To verify the model results, a relative tolerance convergence analysis is conducted and can be found in Appendix C. For the final simulations a relative tolerance of 5e-5 is used to limit computation time.

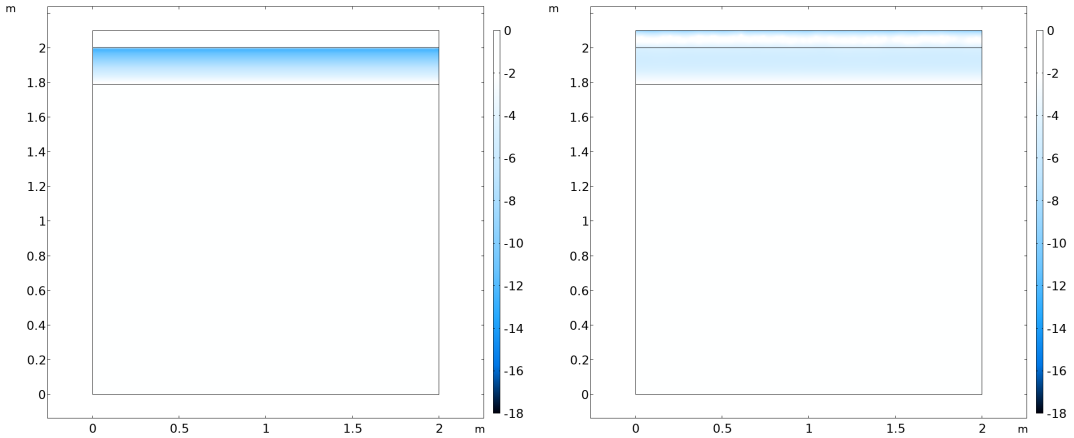

(a) Ice growth and temperature profile in °C directly after flooding

(b) Ice growth and temperature profile in °C 2hr after flooding

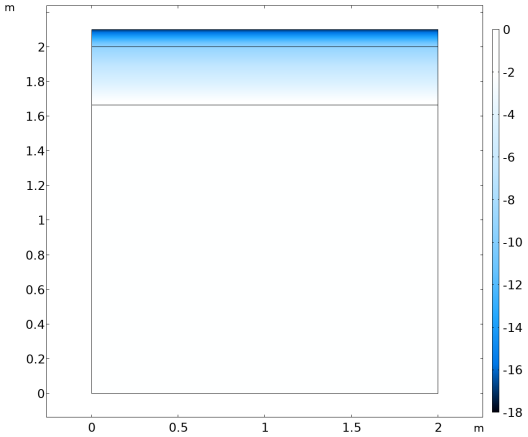

(c) Ice growth and temperature profile in °C 10 days after flooding

Figure 6.10: COMSOL simulation of 10 cm AIM on 21 cm ice at T_a= -20°C

So far, the model did not succeed in merging the AIM and original ice after freezing. This causes a boundary to remain between the two ice layers. Consequently, a linear temperature profile can not be reached, which would be expected based on the experiments by Lozowski et al. [1991] described in Section 6.1, and the natural ice growth at the ice-ocean interface is not correctly simulated. For this reason, the COMSOL model indicates how the temperature profile is affected and the simulations approach but do not simulate exact ice growth with AIM.

Figure 6.11 shows the varying effect on the temperature profile depending on the AIM thickness and initial ice thickness. The initial effect on the temperature profile is similar for 0.21 m and 0.61 m initial ice as shown in Figures 6.11a and 6.11b respectively. However, the temperature profile takes longer to restore for thicker AIM. Furthermore, the simulations for both 5 cm and 10 cm AIM clearly show ice growth at the AIM-ice interface and atmosphere-AIM interface and it takes longer to freeze a thicker AIM layer. When comparing the effects for different initial ice thicknesses, the effects on the temperature profile for 0.61 m ice remain longer. Additionally, the AIM layer freezes faster for 0.61 m ice (as clearly shown for 10 cm AIM), but the temperature profile in the AIM layer takes longer to develop to a linear profile. This can both be a result of the larger difference between the surface temperature prior to flooding and the temperature of the flooding water.

The COMSOL simulation indicates a possible reason for the observed delay during the AIM experiments. The COMSOL simulation shows a duration, longer than the freezing time of the AIM layer, is necessary before the temperature profile has restored. This duration depends on the AIM thickness and can explain the delay observed between the flooding phase and continued ice growth. Figure 6.11 shows the time span decreases for thinner AIM layers and reasonably AIM implementation does concern incremental flooding with thin layers. This restricts the effect on the temperature profile and the restoration time. For this reason, the AIM delay is expected to be limited for full scale implementation.

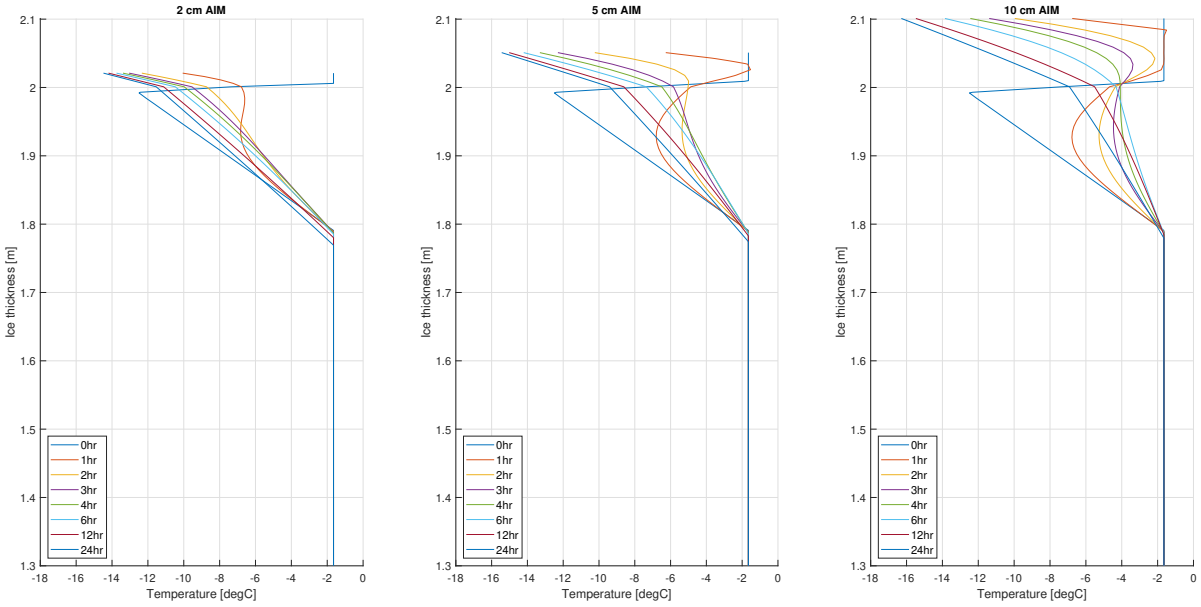

(a) Initial ice thickness of 0.21 m

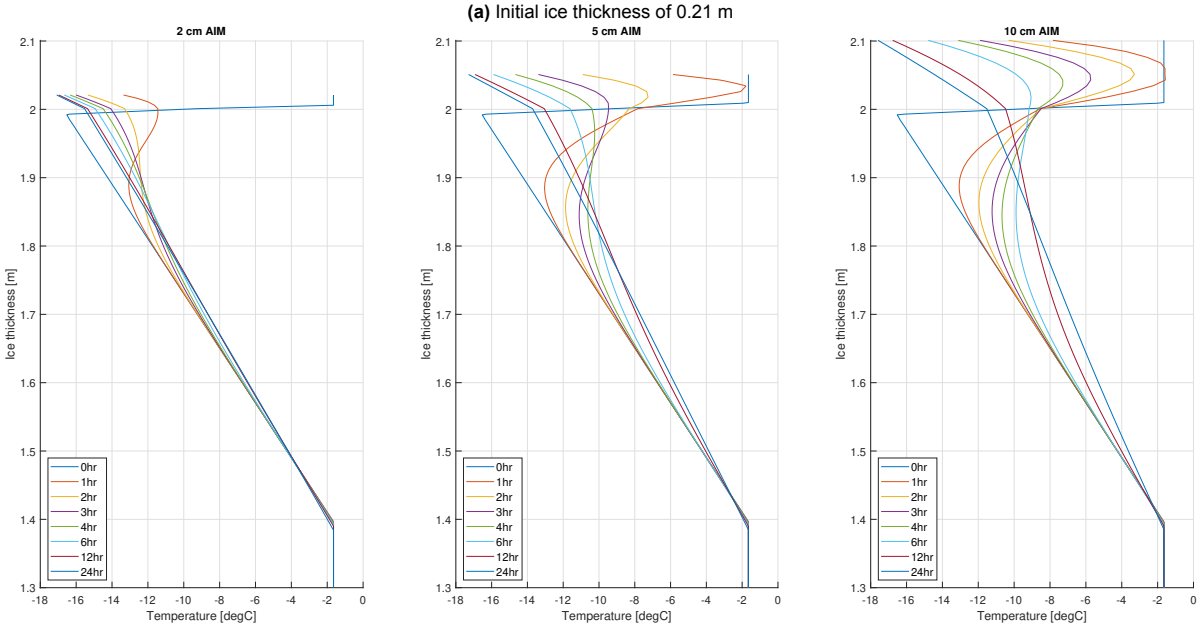

(b) Initial ice thickness of 0.61 m

Figure 6.11: Effect of AIM on temperature profile for different initial ice thicknesses simulated at T_a= -20 °C

6.5. Optimisation of AIM

Desch et al. [2017] concluded the effective ice increase is 70% of the applied AIM. However, based on the findings in this research the AIM effect cannot be generalised to one value. Figure 6.12a shows examples for AIM implementation on FYI for one winter season consisting of 3000 FDD. The figure indicates AIM applied on different ice thicknesses results in different effects, which has two main factors: Initial ice thickness and freezing duration after AIM.

First of all, the initial ice thickness for AIM significantly influences the effective ice thickness increase. Figure 6.12b shows the effective ice thickness increase for different initial ice thicknesses, which is obtained by subtracting natural ice growth from the AIM models. Considering that AIM can be used on MYI and to highlight the development of the effective ice thickness increase, more initial ice thicknesses are simulated. The graph shows a significant enlargement for the effective ice thickness increase for an initial ice thickness of 0.6 m relative to 0.2 m, but this increase flattens for even thicker initial ice. Based on these results it is discouraged to apply AIM on ice thicknesses below 0.6 m and suggested for ice thicknesses approaching 1 m. This is discussed in more detail in Chapter 7.

Secondly, the freezing duration after AIM affects the effective ice thickness increase. As shown in Figure 6.12b, the maximum effect occurs directly after the flooding phase and decreases over time, which is the effect of the growth rate. Theoretically, AIM should be applied late in the winter season to minimise the freezing duration after flooding and obtain the maximum effect. Nevertheless, AIM will result in an effective ice thickness increase regardless of the freezing duration after AIM.

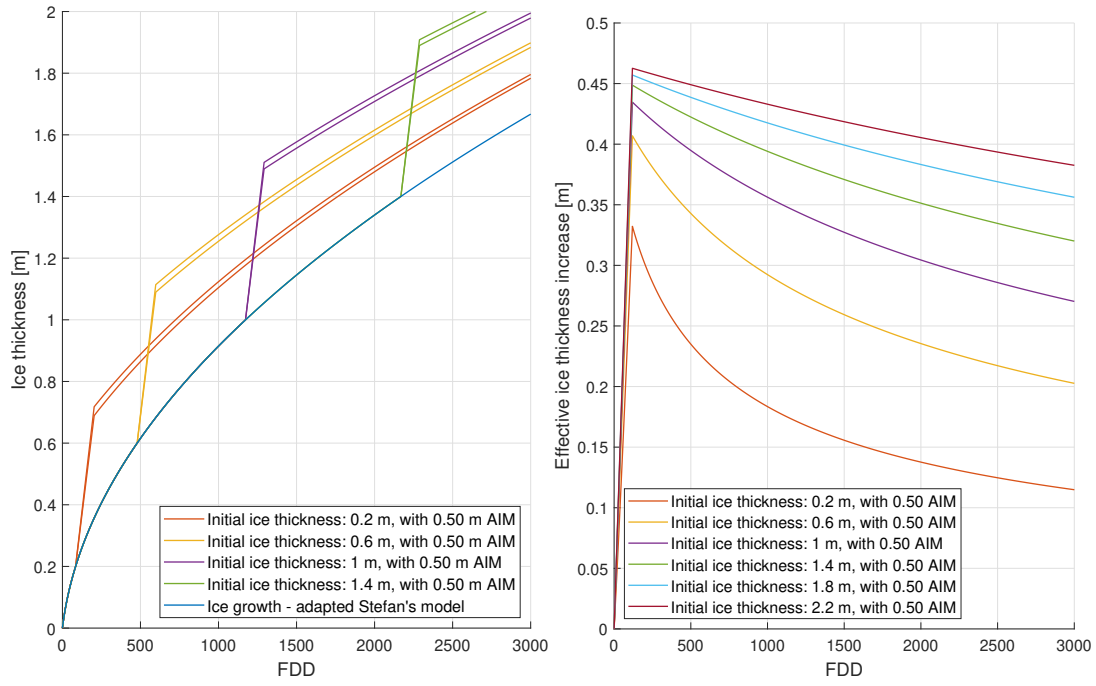

(a) Ice growth model for 0.50 m AIM for different initial ice thicknesses

(b) Effective ice thickness increase due to 0.50 m AIM for different initial ice thicknesses

Figure 6.12: The impact of initial ice thickness and freezing duration after AIM on the effective ice thickness increase

To compare the effects of different AIM thicknesses, the fractional increase ($\frac{\text{Effective increase}}{\text{AIM thickness}}$) is determined for 0.50, 0.75 and 1.0 m as shown in Figure 6.13. For each case, the fractional increase is extracted directly after the flooding phase and after 3000 FDD, as shown in Tables 6.3 and 6.4 respectively. Directly after AIM (Table 6.3), the fractional increase is similar for all AIM thicknesses and increases for thicker initial ice. In other words, the effect of AIM on natural ice growth is larger for thinner ice than for thicker ice. Only for the initial ice thickness of 0.6 m there is a slightly larger difference between the AIM thicknesses. Table 6.4 shows the fractional increase 3000 FDD after AIM and shows a larger difference in fractional increase for the various AIM thicknesses. For all AIM thicknesses, the fractional increase becomes larger for thicker initial ice and the difference between AIM thicknesses decreases for thicker ice.

These results differ from the findings by Desch et al. [2017], who conclude the fractional increase is constant at 70% for different AIM thicknesses. The results in this research suggest that the fractional increase depends on the initial ice thickness and is relatively constant for various AIM thicknesses directly after flooding, but the difference between the AIM thicknesses increases with freezing duration after AIM.

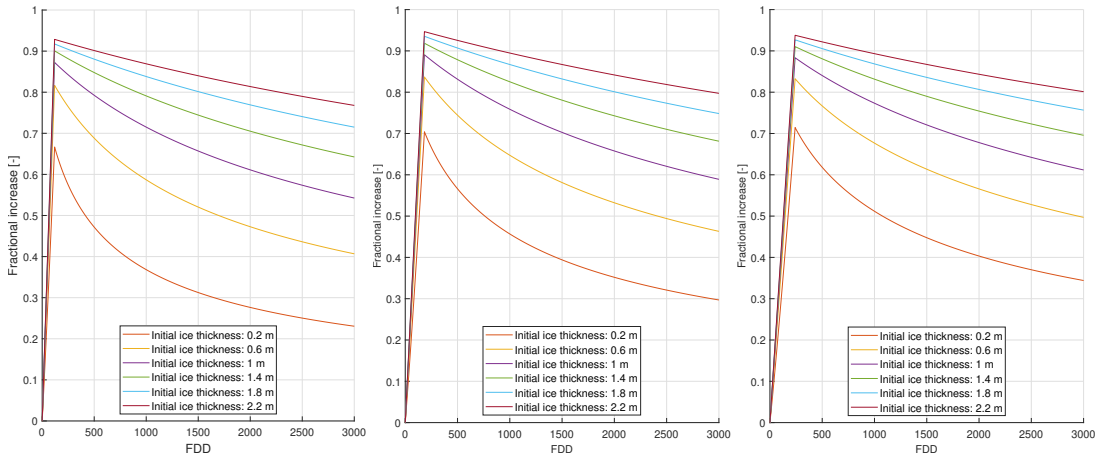

(a) 0.50 m AIM **(b)** 0.75 m AIM **(c)** 1.0 m AIM

Figure 6.13: Fractional increase of different AIM thicknesses

Table 6.3: Maximum fractional increase of AIM thickness directly after the flooding phase for different initial ice thicknesses 'H_i'

	H_i=0.2 m	H_i=0.6 m	H_i=1.0 m	H_i=1.4 m	H_i=1.8 m	H_i=2.2 m
0.50 m AIM	0.67	0.82	0.87	0.90	0.92	0.93
0.75 m AIM	0.70	0.84	0.89	0.92	0.94	0.95
1.0 m AIM	0.71	0.83	0.88	0.91	0.93	0.94

Table 6.4: Fractional increase of AIM after 3000 FDD for different initial ice thicknesses 'H_i'

	H_i=0.2 m	H_i=0.6 m	H_i=1.0 m	H_i=1.4 m	H_i=1.8 m	H_i=2.2 m
0.50 m AIM	0.23	0.41	0.54	0.64	0.71	0.77
0.75 m AIM	0.30	0.46	0.59	0.68	0.75	0.80
1.0 m AIM	0.34	0.50	0.61	0.70	0.76	0.80

7 Implementation of AIM

To define how AIM can be implemented to obtain the desired results, the effects of the different aspects discussed in this research are combined. First of all, Section 7.1 discusses the results of this research and how they, combined, can contribute to AIM implementation. Thereafter, Section 7.2 elaborates on the requirements for an AIM structure. Finally, the effects of AIM on the ice cover and solar radiation management and possible side effects are discussed in Section 7.3.

7.1. Possible AIM methods

The focus of AIM in this research is to counteract the annual Arctic sea ice volume loss. This chapter discusses how the findings in this report can be combined to achieve the target value of 322 km^3. The direct contribution of AIM to the ice volume is considered the primary effect. Additionally, AIM results in secondary effects, which can contribute to the ice volume indirectly. For example, there is an effect on energy absorption (solar radiation management), regional atmospheric temperatures and regional oceanic temperatures. The focus in this research is on the primary effects of AIM, and to account for these secondary effects a climate model is recommended.

First of all, for ice to survive the summer, a survival ice thickness is necessary at the beginning of the melting season. Theoretically, ice that has reached the survival thickness melts away on the last day of the melting season and starts freezing again the day after. Based on an empirical fit, Chapter 4 finds a location dependent melting gradient between -2.1 and -2.7 cm day^{-1} for ice in the Beaufort Sea and between -0.8 and -1.4 cm day^{-1} for ice in the Transpolar Drift. Substituting an average of 91 melting days results in a survival thickness between 1.91 and 2.46 m and between 0.73 and 1.27 m respectively. Secondly, the survival ice thickness is combined with natural ice growth to determine the AIM thickness depending on the desired results. Based on previous winters, 2500 to 3000 FDD are expected during one winter and for further calculations the average of 2750 FDD is used assuming immediate ice growth and no snow formation. COMSOL suggests thinner layers minimise the effect on the temperature profile. For this reason, incremental flooding with a layer thickness of 0.94 cm is considered as a result of the iterative step size. The implementation of AIM on FYI is discussed for the Beaufort Sea and Transpolar Drift in Section 7.1.1 and 7.1.2 and possible implementation for MYI is elaborated in Section 7.1.3.

7.1.1. AIM in the Beaufort Sea for FYI

To explore the possible methods of AIM implementation in the Beaufort Sea, the average survival ice thickness of 2.18 m is considered. Assuming 2750 FDD, 1.6 m ice thickness can develop during one winter, which is insufficient for the survival thickness of the Beaufort Sea. If thick enough, the ice can stay in the Arctic for approximately 5 years or possibly longer if the ice gets trapped in the circular motion of the Beaufort Gyre. This offers various possible methods for AIM implementation. Hereafter, four different methods are suggested for the implementation of AIM: Annual method, biennial method, thermodynamic equilibrium method and predefined target method. The AIM model is simulated for initial ice thickness of 0.6 m and 1.0 m and the ice thicknesses throughout each method are summarised in Table 7.1.

Annual method: Ice can be increased with AIM intending to last the summer season. As discussed in Chapter 5, the initial ice thickness and freezing duration after AIM determine the effective (and necessary) increase. To reach the survival thickness, the AIM model is simulated for 2750 FDD and the results indicate 1.05 m AIM is necessary for an initial ice thickness of 0.6 m and 0.84 m AIM for an initial ice thickness of 1 m. Nevertheless, ice with the survival thickness at the beginning of the summer is expected to melt away on the last day of summer, which is approximately when the September values are obtained. Therefore, this method does not directly contribute to increasing the September ice volume. However, the overall Arctic albedo is increased throughout the melting season and more solar radiation will be reflected resulting in less energy absorption (secondary effects). The implementation of the annual method is shown in Figure 7.1a.

Biennial method: Alternatively, ice can be increased with the intention to last at least two summer seasons, i.e. the biennial method. For ice to reach the survival thickness of 2.18 m independently, an ice thickness of 1.42 m is necessary at the beginning of the second freezing season. This requires AIM to increase the ice to 3.6 m. This two year method can increase the September ice extent and to neutralize the volume decrease, a coverage of approximately 227 000 km^2 is required. To obtain this thickness, a significant amount of AIM is necessary. Initial ice thicknesses of 0.6 m and 1 m require 2.74 m and 2.43 m respectively and this corresponds with water volumes of 621 and 551 km^3. The implementation of the biennial method is shown in Figure 7.1b. Since the natural ice growth is not sufficient to reach the survival thickness again, this two year method is required yearly to continuously increase the September ice volume. At the same time, the AIM contribution is significant and the effectiveness and feasibility is questioned as the thermodynamic equilibrium thickness of 3 m is exceeded. Noteworthy, the thermodynamic equilibrium is related to ice growth at the ice-ocean interface and can be exceeded by AIM.

Thermodynamic equilibrium method: Considering feasibility, AIM can be applied for ice thicknesses to reach the thermodynamic equilibrium of 3 m. For an initial ice thickness of 0.6 m and 1.0 m, this requires 2.09 and 1.8 m AIM respectively as shown in Figure 7.1c. At the end of the first melting season, an ice thickness of 0.82 m is expected. To compensate the Arctic ice volume loss, AIM should cover approximately 393 000 km^2, which corresponds with roughly 12% of the average September ice area (2010-2020) and 3% of the average March ice area (2010-2020). The required water volume equals 821 and 707 km^3 respectively.

Predefined target method, 0.5 m: A last option is targeting a predefined summer ice thickness. For indicative purposes, a target thickness of 0.5 m is considered. This requires an ice thickness of 2.68 m at the end of winter, which corresponds with 1.70 and 1.44 m AIM for initial ice thicknesses of 0.6 m and 1 m. To counteract the volume loss, the AIM should cover 644 000 km^2, which corresponds with approximately 20% of the average September ice area (2010-2020) and 5% of the average March ice area (2010-2020). Figure 7.1d shows the implementation of AIM for 0.6 m and 1.0 m initial ice thickness, which corresponds with required water volumes of 1095 and 927 km^3.

Table 7.1: An example of ice thicknesses at the end of successive freezing seasons (FS) and melting seasons (MS) for different AIM methods in the Beaufort Sea considering 2750 FDD per winter.

	FS 1	MS 1	FS 2	MS 2	FS 3
No AIM FYI	1.6 m	0 m	1.6 m	0 m	1.6 m
Annual method FYI	2.18 m	0 m	1.6 m	0 m	1.6 m
Biennial method FYI	3.6 m	1.42 m	2.18 m	0 m	1.6 m
Thermodynamic equilibrium method FYI	3.0 m	0.82 m	1.83 m	0 m	1.6 m
Predefined target method FYI, 0.5 m	2.68 m	0.5 m	1.70 m	0 m	1.6 m

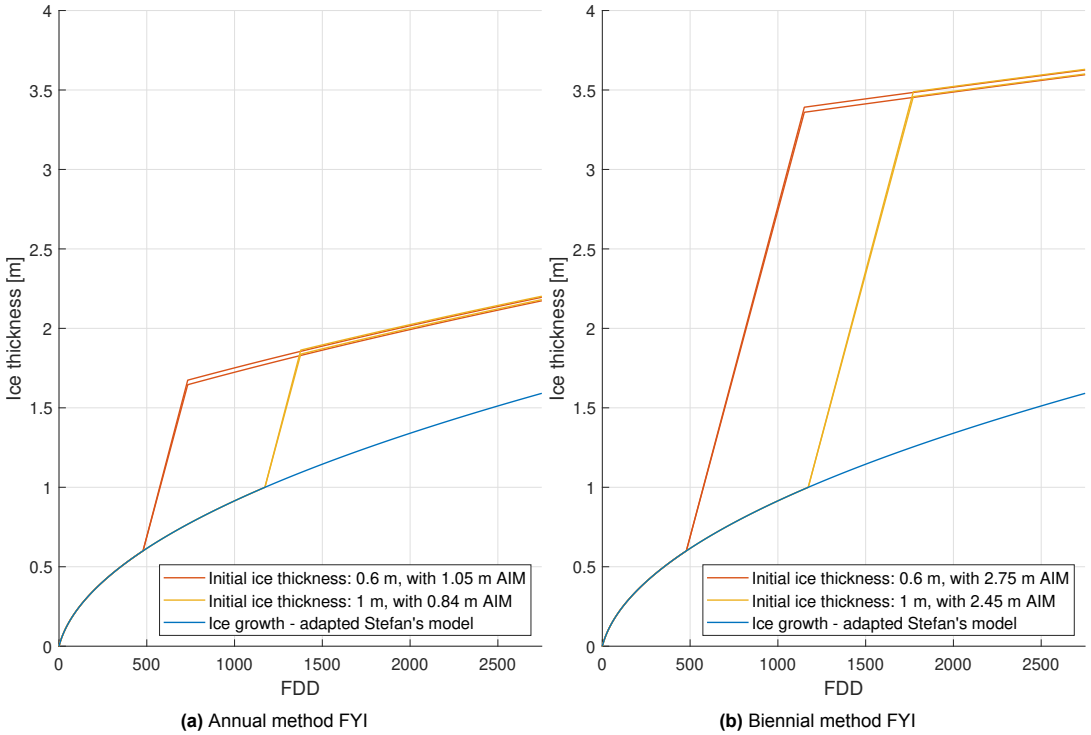

(a) Annual method FYI

(b) Biennial method FYI

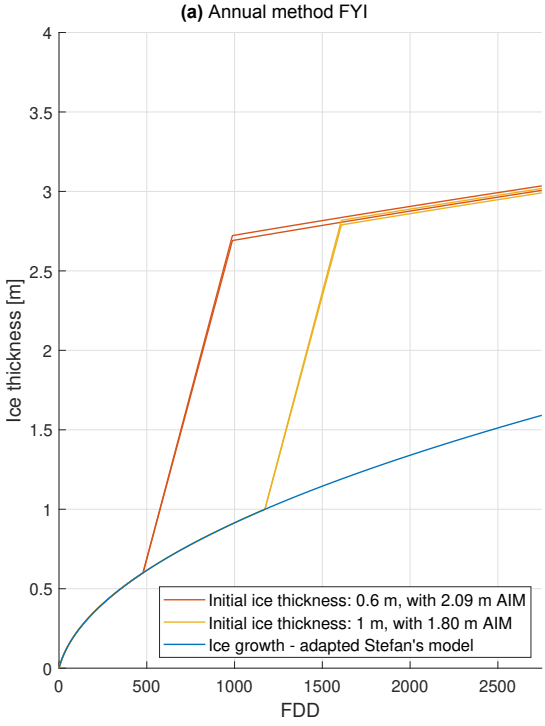

(c) Thermodynamic equilibrium method FYI

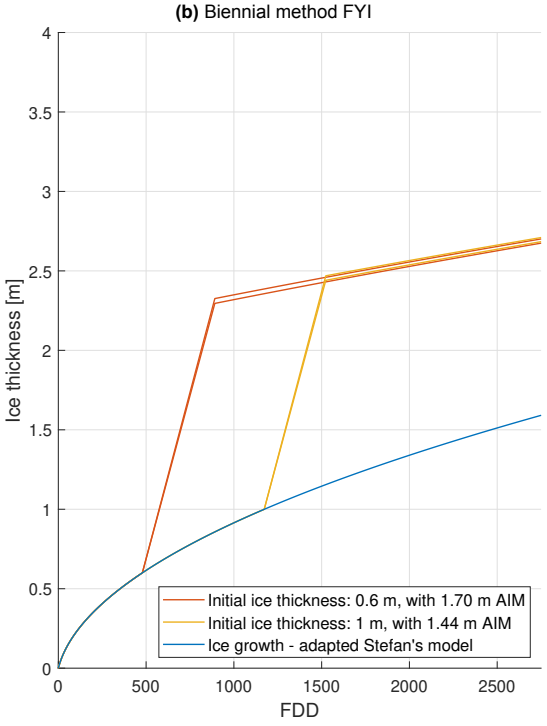

(d) Predefined 0.5 m target for FYI

Figure 7.1: Possible AIM methods in the Beaufort Sea considering 2750 FDD

7.1.2. AIM in the Transpolar Drift for FYI

To analyse the possible AIM methods in the Transpolar Drift, the average survival thickness of 1.0 m is assumed. Considering this survival thickness and a defined number of FDD of 2750, seasonal ice growth would suffice to reach the survival thickness. However, this research focuses on increasing ice which would normally not survive the summer season. For this reason, the AIM model is simulated for 1175 FDD, which corresponds with a naturally feasible ice thickness of 1.0 m. Additionally, ice drift patterns indicate the ice leaving through Fram Strait in one to two years depending on the exact latitude of AIM implementation. To explore the possibilities, the implementation is assumed Northwards in the Transpolar Drift, so the ice stays within the Arctic for two years. For these reasons, two different predefined target methods with initial ice thicknesses of 0.6 and 0.8 m are elaborated. Table 7.2 shows the ice thicknesses throughout each method and the ice is assumed to leave the Arctic between the second melting season and third freezing season. For this reason, it is unlikely that the increased ice directly contributes to the formation of MYI on the long term.

Predefined target method, 0.75 m: To obtain a target value of 0.75 m at the end of the melting season, AIM is used to create a 1.75 m ice thickness. Considering initial ice thicknesses of 0.6 and 0.8 m, 1.02 and 0.9 m AIM are required as shown in Figure 7.2a. To counteract the volume loss of 322 km^3, AIM should cover approximately 429 000 km^2, which is approximately 13.5% of the average September ice area (2015-2020) and 3.5% of the average March ice area (2015-2020). To obtain this, a water volume of 438 and 386 km^3 is required respectively. Furthermore, the ice is expected to enter the Greenland Sea where it will melt completely between the second melting season and third freezing season, therefore the method is required on a yearly basis.

Predefined target method, 0.5 m: To see the effect of reducing the target thickness, the AIM is simulated to obtain a winter thickness of 1.5 m, which results in a summer thickness of 0.5 m. Initial ice thicknesses of 0.6 and 0.8 m are considered again, which requires AIM thicknesses of 0.72 and 0.63 m as shown in Figure 7.2b. To counteract the annual volume loss, the necessary coverage equals 644 000 km^2 and this corresponds with water volumes of 657 and 580 km^3 respectively. Comparing this to the same predefined target method in the Beaufort sea shows that the water requirements for the same primary result is significantly less in the Transpolar Drift.

Table 7.2: An example of ice thicknesses at the end of successive freezing seasons (FS) and melting seasons (MS) for different AIM methods in the Transpolar Drift considering 1175 FDD per winter. The values written in italics are uncertain due to the exact moment of ice export.

	FS 1	MS 1	FS 2	MS 2	FS 3
No AIM FYI	1.0 m	0 m	1.0 m	*0 m*	*1.0 m*
Predefined target method FYI, 0.75 m:	1.75 m	0.75 m	1.30 m	*0.3 m*	*1.07 m*
Predefined target method FYI, 0.5 m:	1.5 m	0.5 m	1.16 m	*0.16 m*	*1.03 m*

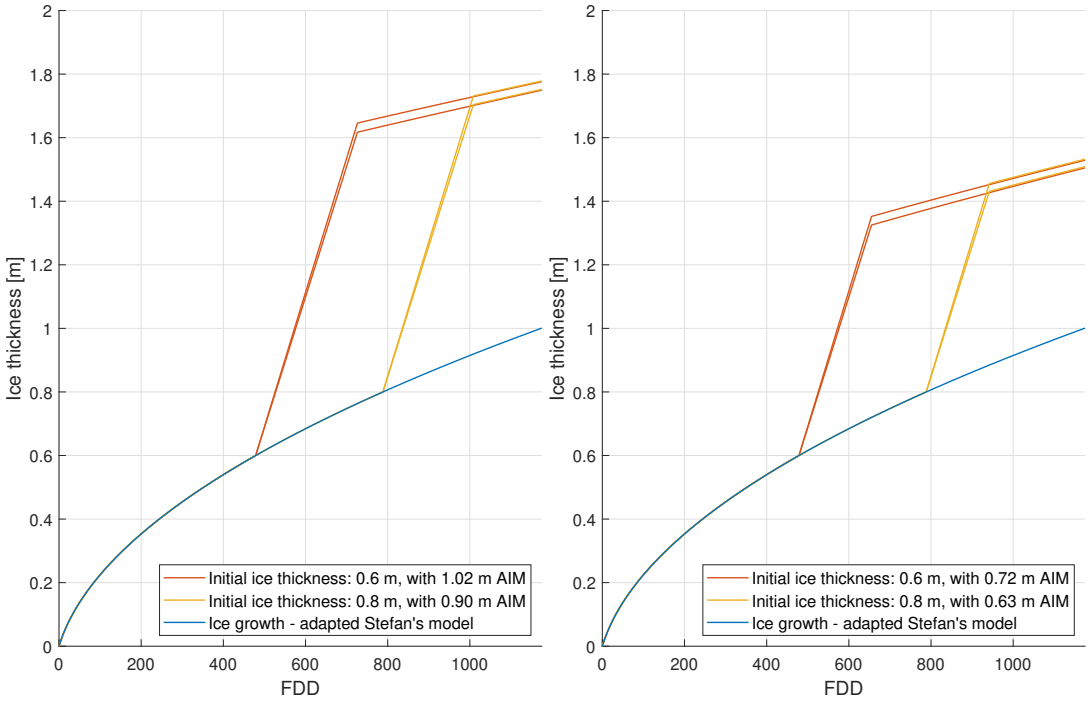

(a) Predefined 0.75 m target for FYI

(b) Predefined 0.5 m target for FYI

Figure 7.2: Requirements for possible AIM methods in the Transpolar Drift considering 1175 FDD

7.1.3. AIM for multi-year ice

Furthermore, MYI also offers possibilities for AIM. However, analysing the options for AIM implementation is more complex, because the initial conditions are varying. Basically, depending on the available ice thicknesses and the desired results, AIM can be applied accordingly.

Considering the results obtained during this research some remarks can be made for the implementation of AIM on MYI. To reach the survival thickness in the Beaufort Sea, it is unnecessary to increase ice with a thickness of 1.7 to 1.85 m or more at the beginning of the freezing season. On the other hand, increasing MYI with an initial ice thickness of 1.4 m or higher at the beginning of the freezing season is advantageous, because the reduction in effectiveness of AIM is minimal. However, the thermodynamic equilibrium should be considered.

Preferably, AIM is combined for both FYI and MYI to achieve optimal results. Based on the initial ice conditions, several AIM implementation plans can be simulated to define the most effective results concerning added ice volume. It is recommended to simulate this using a coupled climate model or standalone ice model, to account for secondary effects as well.

7.2. Structural requirements

Section 7.1 shows possible methods for AIM implementation. To obtain these results, there are certain requirements for the offshore installations concerning necessary pumps and energy. For feasibility reasons, seawater lift pumps are considered as reference, which are currently used in the offshore industry. The capacity of a pump can reach up to 15 000 m^3hr^{-1}, assuming a height of 10 meter this requires approximately 420 kW. Due to efficiencies the actual required power might be higher, on the other hand reducing the height can significantly reduce the required power. An overview of requirements for AIM implementation concerning water volume, number of pumps and energy is shown in Table 7.3. The results give an indication of how the water volume, hence the number of pumps and required energy, varies for different AIM methods. First of all, the table shows that the necessary water volume in the Beaufort Sea is significantly higher than in the Transpolar Drift. Additionally, the water volume decreases for thicker initial ice. At last, reducing the desired winter thickness will increase the necessary coverage to compensate the annual volume loss and results in a water volume increase.

Each pump can be installed as an individual structure, as considered by Desch et al. [2017]. However, in the offshore industry, several seawater lift pumps are installed on one offshore structure, which

is also possible for AIM implementation. The number of offshore structures mainly depends on the achievable coverage of each installation. How to cover large areas with AIM is not discussed in this research, but is expected to depend on the flow rate and the flow duration before the water freezes. Additionally, pumping, storing en distributing water at near freezing temperatures can be challenging. Desch et al. [2017] already suggested to look at comparable existing systems, for example the supply of drink water during the Arctic winter. Furthermore, the AIM structures need to be positioned in locations with suitable ice availability. If the desired AIM thickness is achieved or as the result of ice dynamics, the AIM structure should preferably move or be moved. For this reason, a floating structure with its own propulsion system (a ship) or a floating structure which can easily be towed is recommended. At the same time, the structure should be able to withstand possibly harsh ice conditions.

7.3. Effects of Arctic ice management

Our aim is to counteract the annual ice volume loss using Arctic ice management. Additionally, increasing the ice coverage also contributes to reflecting insolation (solar radiation management). Section 7.3.1 discusses the contribution of AIM to solar radiation management. The possible side effects of AIM are mentioned in Section 7.3.2.

7.3.1. Contribution to solar radiation management

Our aim is the counteract the annual Arctic sea ice volume loss. An illustrative representation of the direct effect of AIM on the ice volume is shown in Figure 7.3a. The added volume increases during the winter and reaches the maximum increase in April after which the increase stays constant during the summer. When the freezing seasons starts again, AIM can be used to generate new ice volume. Additionally, the ice increased in the previous winter also contributes to an ice volume increase. However, this contribution reduces over time, because ice formation would have occurred in a scenario without AIM. When AIM is implemented every year, the ice volume is expected to keep increasing.

Additionally, by counteracting the annual volume loss, the ice area is expected to increase during certain months of the year. An illustrative representation of how AIM can influence the ice area is shown in Figure 7.3b. The idea of the AIM installation is to increase the thickness of existing ice and not initiate new ice formation. In other words, the ice area during the winter is not increased due to AIM. When the melting season begins, ice starts melting at the edges of the ice cover, which is thin FYI and is most likely not increased using AIM (because AIM models have shown increasing thin ice is relatively ineffective). For this reason, the primary effect of AIM on the ice area during the first months of the summer is expected minor. During the second half of the summer, part of the ice that would have melted away has been increased and this contributes to the ice area. For our aim, the additional ice area is estimated to increase during the summer and is maximum during September and October. Afterwards, the added area is expected to decrease over time and it is questioned if AIM directly contributes to the maximum winter ice area. However, the effects of AIM on solar radiation management have an indirect effect.

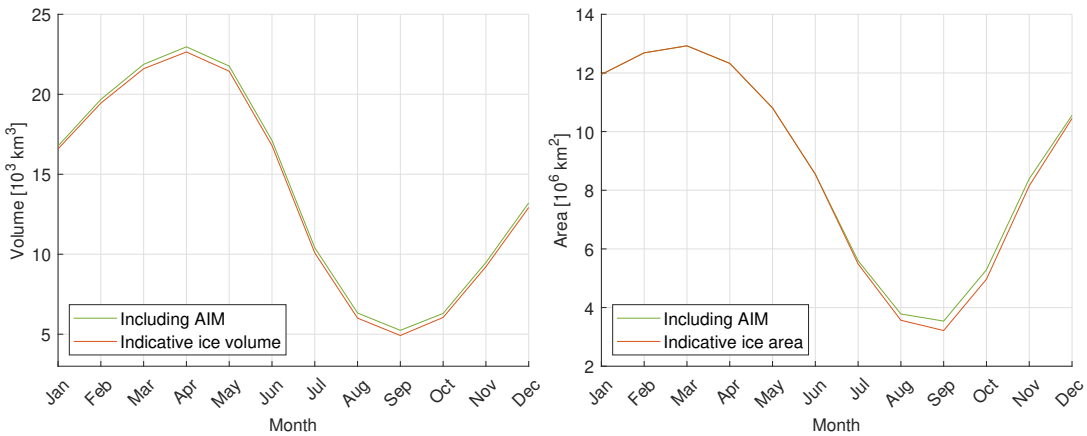

(a) Estimated effect of AIM on ice volume

(b) Estimated effect of AIM on ice area

Figure 7.3: Illustrative representation of the primary effect of AIM on the ice cover

How AIM is contributing to solar radiation management can be expressed in terms of reduced absorbed energy (or increased reflected energy) or in radiative forcing. To calculate the effects of AIM during the year of implementation, the formulae as introduced in Chapter 2.3.2 are used. A scenario including AIM is compared to a scenario without AIM to compare the energy absorption. For the scenario without AIM, the monthly average ice areas during the period 2015-2020 are considered. The scenario including AIM has an increased ice area depending on the AIM method and the interpretation of area increase as shown in Figure 7.3b. Furthermore, an average declination angle of 9° is considered and an average cloud fraction of 0.8. At last, the albedo for ice, land and open ocean is taken as 0.6, 0.78 and 0.06 respectively. The results concerning radiation absorption and radiative forcing for various AIM methods are shown in table 7.3. Depending on the method, the regional absorbed energy can be reduced with 0.7 to 1.2%. This reduction due to the increased coverage might not seem significant. However, the simulations by Caldeira & Wood [2008] show that a regional reduction of 10% can already limit the Arctic temperature increase to +0.68 K instead of +3.46 K without insolation reduction (in a 560 ppm climate relative to a 280 ppm climate). These values are indicative, but emphasizes the impact regional insolation reduction can have on regional temperatures. Alternatively, the impact of AIM can be expressed in terms of effective radiative forcing (ERF). The effective radiative forcing is calculated as the difference in energy absorbed in the Arctic with and without AIM averaged over one year and the Earth's surface. A negative ERF indicates a cooling effect and a positive ERF indicates a warming effect. As expected, increasing the ice coverage during the summer results in negative ERF (i.e. cooling). The IPCC states that the total human-caused radiative forcing in 2019 relative to the pre-industrial state (1750) was +2.72 W m^{-2} with an increasing rate since the 1970s [IPCC, 2021]. Considering recent years, these methods suggests the additional ice area could have compensated approximately 0.98 to 1.6% of the human-caused ERF during the period 2006-2018 (+0.79 W m^{-2}).

Our aim to counteract the annual Arctic sea ice loss does not primarily focus on solar radiation management. To maximise solar radiation management, AIM should target the ice area throughout the summer instead of the September ice volume. By reducing the desired summer thickness and by increasing the coverage, the regionally absorbed energy can be reduced.

These calculations do not include the possible impact of producing and operating AIM devices, the ERF equivalent of production and operation is not calculated in this research. However, for a similar concept Desch et al. [2017] concludes the benefits of increasing the ice cover outweigh the estimated CO_2 release due to steel production, shipping of materials and other industrial processes.

Table 7.3: Overview of requirements for AIM implementation to counteract the annual sea ice volume loss and the primary effects on SRM

Method	Beaufort Sea		Transpolar Drift	
	Thermodynamic equilibrium	**0.5 m target**	**1.0 m target**	**0.5 m target**
Obtained winter thickness	3.0 m	2.68 m	1.75 m	1.5 m
Result summer thickness	0.82 m	0.5 m	0.75 m	0.5 m
Necessary coverage to compensate volume loss	393 000 km^2	644 000 km^2	429 000 km^2	644 000 km^2
	H_i=0.6 m	*H_i=0.6 m*	*H_i=0.6 m*	*H_i=0.6 m*
AIM thickness	2.09 m	1.70 m	1.02 m	0.72 m
Water volume	821 km^3	1095 km^3	438 km^3	464 km^3
Pumps	12500	16700	6670	7058
Power	5.2 GW	7.0 GW	2.8 GW	3.0 GW
	H_i=1.0 m	*H_i=1.0 m*	*H_i=0.8 m*	*H_i=0.8 m*
AIM thickness	1.80 m	1.44 m	0.9 m	0.63 m
Water volume	707 km^3	927 km^3	386 km^3	406 km^3
Pumps	10800	14100	5880	6175
Power	4.5 GW	5.9 GW	2.5 GW	2.6 GW
Effects of the additional ice area in first year of implementation				
Regional absorbed energy	-0.72%	-1.2%	-0.78%	-1.2%
Effective radiative forcing	-0.008 W m^{-2}	-0.013 W m^{-2}	-0.008 W m^{-2}	-0.013 W m^{-2}
Effect on human-caused ERF 2006-2018 (+0.79 Wm^{-2})	-0.98%	-1.61%	-1.07%	-1.61%
Effect on human-caused ERF 1750-2019 (+2.72 Wm^{-2})	-0.29%	-0.47%	-0.31%	-0.47%

7.3.2. Possible side effects of AIM

The use of AIM can bring side effects. Some of the side effects are discussed hereafter, however there are possibly more side effects still undefined. First of all, as mentioned by Desch et al. [2017], the surface temperature warms due to freezing of the additional layer of water. Similarly, Zampieri & Goessling [2019] show an increase in temperature during the winter at locations with simulated AIM installations, but also a direct cooling effect during summer due to both increased latent heat absorption (ice melting) and indirect reduced solar radiative heating (increased surface albedo).

Secondly, effects are expected during ice growth. The AIM installation distributes water over the existing ice cover and will flood the existing snow layer. This reduces the insulating effect of the snow layer, but simultaneously creates a blanketing effect as discussed in Chapter 6. When considering existing literature, the natural process most comparable is the flooding of ice due to a thick snow layer, which creates a layer of snow-ice. Lepparanta [1983] analyses the growth of snow ice and uses half of the ice thermal conductivity for the thermal conductivity of snow ice (frozen slush). Alternatively, Maksym & Jeffries [2001] assume the thermal conductivity of slush as the weighted average of the Maxwell bounds [Kaviany, 1991]. Typically, observed situations of snow ice due to flooding contain 30-50% of snow [Maksym & Jeffries, 2001]. When snow ice is formed using AIM, the fraction of entrained snow is still unknown, and depends on the flow rate of the installation. For this reason the actual thermal conductivity of AIM ice is expected to vary with snow and water fraction.

In third place, there is a possible effect on the salinity of ice. During the process of natural ice growth, the ice decreases in salinity due to formation and rejection of brine pockets. Due to AIM, a new saltier layer is added on top, which will similarly drain the brine. The effect of this might be compared to the natural flooding of ice. Maksym & Jeffries [2001] state the permeability of the underlying ice layer strongly influences the brine drainage by convection. They suggest the salinity increase of the original ice layer might be minimal. This process is expected similar to the effect by AIM, but might be influenced by the flow rate. The possible change in the salinity profile and the increased formation of drainage channels might influence the melt rate and ice strength.

The last effect of AIM discussed also concerns ice decay. Throughout the winter, the existing ice is flooded by the AIM installation. As discussed above, this reduces the natural snow layer present at the beginning of the melting season. During this time of year, snow is known for its high insulating effect which delays the melt of sea ice. A reduced snow layer due to AIM might therefore effect the start of the melting process. Additionally, AIM might change the ice properties which can affect the melting rate.

Besides these effect, AIM might influence biological and chemical processes. For example, Miller et al. [2020] mention a possible increase in gas and aerosol release into the atmosphere, increased brine release in the ocean, reducing photosynthesis by blocking more sunlight and introducing algae in between the original and added ice layer. As mentioned in Chapter 2.3.2, the model by Zampieri & Goessling [2019] show that the ice extent and volume return to their natural state within 10 years, if AIM is ended. This can minimise the side effects of AIM in case of (unforeseen) negative consequences. This paper will not further elaborate these and possible other biological and chemical effects and this is recommended for further research.

8 Conclusion

The Arctic ice cover is decreasing, which not only shows the effects of climate change but is also driving climate change Euskirchen et al. [2013]. In literature several approaches have been mentioned to minimise Arctic amplification. This research has focused on using Arctic ice management (AIM), a solar radiation management technique, to counteract the annual Arctic sea ice loss. Building on the findings for AIM by Desch et al. [2017], this research investigates the required water volume to be distributed on top of sea ice to counteract the annual Arctic sea ice volume loss. To find an answer, five driving aspects are distinguished: Annual Arctic sea ice loss, drift of sea ice, survival ice thickness, effect of natural ice growth and ice growth including AIM.

First of all, the annual Arctic sea ice loss should be expressed in terms of a measurable parameter and value. The annual loss can be defined in either ice extent, ice area or ice volume. All show their maximum relative loss in September, with trends of -83 400 km^2yr^{-1} (-1.19%), -49 200 km^2yr^{-1} (-1.03%) and -322 km^3yr^{-1} (-2.23%) respectively during the period 1979-2020 and relative to the 1979-1996 average. To account for both the absolute ice loss and the overall decreasing thickness of the ice cover, ice volume loss is selected as the target value. Ideally, the ice cover is capable to maintain itself on the long term without AIM. Based on simple calculations and the model by Zampieri & Goessling [2019] for respectively a 560 ppm CO_2 and RCP8.5 scenario, it is questionable if the ice cover can maintain itself after AIM. It is expected that additional solar radiation management and/or negative emission technologies are required for these cases. However, taking The Paris Agreement into account, the greenhouse gas emission are expected to be diminished in the future, enhancing the capabilities of maintaining the ice cover without AIM.

Secondly, the Arctic ice is in constant motion allowing natural processes to enhance or diminish the AIM effects. Literature shows two main long-term ice motions in the Arctic induced equally by the geostrophic wind and current: The Beaufort Gyre and the Transpolar Drift. However, on shorter time scale, 70% of the ice motion is due to the geostrophic wind and the ice motion is highly fluctuating. Considering the main circulation patterns, ice located in the Beaufort Sea generally follows the Beaufort Gyre and is expected to remain in the Arctic for approximately 5 years. In contrast to ice in the Transpolar Drift, which is usually exported within 1 to 2 years through Fram Strait. Besides circulation patterns, the Barents Sea experiences Atlantification which can cause increased ice melt. For these reasons, natural processes south in the Transpolar Drift can have a negative impact on the AIM implementation.

In third place, the survival ice thickness is a fundamental aspect for AIM. The energy balance method proves accurate for ice located in the Beaufort Sea, but over-predicts the ice decay in the Transpolar Drift. Additionally, detailed time and location dependent temperature and cloud coverage forecasts are necessary, which complicates future predictions. Alternatively, an empirical approach shows location based consistency for measurements of the Ice Mass Balance (IMB) Buoy program. The available data shows ice decay between -2.1 and -2.7 cm day^{-1} in the Beaufort Sea and between -0.8 and -1.4 cm day^{-1} in the Transpolar drift. Considering 91 melting days, this results in a survival thickness of 1.91 to 2.46 m and 0.73 to 1.27 m respectively. The difference in ice decay is expected to be the result of differences concerning latitude, oceanic heat flux and snow conditions between the two locations.

Thereafter, natural ice growth indicates the necessary thickness increase. The number of freezing degree days (FDD) for the past 10 years vary between 2500 to 3000 FDD. This allows the growth of first-year ice (FYI) between 1.5 to 1.7 m, but might deviate depending on the moment freezing begins and snow conditions. This exceeds the survival thickness defined for ice in the Transpolar Drift, indicating that ice can survive the melting season naturally. However, snow free conditions are not realistic and the natural achievable ice thickness is expected lower. Additionally, the ice growth rate suggests at

least 0.6 m ice thickness prior to AIM to maintain the fast initial growth rate. Furthermore, the Arctic thermodynamic equilibrium thickness of 3 m can provide an upper limit for AIM implementation.

For the last aspect, a theoretical model of ice growth including AIM is generated to show the effective ice thickness increase. The model is based on Stefan's law and AIM is modelled using an upper and lower limit scenario. Small scale experiments are used for validation and a delay between the flooding phase and the resumed natural ice growth is observed. This causes the experimental results to follow the lower limit scenario. This delay is confirmed by simulations with COMSOL Multiphysics, which indicates additional time is required after the flooding phase to restore the temperature profile. Additionally, the time required for the two ice layers to fully merge can contribute to the delay observed. Based on these findings, AIM is expected to follow the lower limit scenario of the AIM model. The effective ice thickness increase depends on the AIM thickness and increases with thicker initial ice with a maximum effective increase directly after the flooding phase. Due to the growth rate of natural ice, it is discouraged to apply AIM on ice thicknesses below 0.6 m and encouraged for ice thicknesses approaching 1.0 m or higher. Nevertheless, AIM results in an effective increase regardless of initial ice thickness and freezing duration after AIM.

Finally, the combination of all aspects show the possibilities for AIM implementation. Several location dependent methods are elaborated, which all have different requirements. For the Beaufort Sea the necessary water volume varies between 707 and 1095 km^3, and between 386 and 464 km^3 in the Transpolar Drift. The expected energy requirements range from 4.5 to 7.0 GW and 2.5 to 3.0 GW respectively. These methods show the possibilities to counteract the annual volume loss, but indicate AIM has to stay operable to continuously do so. Additionally, the average summer ice area increases for each method, which directly contributes to solar radiation management. Depending on the location and AIM method considered, the regional absorbed energy can be decreased with approximately 0.7 to 1.2%, which corresponds with an effective radiative forcing of -0.008 to -0.013 W m^{-2}. Based on these findings, this research suggests the additional ice area could have compensated 0.98% to 1.6% of the total human-caused effective radiative forcing during the period 2006-2018. However, to maximise the effect of AIM on solar radiation management, the aim should be changed from counteracting volume loss to maximising summer ice area. For each intention, the location dependent survival thickness and AIM model as developed in this research can be used to determine the required water volume to increase the Arctic ice cover as desired.

9 Discussion

This chapter starts with highlighting the relevance of this research in Section 9.1. This is followed by the limitations in Section 9.2. Finally, Section 9.3 shows the recommendations for further research.

9.1. Relevance of the results

Climate models have predicted that all Arctic seas become ice free during the summer months in the 2020s and that the central Arctic reaches this stage in the 2040s. Since the decreasing ice cover not only shows the effects of climate change, but also drives climate change, AIM offers a solution to extent the ice availability. The results shown in this research can be used to prove the effectiveness of AIM. With the increased warming in the Arctic region, local solar radiation management can offer interesting possibilities concerning local temperature reduction, resulting in both local and global benefits. Regardless if AIM can neutralize the annual Arctic sea ice volume loss, this research suggests AIM can increase the ice availability throughout the summer and reduce the regionally absorbed energy. Furthermore, both the location dependent survival ice thickness and AIM model developed in this research can easily be used to explore AIM implementation for other intentions. For example, to show the possibilities of AIM implementation to maximise solar radiation management.

9.2. Limitations of the results

This research has some limiting factors concerning the results of AIM implementation. First of all, a general limiting factor is neglecting secondary effects. The research focuses on neutralizing the annual Arctic ice volume loss and only the effects directly contributing to the ice volume are considered. This neglects the possible secondary effects of temperature decrease due to additional reflection of solar radiation, accelerated ice growth near the increased ice cover or earlier development of initial ice due to cooler water temperatures. These effects can increase the impact of AIM or contribute to minimising the Arctic amplification without directly increasing the September ice volume.

Secondly, the ice decay data considered in this research lacks information of ice thicknesses below 0.5 m. Literature studies have suggested faster ice melt for thin ice in combination with large melt ponds and low albedo. The missing data of complete ice melt can influence the obtained trends.

Furthermore, ice dynamics are only discussed to indicate the main drifting routes and the effect this has on the AIM location selection. However, ice dynamics can influence the natural ice thickness due to ice-ice interaction. This is not included in the obtained and resulting ice thicknesses of the AIM implementation methods and the actual ice thicknesses after AIM can deviate.

At last, the AIM model and the effective ice increase obtained do not account for the possible presence of snow. When ice covered with snow is flooded, some mixture of ice, snow and water will form. This is likely to affect the ice properties and therefore possibly the AIM results.

9.3. Recommendations

Based on the findings in this research, several subjects for further in-depth or extended research have appeared.

First of all, it is recommended to confirm the AIM model with large(r) scale experiments. Mainly the duration of the delay observed between the flooding phase and continued ice growth is of interest. When the recovery time of the temperature profile does not proportionally increase, AIM is expected to follow the lower limit scenario for large(r) scales. Additionally, these experiments can be used to

research if the ice properties change due to AIM. Especially, the possible effects on ice decay and ice strength are expected relevant.

Secondly, implementing AIM in a sea ice model (for example CICE) can allow for incorporation of ice dynamics. Usage of a sea ice model can improve the location selection for implementation of AIM based on current ice availability and can be used to predict the direct effect of AIM on the ice cover for different seasons. Additionally, implementation in coupled climate models can express both direct and secondary effects of AIM for different time scales. This creates the opportunity to compare the effects of the different AIM methods discussed in this research and opens the opportunity for a strategic analysis for the implementation of AIM for FYI and MYI simultaneously.

Furthermore, the results in this research have shown the impact of snow conditions on ice decay. The start of ice melt can generally be identified as the moment when the snow layer had disappeared. This suggests extending the presence of snow or increasing the snow thickness can decrease the number of melting days and hence shorten the melting duration. For this reason, the effects of snow conditions on ice decay and the possibilities to decrease ice decay using snow are recommended for further research.

References

Abels, G. (1892). Measurement of the snow density at Ekaterinburg during the winter of 1890-1891. *Academia Nauk*, *19*.

Anderson, D. L. (1961). Growth rate of sea ice. *Journal of Glaciology*, *3*(30), 1170–1172.

Arctic Monitoring and Assessment Programme (AMAP). (1998). AMAP Assessment Report: Arctic Pollution Issues. *AMAP Assessment Report: Arctic Pollution Issues*, 1–8. Retrieved from https://oaarchive.arctic-council.org/handle/11374/924

Årthun, M., Eldevik, T., Smedsrud, L. H., Skagseth, & Ingvaldsen, R. B. (2012, 7). Quantifying the Influence of Atlantic Heat on Barents Sea Ice Variability and Retreat. *Journal of Climate*, *25*(13), 4736–4743. doi: 10.1175/JCLI-D-11-00466.1

Årthun, M., Onarheim, I. H., Dörr, J., & Eldevik, T. (2021, 1). The Seasonal and Regional Transition to an Ice-Free Arctic. *Geophysical Research Letters*, *48*(1). doi: 10.1029/2020GL090825

Ashton, G. D. (1983, 6). Predicting Lake Ice Decay. *CRREL Report 83-19*.

Barry, R. G., Serreze, M. C., Maslanik, J. A., & Preller, R. H. (1993). The Arctic Sea Ice□Climate System: Observations and modeling. *Reviews of Geophysics*, *31*(4), 397–422. doi: 10.1029/93RG01998

Berdahl, M., Robock, A., Ji, D., Moore, J. C., Jones, A., Kravitz, B., & Watanabe, S. (2014, 2). Arctic cryosphere response in the geoengineering model intercomparison project G3 and G4 scenarios. *Journal of Geophysical Research*, *119*(3), 1308–1321. doi: 10.1002/2013JD020627

Bilello, M. A. (1961). Formation, Growth, and Decay of Sea-Ice in the Canadian Arctic Archipelago. *ARCTIC*, *14*(1). doi: 10.14430/arctic3658

Bilello, M. A. (1980). Maximum thickness and subsequent decay of lake, river and fast sea ice in Canada and Alaska. *CRREL Report 80-6*.

Box, J. E., Fettweis, X., Stroeve, J. C., Tedesco, M., Hall, D. K., & Steffen, K. (2012). Greenland ice sheet albedo feedback: thermodynamics and atmospheric drivers Greenland ice sheet albedo feedback. *TCD*, *6*, 593–634. doi: 10.5194/tcd-6-593-2012

Caldeira, K., & Wood, L. (2008, 11). Global and Arctic climate engineering: numerical model studies. *Philosophical Transactions of the Royal Society A: Mathematical, Physical and Engineering Sciences*, *366*(1882), 4039–4056. doi: 10.1098/rsta.2008.0132

Cavalieri, D. J., C. L. Parkinson, P. Gloersen, & H. J. Zwally. 1996. (1996). *Sea Ice Concentrations from Nimbus-7 SMMR and DMSP SSM/I-SSMIS Passive Microwave Data, Version 1.* Boulder, Colorado USA: NASA National Snow and Ice Data Center Distributed Active Archive Center. doi: https://doi.org/10.5067/8GQ8LZQVL0VL

Cavalieri, D. J., & Parkinson, C. L. (2012, 8). Arctic sea ice variability and trends, 1979–2010. *The Cryosphere*, *6*(4), 881–889. doi: 10.5194/tc-6-881-2012

Colony, R., & Thorndike, A. S. (1984). An estimate of the mean field of Arctic sea ice motion. *Journal of Geophysical Research*, *89*(C6), 10623. doi: 10.1029/JC089IC06P10623

Colony, R., & Thorndike, A. S. (1985). Sea ice motion as a drunkard's walk. *Journal of Geophysical Research*, *90*(C1), 965–974. doi: 10.1029/JC090IC01P00965

Comiso, J. C. (2001). Satellite-observed variability and trend in sea-ice extent, surface temperature, albedo and clouds in the Arctic. *Annals of Glaciology*, *33*. doi: 10.3189/172756401781818617

Comiso, J. C. (2002, 10). A rapidly declining perennial sea ice cover in the Arctic. *Geophysical Research Letters*, *29*(20). doi: 10.1029/2002GL015650

Comiso, J. C. (2012, 2). Large Decadal Decline of the Arctic Multiyear Ice Cover. *Journal of Climate*, *25*(4), 1176–1193. doi: 10.1175/JCLI-D-11-00113.1

Croll, J. (1875, 6). Climate and Time in their Geological Relations; a theory of Secular Changes of the Earth's Climate. *Nature*, *12*(295), 141–144. doi: 10.1038/012141a0

Crook, J. A., Forster, P. M., & Stuber, N. (2011, 7). Spatial patterns of modeled climate feedback and contributions to temperature response and polar amplification. *Journal of Climate*, *24*(14), 3575–3592. doi: 10.1175/2011JCLI3863.1

Danish Meteorological Institute. (n.d.). *Sea Ice Thickness and Volume.* Retrieved from http://polarportal.dk/en/sea-ice-and-icebergs/sea-ice-thickness-and-volume/

Day, J. J., Tietsche, S., Collins, M., Goessling, H. F., Guemas, V., Guillory, A., … Hawkins, E. (2016, 6). The Arctic Predictability and Prediction on Seasonal-to-Interannual TimEscales (APPOSITE) data set version 1. *Geoscientific Model Development*, *9*(6), 2255–2270. doi: 10.5194/GMD-9-2255-2016

Dee, D., & National Center for Atmospheric Research Staff (Eds). (2022). *The Climate Data Guide: ERA5 atmospheric reanalysis.* Retrieved from https://climatedataguide.ucar.edu/climate-data/era5-atmospheric-reanalysis

Desch, S. J., Smith, N., Groppi, C., Vargas, P., Jackson, R., Kalyaan, A., … Hartnett, H. E. (2017, 1). Arctic ice management. *Earth's Future*, *5*(1), 107–127. doi: 10.1002/2016EF000410

Docquier, D., Massonnet, F., Barthélemy, A., Tandon, N. F., Lecomte, O., & Fichefet, T. (2017, 12). Relationships between Arctic sea ice drift and strength modelled by NEMO-LIM3.6. *Cryosphere*, *11*(6), 2829–2846. doi: 10.5194/TC-11-2829-2017

Ekman, V. W. (1905). *On the influence of the earth's rotation on ocean-currents.* Almqvist & Wiksells boktryckeri, A.-B.,.

Emery, W. J., Fowler, C. W., & Maslanik, J. A. (1997). Satellite-derived maps of Arctic and Antarctic sea ice motion: 1988 to 1994. *Geophysical Research Letters*, *24*(8), 897–900. doi: 10.1029/97GL00755

EUMETSAT SAFs. (n.d.). *Sea ice products.* Retrieved from https://osi-saf.eumetsat.int/products/sea-ice-products

Euskirchen, E. S., Goodstein, E. S., & Huntington, H. P. (2013, 12). An estimated cost of lost climate regulation services caused by thawing of the Arctic cryosphere. *Ecological Applications*, *23*(8), 1869–1880. doi: 10.1890/11-0858.1

Fetterer, F., Knowles, K., Meier, W. N., Savoie, M., & Windnagel, A. K. (2017). *Sea Ice Index, Version 3. Monthly Data With Statistics.* Boulder, Colorado USA: NSIDC: National Snow and Ice Data Center.

Field, L., Ivanova, D., Bhattacharyya, S., Mlaker, V., Sholtz, A., Decca, R., … Katuri, K. (2018, 6). Increasing Arctic Sea Ice Albedo Using Localized Reversible Geoengineering. *Earth's Future*, *6*(6), 882–901. doi: 10.1029/2018EF000820

Flannery, B. P., Kheshgi, H., Marland, G., & Maccraken, M. C. (1997). Geoengineering Climate. In R. G. Watts (Ed.), *Engineering response to global climate change* (pp. 379–427).

Flato, G., Marotzke, J., Abiodun, B., Braconnot, P., Chou, S., Collins, W., … Rummukainen, M. (2013). Evaluation of Climate Models. In Stocker T.F. et al. (Eds.), *Ipcc, 2013: Climate change 2013: The physical science basis. contribution of working group i to the fifth assessment report of the intergovernmental panel on climate change* (chap. 9). Cambridge, New York: Cambridge University Press.

Fletcher, J. O. (1965). *The heat budget of the Arctic Basin and its relation to climate.*

Forsström, S., Gerland, S., & Pedersen, C. A. (2011). Thickness and density of snow-covered sea ice and hydrostatic equilibrium assumption from in situ measurements in Fram Strait, the Barents Sea and the Svalbard coast. *Annals of Glaciology*, *52*(57 PART 2), 261–270. doi: 10.3189/172756411795931598

Francis, J. A., & Wu, B. (2020, 11). Why has no new record-minimum Arctic sea-ice extent occurred since September 2012? *Environmental Research Letters*, *15*(11), 114034. doi: 10.1088/1748-9326/abc047

Freeman, J., Blunden, J., & Arndt, D. (2011, 2). State of the Climate in 2010. *Bulletin of the American Meteorological Society*, *92*, S180.

Fruchtzwerg's world. (2011). *morning wanderer | fruchtzwerg's world | Flickr.* Retrieved from https://www.flickr.com/photos/fruchtzwergsworld/6270013023/in/album-72157607376794097/

Goosse, H., Kay, J. E., Armour, K. C., Bodas-Salcedo, A., Chepfer, H., Docquier, D., … Vancoppenolle, M. (2018, 12). Quantifying climate feedbacks in polar regions. *Nature Communications*, *9*(1). doi: 10.1038/S41467-018-04173-0

Govindasamy, B., & Caldeira, K. (2000, 7). Geoengineering Earth's radiation balance to mitigate CO2-induced climate change. *Geophysical Research Letters*, *27*(14), 2141–2144. doi: 10.1029/1999GL006086

Hall, A. (2004, 4). The Role of Surface Albedo Feedback in Climate. *Journal of Climate*, *17*(7), 1550–1568. doi: 10.1175/1520-0442(2004)017<1550:TROSAF>2.0.CO;2

Hartmann, D. L. (2016). The Global Energy Balance. In D. L. Hartmann (Ed.), *Global physical climatology* (Second Edition ed., pp. 25–48). Boston: Elsevier. doi: 10.1016/B978-0-12-328531-7.00002-5

Herman, G. F., & Curry, J. A. (1984, 1). Observational and Theoretical Studies of Solar Radiation in Arctic Stratus Clouds. *Journal of Climate and Applied Meteorology*, *23*(1), 5–24. doi: 10.1175/1520-0450(1984)023<0005:OATSOS>2.0.CO;2

Hibler, W. D. (1979, 7). A Dynamic Thermodynamic Sea Ice Model. *Journal of Physical Oceanography*, *9*(4), 815–846. doi: 10.1175/1520-0485(1979)009<0815:ADTSIM>2.0.CO;2

Hibler, W. D., & Tucker, W. B. (1979, 1). Some Results from a Linear-Viscous Model of the Arctic Ice Cover. *Journal of Glaciology*, *22*(87), 293–304. doi: 10.3189/S0022143000014283

Hole, G. M., & Macias-Fauria, M. (2017, 9). Out of the woods: Driftwood insights into Holocene pan-Arctic sea ice dynamics. *Journal of Geophysical Research: Oceans*, *122*(9), 7612–7629. doi: 10.1002/2017JC013126

Høyland, K. V. (2021). *Ice actions on structures [Class handout].* Norwegian University of Science and Technology (NTNU), TBA4260.

Hunke, E. C. (2010, 1). Thickness sensitivities in the CICE sea ice model. *Ocean Modelling*, *34*(3-4), 137–149. doi: 10.1016/j.ocemod.2010.05.004

Hunke, E. C., Lipscomb, W. H., Turner, A. K., Jeffery, N., & Elliott, S. (2015). *CICE: the Los Alamos Sea Ice Model Documentation and Software User's Manual Version 5.1 LA-CC-06-012.*

IBRU Durham University. (n.d.). *Arctic Maps Series - Durham University.* Retrieved from https://www.durham.ac.uk/research/institutes-and-centres/ibru-borders-research/maps-and-publications/maps/arctic-maps-series/

IPCC, Masson-Delmotte, V., Zhai, P., Pirani, A., Connors, S., Péan, C., … Zhou, B. (2021). Summary for Policymakers. *Climate Change 2021: The Physical Science Basis. Contribution of Working Group I to the Sixth Assessment Report of the Intergovernmental Panel on Climate Change*, 3–32.

Kaviany, M. (1991). *Principles of Heat Transfer in Porous Media*. New York, NY: Springer US. doi: 10.1007/978-1-4684-0412-8

Kwok, R., Cunningham, G. F., Wensnahan, M., Rigor, I., Zwally, H. J., & Yi, D. (2009, 7). Thinning and volume loss of the Arctic Ocean sea ice cover: 2003–2008. *Journal of Geophysical Research*, *114*(C7), C07005. doi: 10.1029/2009JC005312

Kwok, R., Kacimi, S., Webster, M. A., Kurtz, N. T., & Petty, A. A. (2020, 3). Arctic Snow Depth and Sea Ice Thickness From ICESat-2 and CryoSat-2 Freeboards: A First Examination. *Journal of Geophysical Research: Oceans*, *125*(3). doi: 10.1029/2019JC016008

Kwok, R., Spreen, G., & Pang, S. (2013, 5). Arctic sea ice circulation and drift speed: Decadal trends and ocean currents. *Journal of Geophysical Research: Oceans*, *118*(5), 2408–2425. doi: 10.1002/JGRC.20191

Kwok, R., & Untersteiner, N. (2011). The thinning of Arctic sea ice. *Citation: Physics Today*, *64*, 36. doi: 10.1063/1.3580491

Laevastu, T. (1960). Factors affecting the temperature of the surface layer of the sea. *Comment. Phys. Math.*, *25*, 1–136.

Lebedev, V. V. (1938). Rost l'da v arkticheskikh rekakh i moriakh v zavisimosti ot otritsatel'nykh temperatur vozdukha. *Problemy arktiki*, *5*(6), 9–25.

Ledley, T. S. (1991). Snow on sea ice: competing effects in shaping climate. *Journal of Geophysical Research*, *96*(D9). doi: 10.1029/91JD01439

Lenton, T. M., & Vaughan, N. E. (2009). The radiative forcing potential of different climate geoengineering options. *Atmospheric Chemistry and Physics*, *9*(15), 5539–5561. doi: 10.5194/ACP-9-5539-2009

Lepparanta, M. (1983). A Growth Model for Black Ice, Snow Ice and Snow Thickness in Subarctic Basins. *Nordic Hydrology*, 59–70.

Leppäranta, M. (2011). *The Drift of Sea Ice*. Berlin, Heidelberg: Springer Berlin Heidelberg. doi: 10.1007/978-3-642-04683-4

Lin, L., & Zhao, J. (2019, 6). Estimation of Oceanic Heat Flux Under Sea Ice in the Arctic Ocean. *Journal of Ocean University of China*, *18*(3), 605–614. doi: 10.1007/S11802-019-3877-7

Lindsay, R., & Schweiger, A. (2015). Arctic sea ice thickness loss determined using subsurface, aircraft, and satellite observations. *Cryosphere*, *9*(1). doi: 10.5194/tc-9-269-2015

Lozowski, E., Jones, S., & Hill, B. (1991, 11). Laboratory measurements of growth in thin ice and flooded ice. *Cold Regions Science and Technology*, *20*(1), 25–37. doi: 10.1016/0165-232X(91)90054-K

Maeda, K., Kimura, N., & Yamaguchi, H. (2020). Temporal and spatial change in the relationship between sea-ice motion and wind in the arctic. *Polar Research*, *39*. doi: 10.33265/POLAR.V39.3370

Maksym, T., & Jeffries, M. O. (2001, 9). Phase and compositional evolution of the flooded layer during snow-ice formation on Antarctic sea ice. *Annals of Glaciology*, *33*, 37–44. doi: 10.3189/172756401781818860

Maykut, G. (1986). The Surface Heat and Mass Balance. In *The geophysics of sea ice* (pp. 395–463). Boston, MA: Springer US. doi: 10.1007/978-1-4899-5352-0{_}6

Maykut, G., & Untersteiner, N. (1969). *Numerical Prediction of the Thermodynamic Response of Arctic Sea Ice to Environmental Changes*. Santa Monica, CA: RAND Corporation.

Maykut, G., & Untersteiner, N. (1971). Some results from a time- dependent thermodynamic model of sea ice. *J Geophys Res*, *76*(6), 1550–1575. doi: 10.1029/JC076I006P01550

Mcphee, M. G. (1980). An Analysis of Pack Ice Drift in Summer. In *Sea ice processes and models* (pp. 62–75).

Merkouriadi, I., Gallet, J. C., Graham, R. M., Liston, G. E., Polashenski, C., Rösel, A., & Gerland, S. (2017, 10). Winter snow conditions on Arctic sea ice north of Svalbard during the Norwegian young sea ICE (N-ICE2015) expedition. *Journal of Geophysical Research: Atmospheres*, *122*(20), 837–10. doi: 10.1002/2017JD026753

Miller, L., Fripiat, F., Moreau, S., Nomura, D., Stefels, J., Steiner, N., … Vancoppenolle, M. (2020, 9). Implications of Sea Ice Management for Arctic Biogeochemistry. *Eos*, *101*. doi: 10.1029/2020EO149927

Millero, F. J. (1978, 1). Freezing point of seawater. *Eighth Report of the Joint Panel on Oceanographic Tables and Standards*, *28*, 29–31.

Moon, T. A., Overeem, I., Druckenmiller, M., Holland, M., Huntington, H., Kling, G., … Wong, G. (2019, 3). The Expanding Footprint of Rapid Arctic Change. *Earth's Future*, *7*(3), 212–218. doi: 10.1029/2018EF001088

Nakawo, M., & Sinha, N. K. (2022). GROWTH RATE AND SALINITY PROFILE OF FIRST-YEAR SEA ICE IN THE HIGH ARCTIC. *Journal 01 Glaciolog;>*, *27*(g6), 81.

National Snow and Ice Data Center. (n.d.). *Arctic Sea Ice News & Analysis.* Retrieved from https://nsidc.org/arcticseaicenews/

Nayar, K. G., Sharqawy, M. H., Banchik, L. D., & Lienhard V, J. H. (2016, 7). Thermophysical properties of seawater: A review and new correlations that include pressure dependence. *Desalination*, *390*, 1–24. doi: 10.1016/j.desal.2016.02.024

NOAA Climate.gov. (n.d.). *Climate Variability: Arctic Oscillation.* Retrieved from https://www.climate.gov/news-features/understanding-climate/climate-variability-arctic-oscillation#

Notz, D., & Community, S. (2020, 5). Arctic Sea Ice in CMIP6. *Geophysical Research Letters*, *47*(10). doi: 10.1029/2019GL086749

Olason, E., & Notz, D. (2014, 9). Drivers of variability in Arctic sea-ice drift speed. *Journal of Geophysical Research: Oceans*, *119*(9), 5755–5775. doi: 10.1002/2014JC009897

Onarheim, I. H., Eldevik, T., Smedsrud, L. H., & Stroeve, J. C. (2018). Seasonal and regional manifestation of Arctic sea ice loss. *Journal of Climate*, *31*(12). doi: 10.1175/JCLI-D-17-0427.1

Ono, N. (1967). Specific Heat and Heat of Fusion of Sea Ice. *Physics of Snow and Ice*, *1*(1), 599–610.

Overland, J., Dunlea, E., Box, J. E., Corell, R., Forsius, M., Kattsov, V., … Wang, M. (2019). *The urgency of Arctic change* (Vol. 21). doi: 10.1016/j.polar.2018.11.008

Overland, J. E., & Pease, C. H. (1988). Modeling ice dynamics of coastal seas. *JGR*, *93*(C12), 619–15. doi: 10.1029/JC093IC12P15619

Overland, J. E., & Wang, M. (2013, 5). When will the summer Arctic be nearly sea ice free? *Geophysical Research Letters*, *40*(10), 2097–2101. doi: 10.1002/GRL.50316

Park, H. S., & Stewart, A. L. (2016). An analytical model for wind-driven Arctic summer sea ice drift. *Cryosphere*, *10*(1), 227–244. doi: 10.5194/TC-10-227-2016

Parkinson, C. L., & Cavalieri, D. J. (2008, 7). Arctic sea ice variability and trends, 1979–2006. *Journal of Geophysical Research*, *113*(C7), C07003. doi: 10.1029/2007JC004558

Parkinson, C. L., Cavalieri, D. J., Gloersen, P., Zwally, H. J., & Comiso, J. C. (1999, 9). Arctic sea ice extents, areas, and trends, 1978-1996. *Journal of Geophysical Research: Oceans*, *104*(C9), 20837–20856. doi: 10.1029/1999JC900082

Perovich, D. K., Nghiem, S. V., Markus, T., & Schweiger, A. (2007, 3). Seasonal evolution and interannual variability of the local solar energy absorbed by the Arctic sea ice-ocean system. *Journal of Geophysical Research: Oceans*, *112*(3). doi: 10.1029/2006JC003558

Perovich, D. K., & Polashenski, C. (2012, 4). Albedo evolution of seasonal Arctic sea ice. *Geophysical Research Letters*, *39*(8), n/a-n/a. doi: 10.1029/2012GL051432

Perovich, D. K., & Richter-Menge, J. A. (2009, 1). Loss of Sea Ice in the Arctic. *Annual Review of Marine Science*, *1*(1), 417–441. doi: 10.1146/annurev.marine.010908.163805

Pithan, F., & Mauritsen, T. (2014). Arctic amplification dominated by temperature feedbacks in contemporary climate models. *Nature Geoscience*, *7*(3), 181–184. doi: 10.1038/NGEO2071

Polar Science Center. (2022). *PIOMAS Arctic Sea Ice Volume Reanalysis.* Retrieved from http://psc.apl.uw.edu/research/projects/arctic-sea-ice-volume-anomaly/

Polyakov, I. V., Pnyushkov, A. V., Alkire, M. B., Ashik, I. M., Baumann, T. M., Carmack, E. C., … Yulin, A. (2017, 4). Greater role for Atlantic inflows on sea-ice loss in the Eurasian Basin of the Arctic Ocean. *Science*, *356*(6335), 285–291. doi: 10.1126/science.aai8204

Pomeroy, J. W., & Brun, E. (2001). Physical Properties of Snow. *Snow ecology: An interdisciplinary examination of snow-covered ecosystems*, *45*, 118.

Previdi, M., Smith, K. L., & Polvani, L. M. (2021, 9). Arctic amplification of climate change: a review of underlying mechanisms. *Environmental Research Letters*, *16*(9), 093003. doi: 10.1088/1748-9326/ac1c29

Rampal, P., Weiss, J., & Marsan, D. (2009, 5). Positive trend in the mean speed and deformation rate of Arctic sea ice, 1979-2007. *Journal of Geophysical Research: Oceans*, *114*(5). doi: 10.1029/2008JC005066

Rigor, I. G., Wallace, J. M., & Colony, R. L. (2002, 9). Response of Sea Ice to the Arctic Oscillation. *Journal of Climate*, *15*(18), 2648–2663. doi: 10.1175/1520-0442(2002)015<2648:ROSITT>2.0.CO;2

Roberts, A. F., Hunke, E. C., Allard, R., Bailey, D. A., Craig, A. P., Lemieux, J.-F., & Turner, M. D. (2018, 9). Quality control for community-based sea-ice model development. *Philosophical Transactions of the Royal Society A: Mathematical, Physical and Engineering Sciences*, *376*(2129), 20170344. doi: 10.1098/rsta.2017.0344

Schweiger, A., Lindsay, R., Zhang, J., Steele, M., Stern, H., & Kwok, R. (2011). Uncertainty in modeled Arctic sea ice volume. *Journal of Geophysical Research: Oceans*, *116*(9). doi: 10.1029/2011JC007084

Screen, J. A., & Simmonds, I. (2010, 4). The central role of diminishing sea ice in recent Arctic temperature amplification. *Nature*, *464*(7293), 1334–1337. doi: 10.1038/nature09051

Semtner, A. J. (1976). A Model for the Thermodynamic Growth of Sea Ice in Numerical Investigations of Climate. *Journal of Physical Oceanography*, *6*(3). doi: 10.1175/1520-0485(1976)006<0379:amfttg>2.0.co;2

Serreze, M. C., Barry, R. G., & Mclaren, A. S. (1989, 8). Seasonal variations in sea ice motion and effects on sea ice concentration in the Canada Basin. *Journal of Geophysical Research: Oceans*, *94*(C8), 10955–10970. doi: 10.1029/JC094IC08P10955

Serreze, M. C., & Francis, J. A. (2006, 6). The Arctic Amplification Debate. *Climatic Change*, *76*(3-4), 241–264. doi: 10.1007/s10584-005-9017-y

Serreze, M. C., & Meier, W. N. (2019, 1). The Arctic's sea ice cover: trends, variability, predictability, and comparisons to the Antarctic. *Annals of the New York Academy of Sciences*, *1436*(1), 36–53. doi: 10.1111/nyas.13856

Sharqawy, M. H., Lienhard, J. H., & Zubair, S. M. (2010, 4). Thermophysical properties of seawater: a review of existing correlations and data. *Desalination and Water Treatment*, *16*(1-3), 354–380. doi: 10.5004/dwt.2010.1079

Smedsrud, L. H., Halvorsen, M. H., Stroeve, J. C., Zhang, R., & Kloster, K. (2017). Fram Strait sea ice export variability and September Arctic sea ice extent over the last 80 years. *The Cryosphere*, *11*, 65–79. doi: 10.5194/tc-11-65-2017

Smith, I. J., Langhorne, P. J., Frew, R. D., Vennell, R., & Haskell, T. G. (2012, 12). Sea ice growth rates near ice shelves. *Cold Regions Science and Technology*, *83-84*, 57–70. doi: 10.1016/j.coldregions .2012.06.005

Spreen, G., Steur, L., Divine, D., Gerland, S., Hansen, E., & Kwok, R. (2020, 6). Arctic Sea Ice Volume Export Through Fram Strait From 1992 to 2014. *Journal of Geophysical Research: Oceans*, *125*(6). doi: 10.1029/2019JC016039

Stefan, J. (1891). Ueber die Theorie der Eisbildung, insbesondere über die Eisbildung im Polarmeere. *Annalen der Physik*, *278*(2), 269–286. doi: 10.1002/andp.18912780206

Stockdale, T. N., Molteni, F., & Ferranti, L. (2015, 2). Atmospheric initial conditions and the predictability of the Arctic Oscillation. *Geophysical Research Letters*, *42*(4), 1173–1179. doi: 10.1002/2014GL062681

Sturm, M., Holmgren, J., König, M., & Morris, K. (1997). The thermal conductivity of seasonal snow. *Journal of Glaciology*, *43*(143), 26–41. doi: 10.3189/S0022143000002781

Sturm, M., Perovich, D. K., & Holmgren, J. (2002, 10). Thermal conductivity and heat transfer through the snow on the ice of the Beaufort Sea. *Journal of Geophysical Research: Oceans*, *107*(10). doi: 10.1029/2000JC000409

Taylor, P. C., Cai, M., Hu, A., Meehl, J., Washington, W., & Zhang, G. J. (2013, 9). A Decomposition of Feedback Contributions to Polar Warming Amplification. *Journal of Climate*, *26*(18), 7023–7043. doi: 10.1175/JCLI-D-12-00696.1

Tesi, T., Muschitiello, F., Mollenhauer, G., Miserocchi, S., Langone, L., Ceccarelli, C., … Capotondi, L. (2021, 11). Rapid Atlantification along the Fram Strait at the beginning of the 20th century. *Science Advances*, *7*(48), 2946. doi: 10.1126/SCIADV.ABJ2946

The Climate Prediction Center. (n.d.). *CPC - Monitoring & Data: Daily Arctic Oscillation Index.* Retrieved from https://www.cpc.ncep.noaa.gov/products/precip/CWlink/daily_ao_index/ao_index.html

Thompson, D. W., & Wallace, J. M. (1998, 5). The Arctic oscillation signature in the wintertime geopotential height and temperature fields. *Geophysical Research Letters*, *25*(9), 1297–1300. doi: 10.1029/98GL00950

Thorndike, A. S. (1986). Kinematics of Sea Ice. In *The geophysics of sea ice* (pp. 489–549). Boston, MA: Springer US. doi: 10.1007/978-1-4899-5352-0{_}8

Thorndike, A. S., & Colony, R. (1982). Sea ice motion in response to geostrophic winds. *Journal of Geophysical Research*, *87*(C8), 5845. doi: 10.1029/JC087IC08P05845

Timmermans, M. L., & Marshall, J. (2020, 4). Understanding Arctic Ocean Circulation: A Review of Ocean Dynamics in a Changing Climate. *Journal of Geophysical Research: Oceans*, *125*(4). doi: 10.1029/2018JC014378

Trodahl, H. J., Wilkinson, S. O., McGuinness, M. J., & Haskell, T. G. (2001, 4). Thermal conductivity of sea ice; dependence on temperature and depth. *Geophysical Research Letters*, *28*(7), 1279–1282. doi: 10.1029/2000GL012088

Turner, K. E., Smith, I. J., Tison, J. L., Verbeke, V., McGuinness, M., Ingham, M., … Trodahl, J. (2017, 6). Sea ice growth rates from tide-driven visible banding. *Journal of Geophysical Research: Oceans*, *122*(6), 4675–4684. doi: 10.1002/2016JC012524

US Department of Commerce, N. O., & Administration, A. (n.d.). *The Ekman Spiral - Currents: NOAA's National Ocean Service Education.* Retrieved from https://oceanservice.noaa.gov/education/tutorial_currents/04currents4.html

Vowinckel, E., & Orvig, S. (1962, 12). Relation between Solar Radiation Income and Cloud Type in the Arctic. *Journal of Applied Meteorology*, *1*(4), 552–559. doi: 10.1175/1520-0450(1962)001<0552:RBSRIA>2.0.CO;2

Walsh, J. E. (2014). Intensified warming of the Arctic: Causes and impacts on middle latitudes. *Global and Planetary Change*, *117*, 52–63. doi: 10.1016/J.GLOPLACHA.2014.03.003

Wang, Q., Ricker, R., & Mu, L. (2021, 2). Arctic Sea Ice Decline Preconditions Events of Anomalously Low Sea Ice Volume Export Through Fram Strait in the Early 21st Century. *Journal of Geophysical Research: Oceans*, *126*(2). doi: 10.1029/2020JC016607

Warren, S. G., Rigor, I. G., Untersteiner, N., Radionov, V. F., Bryazgin, N. N., Aleksandrov, Y. I., & Colony, R. (1999). Snow depth on Arctic sea ice. *Journal of Climate*, *12*(6), 1814–1829. doi: 10.1175/1520-0442(1999)012<1814:SDOASI>2.0.CO;2

Winton, M. (2006, 2). Amplified Arctic climate change: What does surface albedo feedback have to do with it? *Geophysical Research Letters*, *33*(3). doi: 10.1029/2005GL025244

Wu, X., Budd, W. F., Lytle, V. I., & Massom, R. A. (1999, 1). The effect of snow on Antarctic sea ice simulations in a coupled atmosphere-sea ice model. *Climate Dynamics*, *15*(2), 127–143. doi: 10.1007/s003820050272

Yen, Y. C. (1981). REVIEW OF THERMAL PROPERTIES OF SNOW, ICE AND SEA ICE. *CRREL Report (US Army Cold Regions Research and Engineering Laboratory)*.

Zampieri, L., & Goessling, H. F. (2019, 12). Sea Ice Targeted Geoengineering Can Delay Arctic Sea Ice Decline but not Global Warming. *Earth's Future*, *7*(12), 1296–1306. doi: 10.1029/2019EF001230

Zhang, J. (2021, 9). Recent Slowdown in the Decline of Arctic Sea Ice Volume Under Increasingly Warm Atmospheric and Oceanic Conditions. *Geophysical Research Letters*, *48*(18). doi: 10.1029/2021GL094780

Zhang, J., Lindsay, R., Schweiger, A., & Rigor, I. (2012, 10). Recent changes in the dynamic properties of declining Arctic sea ice: A model study. *Geophysical Research Letters*, *39*(20). doi: 10.1029/2012GL053545

Zwally, H. J., & Gloersen, P. (2008, 9). Arctic sea ice surviving the summer melt: interannual variability and decreasing trend. *Journal of Glaciology*, *54*(185), 279–296. doi: 10.3189/002214308784886108

A

Map of the different Arctic regions

Figure A.1 shows a map of the different Arctic regions as defined by the NSIDC.

Figure A.1: The different regions in the Arctic. Credit: National Snow and Ice Data Center.

B

AIM full test results

Four different test set-ups, summarised in Table B.1, are used for small scale AIM experiments. Each experiment is conducted twice, however the cooling time prior to flooding is kept constant and due to different initial water temperatures the initial ice thickness is not equal but of similar height. Figures B.1, B.2, B.3 and B.4 show the same behaviour and for this reason the results are considered reliable. An additional test (Test V) is conducted to exclude possible sawing effects on the ice growth. Two coolers with the same initial freezing moment were flooded and the ice thickness in each cooler was measured once. Figure B.5 is in line with the other results, indicating there is no effect of the sawing process.

Table B.1: Overview of experiments used to validate the AIM model

Experiment	Flooding phase	Cooling time prior to flooding	
Test I	Instantly 2.5 cm (4.5 L)	24 h	Figure B.1
Test II	Instantly 2.5 cm (4.5 L)	48 h	Figure B.2
Test III	Incrementally 9x0.28 cm (9x0.5L)	24 h	Figure B.3
Test IV	Incrementally 9x0.28 cm (9x0.5L)	48 h	Figure B.4

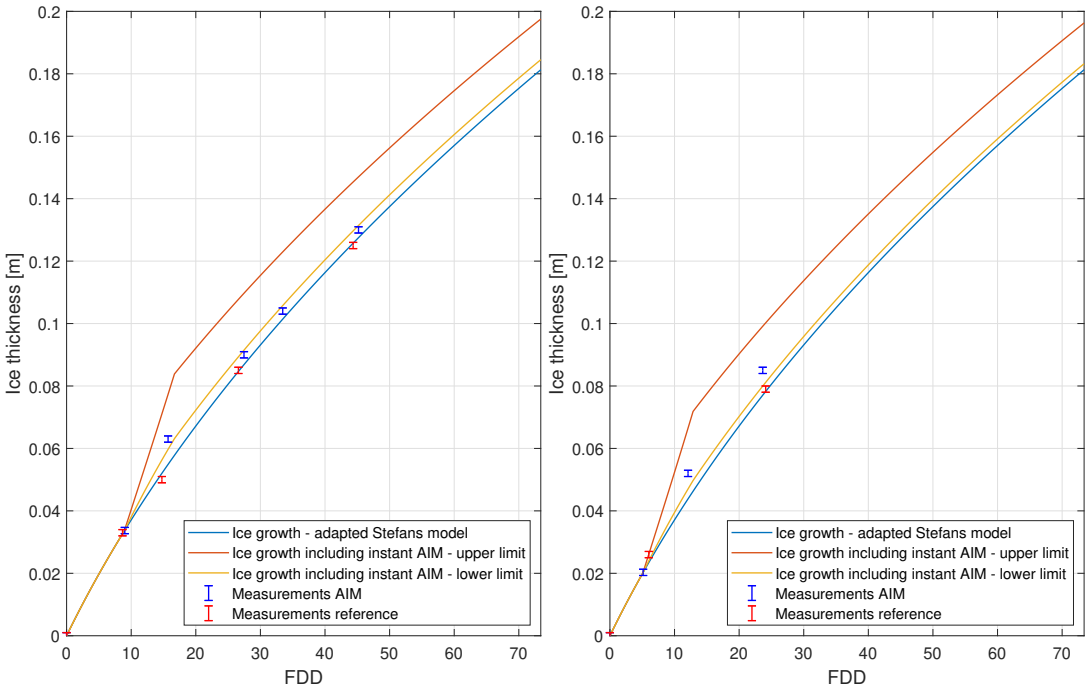

(a) Test I **(b)** Test Ib

Figure B.1: Results for instant flooding after 24 h cooling time

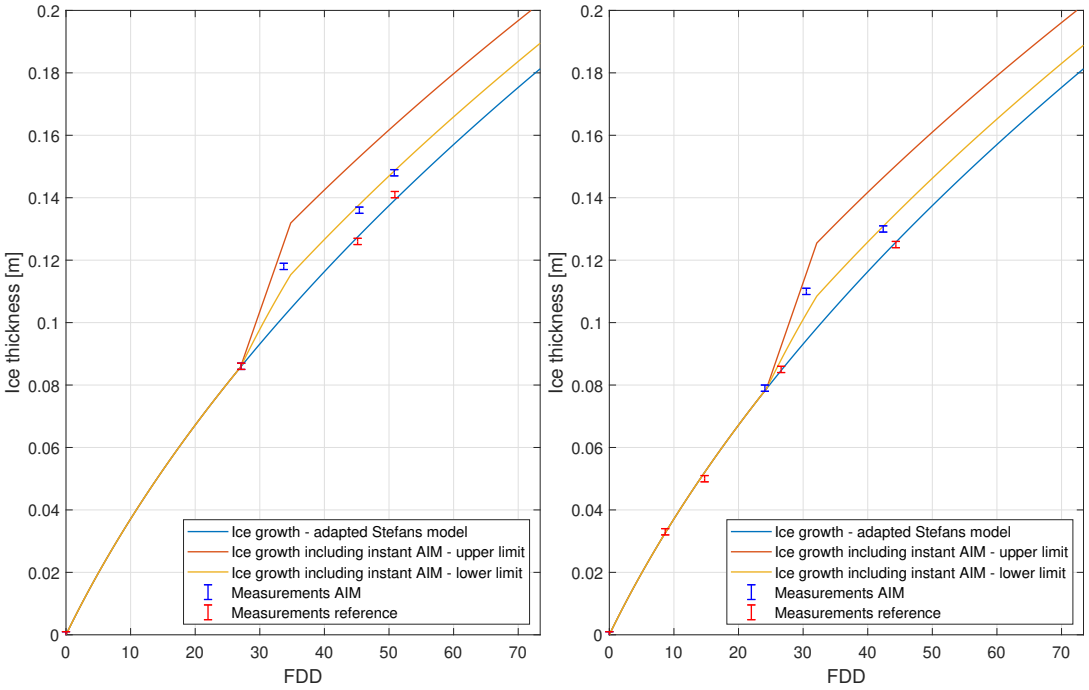

(a) Test II - Flooding at once **(b)** Test IIb

Figure B.2: Results for instant flooding after 48 h cooling time

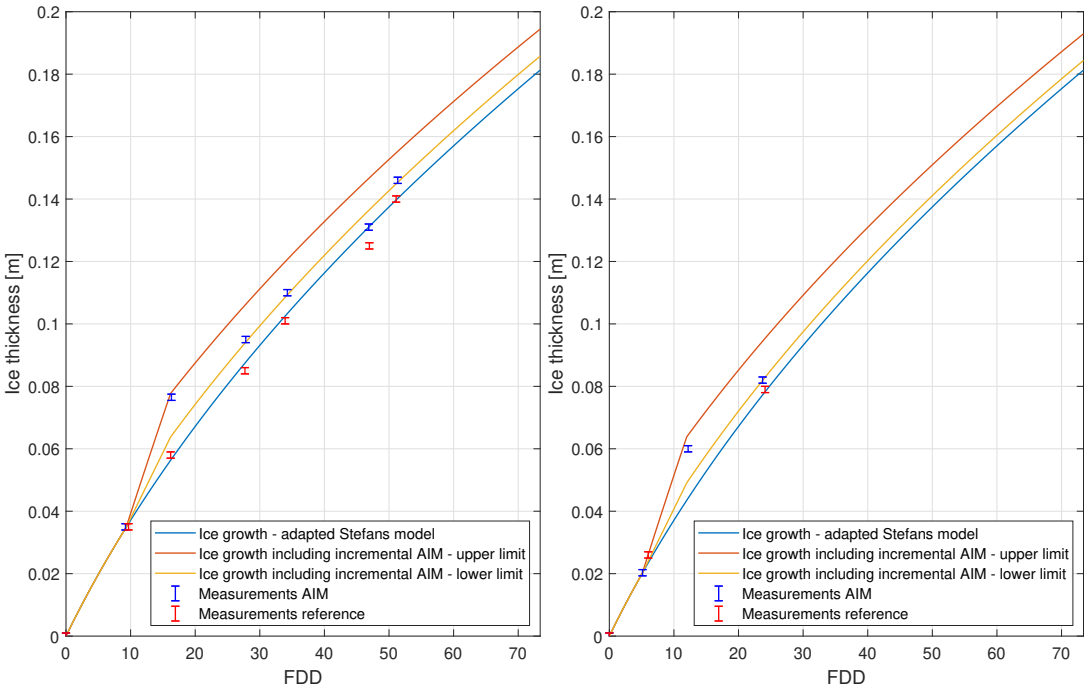

(a) Test III **(b)** Test IIIb

Figure B.3: Results for incremental flooding after 24 h cooling time

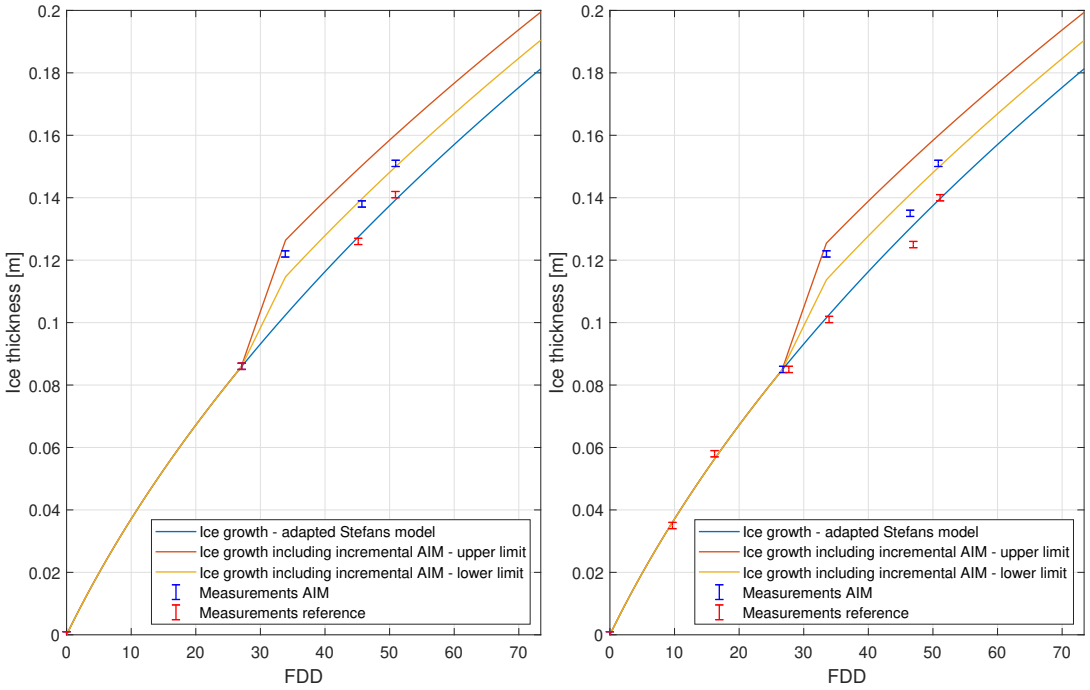

(a) Test IV **(b)** Test IVb

Figure B.4: Results for incremental flooding after 48 h cooling time

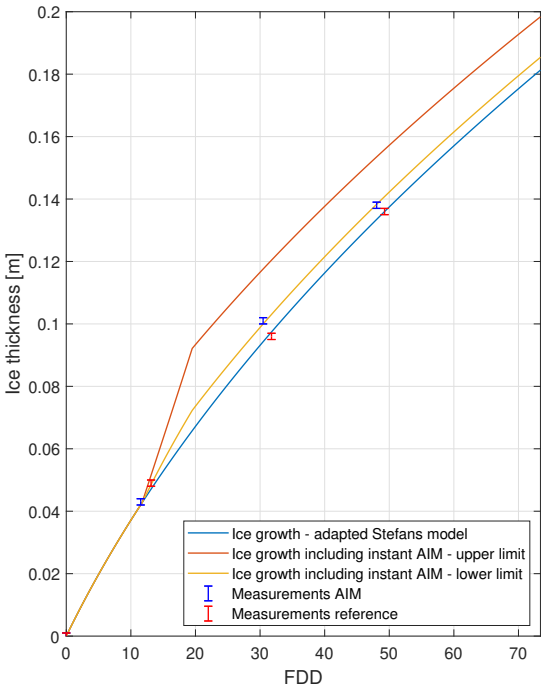

Figure B.5: Test V: Confirming ice growth without sawing effects

C

Convergence study COMSOL

A relative tolerance convergence study is conducted for the COMSOL Multiphysics simulations, shown in Figure C.1, to ensure reliable results. Based on this study, a relative tolerance of 5e-5 is used for the final simulations to balance accuracy and computation time.

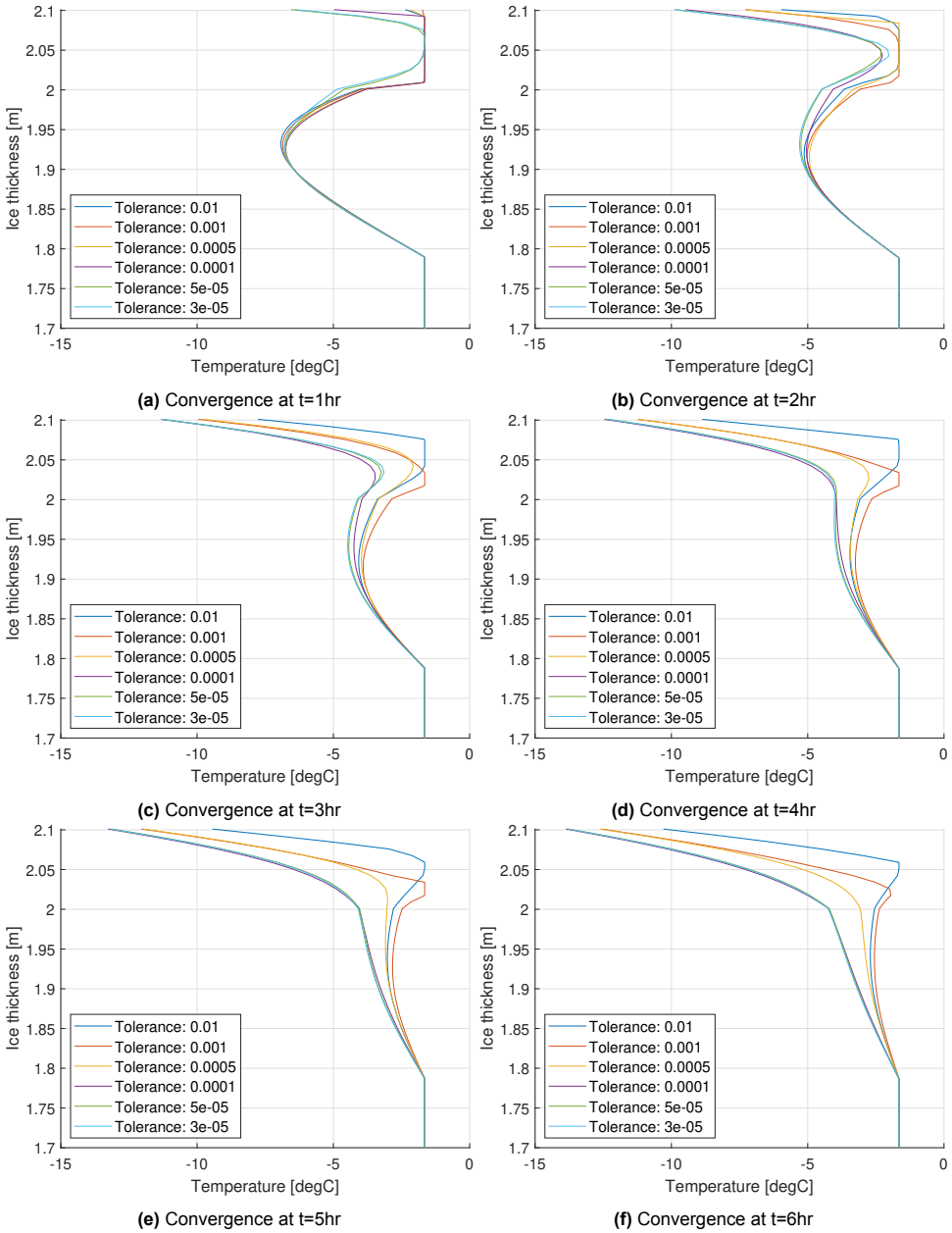

(a) Convergence at t=1hr

(b) Convergence at t=2hr

(c) Convergence at t=3hr

(d) Convergence at t=4hr

(e) Convergence at t=5hr

(f) Convergence at t=6hr

Figure C.1: Convergence study at several time intervals